

## Stellingen

Zogeheten service-practica en service-onderwijs, die door de ene discipline in het hoger onderwijs worden verzorgd voor een andere discipline, dienen zorgvuldig op de vragende discipline te worden afgestemd.

E.F.M. Jansen en A.H. Verdonk, *J. Mater. Educ.* **11** (1989) 181-199.

De door Popov *et.al.* door middel van impedantiemetingen over een groot frequentiegebied (1 mHz - 100 kHz) onderzochte veranderingen van gedrag van een organische coating gerepresenteerd met behulp van een equivalent circuit kunnen slechts correct geïnterpreteerd worden nadat de frequentieafhankelijkheid van de componenten van het equivalente circuit onderzocht is en nihil bevonden.

B.N. Popov, M.A. Alwohaibi en R.E. White, *J. Electrochem. Soc.* **140** (1993) 947-951.

Het ontbreken van de actief-passief overgang in de door Babic en Metikos-Hukovic beschreven potentiodynamische meting aan een roestvast stalen electrode is niet afdoende verklaard met het feit dat kort contact van de electrode met vochtige lucht voldoende is om een dunne oxidelaag te doen ontstaan op het oppervlak.

R. Babic en M. Metikos-Hukovic, *J. Appl. Electrochem.* **23** (1993) 352-357.

Voor het monitoren van wateropnamen door organische deklagen met een typisch barrière-gedrag verdient het gebruik van een eenvoudige capaciteitsmeter de voorkeur boven impedantieapparatuur.

Teneinde de gevoeligheid voor putvormige corrosie van een roestvast staal beter te kunnen beoordelen verdient het aanbeveling om in de certificaten van roestvast staal halffabrikaten gegevens op te nemen over de insluitsels in het betreffende staal, met name het aantal en de grootteverdeling van mangaansulfide insluitsels.

Dit proefschrift.

De spreiding in de standaard potentiodynamische polarisatiecurven (voorwaartse scan) volgens ASTM G61 van type 304 roestvast staal geeft reeds de beperkte bruikbaarheid aan van deze techniek voor het ordenen van roestvaste staalsoorten naar gevoeligheid voor initiatie van lokale corrosie op basis van de pittingpotentiaal.

ASTM G61, Standard test method for conducting cyclic potentiodynamic polarization measurements for localized corrosion susceptibility of iron-, nickel- or cobalt-based alloys, 1992 Annual Book of ASTM standards, Vol. 03.02, American Society for Testing and Materials, Philadelphia, USA (1992), 231-235.

Het verdient aanbeveling om kunstenaars aan te merken als onderzoekers teneinde de voor diverse regelingen noodzakelijke beoordelingen te verbeteren.

De kosten van de gezondheidszorg in Nederland kunnen worden teruggedrongen door vermindering van het aantal tv-programma's met een medisch thema.

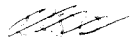
Teneinde het aantal dragers van een donorcodicil te vergroten zou in nieuwe portefeuilles naast de vakjes met een dummy rijbewijs en dummy creditcards een vakje met een blanco codicil aangebracht moeten worden.

Twee carrières op één kussen, daar slaapt de duivel tussen.

De reputatie van een chemicus in 1993 is niet beter dan die van een alchemist in 1623.

J. van Kasteren, *Chemisch Magazine*, juni 1993, 270-272.

Constantijn Huygens, *Een Alchymist*, 1623



2252  
TR diss  
TR diss 2252

**TR diss  
2252**

# Pitting Corrosion of Stainless Steels

The Role of Inclusions and the  
Effect of Surface Deformation

CIP-GEGEVENS KONINKLIJKE BIBLIOTHEEK, DEN HAAG

Jansen, Elisabeth Francisca Maria

Pitting corrosion of stainless steels : the role of inclusions and the effect of surface deformation / Elisabeth Francisca Maria Jansen. - [S.l. : s.n.]. - III.

Proefschrift Technische Universiteit Delft. - met lit. opg. - Met samenvatting in het Nederlands.

ISBN 90-9006403-6

Trefw.: corrosie.

cover design: Agnes Roothaan

sponsored by



**Pitting Corrosion of Stainless Steels**  
The Role of Inclusions and the Effect of Surface Deformation

**Putvormige Corrosie van Roestvaste Staalsoorten**  
De Rol van Insluitsels en het Effect van Oppervlakteformatie

proefschrift

ter verkrijging van de graad van doctor aan de Technische  
Universiteit Delft, op gezag van de Rector Magnificus,  
Prof. Ir. K.F. Wakker, in het openbaar te verdedigen ten  
overstaan van een commissie aangewezen door het College  
van Dekanen op dinsdag 7 september 1993 te 14.00 uur

door

**Elisabeth Francisca Maria Jansen**

geboren op 7 januari 1960 te Altforst (Gld.), chemicus



Dit proefschrift is goedgekeurd door de promotor, prof. dr. J.H.W. de Wit.

# CONTENTS

<b>1 Introduction</b>	1
1.1 The purpose of the research project	1
1.2 Stainless steel and its history	2
1.3 Corrosion testing and pitting	3
1.4 The outline of this thesis	6
1.5 References	7
<b>2 Literature Review</b>	9
2.1 Introduction	9
2.2 Pit initiation at inclusions	10
2.2.1 Number and type of inclusions in stainless steels	10
2.2.2 Attack at inclusion sites	11
2.3 Stabilization of pit growth	12
2.3.1 Introduction	12
2.3.2 The influence of anions	14
2.3.3 Dissolution products from manganese sulphide inclusions	16
2.3.4 General stabilization theories	17
2.4 References	20
<b>3 The Meaning of Current Spikes</b>	23
3.1 Introduction	23
3.2 Experimental	24
3.3 Results and discussion	28
3.3.1 Current-potential curves and current spikes	28
3.3.2 Current spikes and manganese sulphide inclusions	35
3.3.3 The influence of anions	47
3.3.4 The relation between spikes and pitting	52
3.4 Conclusions	60
3.5 References	60

<b>4 Comparison of 6 Stainless Steels</b>	63
4.1 Introduction	63
4.2 Experimental	64
4.3 Results and discussion	65
4.3.1 Current-potential curves	65
4.3.2 Current spikes	67
4.3.3 Surface analyses	71
4.4 Conclusions	79
4.5 References	80
<b>5 The Effect of Surface Deformation</b>	81
5.1 Introduction	81
5.2 Experimental	83
5.3 Results	84
5.3.1 Current-potential curves	84
5.3.2 Current spikes	89
5.4 Discussion	96
5.5 Conclusions	98
5.6 References	99
<b>6 General Conclusions and Recommendations</b>	101
6.1 General conclusions	101
6.2 Recommendations	104
6.3 Literature	105
<b>appendix A Information on the Stainless Steels</b>	107
<b>appendix B Structure of the Computer Programs</b>	111
B.1 Data acquisition	111
B.2 Data analysis	113
<b>Summary</b>	117
<b>Samenvatting</b>	119
<b>Dankwoord / Acknowledgement</b>	123
<b>Curriculum vitae</b>	125



# INTRODUCTION

## 1.1 The purpose of the research project

Stainless steels are popular construction materials because of their good corrosion resistance. But especially in aggressive industrial environments most of these steels are susceptible to localized corrosion, for example pitting and crevice corrosion. These are dangerous types of corrosion because attack is often unpredictable, proceeds fast and causes serious damage. Despite the availability of many data on localized corrosion phenomena, both from experience and laboratory research, information on mechanisms is quite incomplete.

This thesis is a result of studies on pitting corrosion of stainless steels and the effect of surface deformation by micropeening on this type of corrosion. Micropeening is a technique for the cold working of a metallic surface by pelting it with small glass beads. One of the resulting effects is a compressive stress in the surface layer, which is known to be often beneficial for a number of mechanical properties. In the project\* described in this thesis the consequences of micropeening for the pitting susceptibility of stainless steel were to be studied. In order to do so, first an appropriate method to characterize the susceptibility of stainless steel to pitting corrosion had to be found. It proved also necessary to investigate the role of inclusions in this process, in order to obtain sensible experimental results on the pitting corrosion behaviour. In this way the influence of micropeening could be studied in more detail.

---

\* This project was supported by the Dutch Ministry of Economic Affairs / SENTER within the scope of IOP-metals (*IOP : Innovatiegerichte Onderzoeks Programma's*).

## 1.2 Stainless steel and its history

Stainless steels are iron-base alloys with chromium and ten to fifteen other alloying elements. They are widely used for a variety of applications in architecture, chemical, dairy and food-processing plants, transportation industries, sculpture, cooking utensils and cutlery for instance. The composition of the steel together with the mechanical and heat treatments determines the structure of the material and thus the mechanical properties. Structure and composition also determine the corrosion behaviour the steel. The iron-chromium alloys with at least 10.5%\* chromium have a ferritic (body-centered cubic) structure. The iron-chromium-nickel alloys have an austenitic (face-centered cubic) structure, provided their carbon content is low and they are properly heat treated. These alloys are tougher and more ductile and have a better general corrosion resistance than the ferritic alloys.

Reports on the properties of iron-chromium alloys exist from the beginning of last century. Twenty-three years after the discovery of chromium (1797), Faraday and Stodart started experiments with the alloys. They inspired P. Berthier to do more extensive research, which was reported in 1821<sup>1</sup>. He noticed that the resistance of iron-chromium against attack by acids improved with higher chromium content. Because the alloys also had good mechanical properties they were suggested to be suitable for cutlery and sabres "*damassées, solides, dures et d'un bel effet*". In 1892 however, R.A. Hadfield<sup>2</sup> reported that the more chromium was added to iron alloys, the more they were attacked after immersion in sulphuric acid. The behaviour after immersion in sulphuric acid was considered to indicate the general corrosion behaviour of the metal. Hadfield only tested alloys containing up to 9.18% chromium (with 0.71% carbon). Not until the beginning of this century commercial "stainless steels" were developed. It was H. Brearley who, in 1913, initiated the production in England<sup>3</sup>. He was engaged in research on various steels for rifles and naval guns, when he found that he could not etch polished samples of iron alloyed with 12.8% chromium and 0.24% carbon, which he prepared for microscopic examination. He noticed the effect of heat treatments and investigated limiting ranges of composition, factors that

were formerly not recognized as being very important. He interested E. Stuart, employed in Sheffield, in the alloy which led to the introduction of stainless steel cutlery in 1914. Laboratory search for scaling resistant materials to be used as protective tubes for thermoelectric couples, by Benno Strauss and Eduard Maurer at Krupp works in Essen, Germany, led to the discovery of the austenitic chromium-nickel-iron alloys<sup>4</sup>. In 1912, patents were applied for by Krupp, for both martensitic (0.15% carbon, 14% chromium and 1.8% nickel) and austenitic (0.25% carbon, 20% chromium and 7% nickel) alloys. Adding molybdenum to austenitic steel further improved its corrosion resistance. Patents, also held by Krupp, date from 1923. Now, 70 years later, basically the same austenitic alloys known as AISI 304 (FeCrNi, "18-8") and AISI 316 (FeCrNiMo) are the most familiar stainless steels.

More information on AISI 304, AISI 316 and other steels relevant for this thesis can be found in appendix A.

### **1.3 Corrosion testing and pitting**

In the beginning of this century the corrosion resistance of materials for cutlery was regularly tested by placing a drop of "pure malt vinegar" on the polished surface<sup>3</sup>. The dry residues from the drop were washed off in water and the surface was examined for any signs of a stain. Steels with a low carbon content, alloyed with a sufficient amount of chromium and heat treated in an appropriate way, proved to resist staining; they were "stainless".

More in general, metals used to be (and still are) tested by exposing them to the atmosphere, hanging panels in the sea or river or burying them and inspecting them afterwards for corrosion products, loss in weight, maximum depth of pitting and physical properties for instance<sup>5,6</sup>. Important laboratory tests were salt spray tests and intermittent and total immersion tests.

Since 1926, the electrochemical ('corrosion') behaviour of metals is being studied by measuring the current-potential relation<sup>6</sup>. Current-potential curves are still very important in corrosion research and are often used to characterize the pitting susceptibility of a metal. A schematic

current-potential curve obtained under steady-state conditions, called a polarisation curve, is shown in figure 1.1.

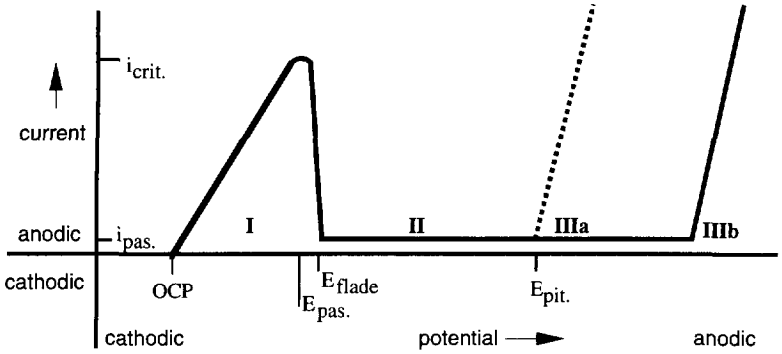


Figure 1.1. Schematic polarization curve.

The potential of a metal submerged in an electrolyte solution is shifted slowly from the initial Open Circuit Potential OCP (for a corroding system also called the corrosion potential) towards more anodic values. Upon this anodic polarisation of an initially clean metal electrode the metal oxidation ( $Me \rightarrow Me^{z+} + z e^-$ ) is stimulated. This corresponds to region I in figure 1.1, which shows an increasing current with increasing anodic potential. Some metals, such as stainless steel and aluminium, form a solid product, e.g. an oxide, during this process, that may adhere to the surface and impede further dissolution. The sudden decrease of the current seen in figure 1.1 as the transition from region I to region II, starting at the primary passive potential  $E_{pas}$  and ending at the Flade potential  $E_{flade}$ , reflects this process. The maximum current in the active region I is called the critical current  $i_{crit}$ . In region II the surface is completely covered with a solid product: the passive layer or passive film. The metal is now called passive and the corresponding low current is called the passive current  $i_{pas}$ . Upon anodic polarization from  $E_{flade}$ , the passive film (chromium oxide like in case of stainless steel) initially keeps the metal covered and protected. This lasts until a potential is reached at which the film breaks or oxidizes further to soluble components or/and water is oxidized to oxygen, region III in figure 1.1. Local film breakthrough as indicated by a current

increase at IIIa, is observed in halide containing electrolyte solutions and is associated with pitting. The potential at which this occurs is called the pitting potential  $E_{pit}$ . In halide free solutions at more anodic potentials the passive film on stainless steel can oxidize further to soluble chromates: transpassivity in region IIIb. Passivity is then lost over the whole exposed surface. Depending on the alloy composition, transpassive dissolution of the film is accompanied by oxygen evolution.

The oxide film on stainless steel can be formed directly in humid air or at exposure to a solution. The oxide film can fail at weak spots, for example in chromium depleted zones (created by a wrong heat treatment or welding) or near inclusions which are present in large amounts in commercial stainless steels. If, in-service, at a particular place the 'bare' metal gets exposed to an aggressive solution, while the surrounding surface is still covered by an oxide film, the local metal dissolution can proceed very fast. The cathodic current, oxygen reduction for example, which flows over an important surface area near the defect, is balanced by the anodic current in the defect, see figure 1.2. Because of the low surface area ratio  $A_{anode}/A_{cathode}$ , the current density in the defect is high, corresponding to high local dissolution rates. (The electronic conductivity of the passive film and the ionic conductivity of the electrolyte are generally sufficient for this process to occur.)

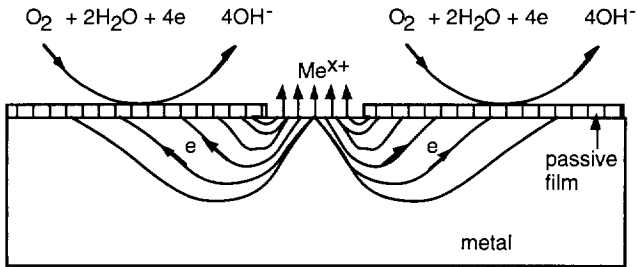
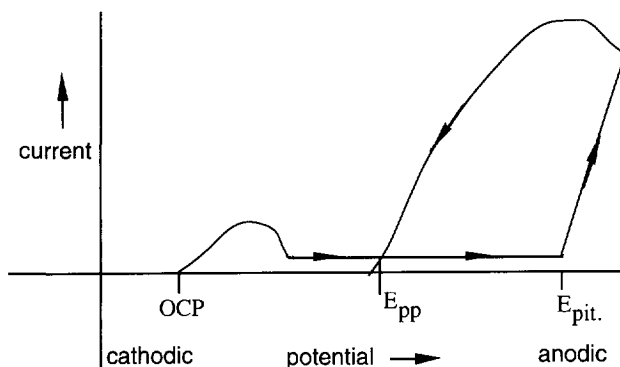


Figure 1.2. Schematic representation of pitting corrosion.

There is a standardized exposure test for pitting corrosion, known as ASTM G48, and a standardized test for determination of the pitting potential, ASTM G617. In the former test specimens are exposed to 6%  $FeCl_3$  and inspected afterwards for weight loss, pit depth, pit density and

appearance. The latter test prescribes a cyclic potentiodynamic polarization measurement: scanning with 0.6 V/h from the OCP in anodic direction and reversing when the current density reaches 5 mA/cm<sup>2</sup>, in order to determine the pitting (or pit nucleation) potential, from the anodic part of the curve, and the protection potential,  $E_{pp}$ , from the cathodic part of the scan, see figure 1.3. Pits are believed not to propagate below the protection potential. The preparation of the specimen and the design of the specimen holder are prescribed into detail. The pitting potential and the protection potential thus determined are being used for metals ranking.



*Figure 1.3. Schematic showing the use of a current-potential curve to determine the pitting potential and the protection potential.*

Although corrosion testing and research has quite a history, it is still difficult to predict the in-service behaviour of a metal on the basis of laboratory tests. Evans<sup>6</sup> talked in 1946 on "The fallacy of anodic testing", referring to tests in which the metallic specimen is made the anode in an electrolytic cell. Now, in 1993, this translation step is still most delicate.

#### **1.4 The outline of this thesis**

In chapter two of this thesis literature on the initiation of pitting corrosion at inclusion sites and stabilization of pit growth is reviewed. The subsequent chapters cover the results and discussion of experimental work. Subject of chapter three is the relation between pitting and inclusions in

AISI 304 and AISI 316. Current spikes have been measured in sodium chloride solutions under potentiostatic control in the passive potential region. These spikes are related to macroscopic pitting phenomena, studied with a video camera, on the one hand and to inclusions, studied with surface analytical techniques, on the other hand. In chapter four the corrosion behaviour of several highly alloyed, molybdenum containing stainless steels in sodium chloride solutions is compared. Special attention is given to the inclusions in these steels. Experiments with stainless steels deformed by micropeening or rolling are reported in chapter five. Deformed and undeformed specimens are compared with respect to their behaviour under potentiostatic and potentiodynamic conditions in sodium chloride solutions. Conclusions and recommendations are formulated in chapter six. Appendices with details on the developed computer programs and on the stainless steels discussed in this thesis, and a summary, in English and in Dutch, have been added.

## 1.5 References

- 1 P. Berthier, *Annales de Chimie et de Physique* **17** (1821) 55-64.
- 2 R.A. Hadfield, *Journal of the Iron and Steel Institute* **II** (1892) 49-110.
- 3 J.H.G. Monypenny, *Stainless Iron and Steel*, Chapman&Hall, London, UK (1926).
- 4 E.E. Thum (ed.), *The Book of Stainless Steels*, The American Society for Metals, Cleveland, Ohio, USA (1935).
- 5 *Metals Handbook Ninth Edition*, Vol 13, Corrosion, American Society for Metals, Metals Park, Ohio, USA (1987).
- 6 U.R. Evans, *Metallic Corrosion passivity and Protection*, Second Edition, Edward Arnold & Co., London, UK (1946).
- 7 ASTM G48, ASTM G61, 1982 Annual Book of ASTM standards, part 10, American Society for Testing and Materials, Philadelphia, USA (1982).

# LITERATURE REVIEW

## PIT INITIATION AT INCLUSIONS AND STABILIZATION OF PIT GROWTH

### 2.1 Introduction

The corrosion behaviour of a steel is not only determined by the composition, but also by the metallurgical structure of the steel. With respect to pitting corrosion of commercial stainless steels such as AISI 304 and AISI 316, sulphide inclusions, and especially manganese sulphide inclusions, have been recognized as promoting agents. Accordingly, reduction of the sulphur and/or manganese content of these steels results in an improved resistance against pitting and crevice\* corrosion<sup>1-4</sup>. Removal of sulphide inclusions at the surface by pickling with nitric acid also leads to a reduction of the pitting susceptibility as determined by potentiostatic techniques and immersion tests<sup>5-7</sup>. But it should be noted that changing the alloy composition to reduce the susceptibility to localized corrosion will at the same time alter other properties like the weldability and machinability, which is not always desired. Pickling a surface is a polluting activity and its effect on the resistance to localized corrosion will only be temporary.

Descriptions of the mechanism of attack at inclusions given by Eklund<sup>8</sup> and Wranglén<sup>9</sup> almost twenty years ago, have been followed by a vast amount of literature on pitting mechanisms. High resolution micro-analytical techniques have enabled detailed studies of inclusions and localized corrosion. In this chapter a review of the recent literature on the

---

\* It is believed that pitting and crevice corrosion of stainless steel are closely related.



role of inclusions in pitting corrosion is given. Reports on the number and type of inclusions in austenitic stainless steels, attack at inclusion sites and factors determining whether or not attack proceeds, are surveyed.

## **2.2 Pit initiation at inclusions**

### **2.2.1 Number and type of inclusions in stainless steels**

Some recent articles give more or less detailed information on the number and type of inclusions in stainless steels. Stewart<sup>10</sup>, using an optical microscope with an image analysis system, energy dispersive spectroscopy and an electron microprobe system, found in a commercial purity AISI 304 steel (0.011% S) 748 elliptically shaped inclusions per mm<sup>2</sup> with a mean area of 2.3 μm<sup>2</sup>. One fourth contained sulphur, and most of these inclusions also contained iron and chromium. Most of the sulphides were found to be associated with oxides. The larger inclusions were generally rich in sulphur.

The inclusions in two AISI 304L steels, with a sulphur content of 0.010% and 0.007%, were studied by Daufin<sup>11</sup>. Microprobe analyses revealed that the alloys contained 1242 and 600 inclusions per mm<sup>2</sup> respectively. In the former alloy 95% of the inclusions consisted of several types of oxides. Large manganese/chromium sulphide inclusions were found to be associated with small calcium aluminosilicate inclusions. In the latter alloy only traces of sulphides were found. Sulphides were sometimes found around oxide particles.

A scanning Auger microscope fitted with an X-ray analysis system was used both by Ke<sup>12</sup> and Castle<sup>13</sup>. Ke<sup>12</sup> distinguished three groups of inclusions in AISI 304 (no data on the composition): oxides (Cr<sub>2</sub>O<sub>3</sub> and MnO with some Al<sub>2</sub>O<sub>3</sub>), manganese sulphide inclusions and mixed oxide/sulphide inclusions. The number of manganese sulphide inclusions was estimated at 3000 per mm<sup>2</sup> and the diameter of these inclusions was less than 2 μm. Castle<sup>13</sup> investigated AISI 316 (0.009% S) and found two types of inclusions: separate sulphide particles and sulphides associated with complex oxide inclusions.

Titanium rich AISI 301 (0.01% S) and AISI 316 (0.015% S) were investigated by Srivastava<sup>14</sup>. Using scanning electron microscopy, energy dispersive X-ray analysis and scanning Auger electron spectroscopy, oxide and sulphide inclusions were found. The iron/manganese sulphide inclusions were generally associated with oxides of titanium, often surrounding them, but isolated sulphide stringers were also common.

This survey illustrates that the number and type of inclusions reported to be found in several stainless steels vary considerably. Although the differences will certainly be partly due to differences in experimental circumstances, the inclusions are sure to differ from batch to batch.

### 2.2.2 Attack at inclusion sites

A general classification scheme for the possible mechanisms of pit initiation at inclusions has been proposed by Ives<sup>15</sup>. Four types are distinguished (see figure 2.1): (I) dissolution of soluble (anodic) inclusion in an immune or protected matrix, (II) selective attack of a multiphase inclusion in an immune or protected matrix, (III) dissolution of the matrix next to a cathodic inclusion and (IV) a physical crevice between an (under the given conditions) unreactive inclusion and matrix (no mechanical bond) where pit growth can start because of occluded cell effects (to be discussed in 2.3).

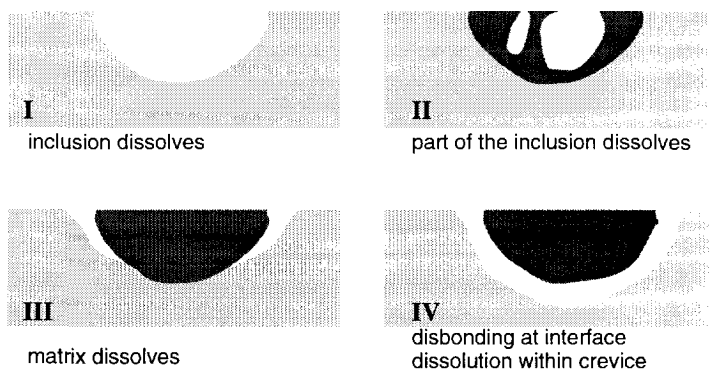


Figure 2.1. Classification of pit nucleation processes according to Ives<sup>15</sup>.

The various types of attack at different inclusions in stainless steels which have been described in the literature, can readily be classified according to this scheme. Manganese sulphide inclusions dissolve easily in neutral or acidic sodium chloride solutions<sup>9,10,12,13,15,16</sup>, and the attack is therefore of type I. The same type of attack has been observed for calcium oxide inclusions<sup>15</sup>. Preferential dissolution of manganese sulphide around or next to an oxide inclusion is frequently reported<sup>13-17</sup> and clearly of type II. Initiation of type III is seen at chromium-rich, titanium-rich and copper-rich inclusions<sup>15</sup>. There is no evidence of type IV occurring in austenitic stainless steels, although it has been suggested that crevices can be formed by cold deformation<sup>14,15</sup>.

The (globular) inclusions consisting of only manganese sulphide are sometimes believed to be not, or less, harmful as opposed to oxide-sulphide inclusions<sup>10,13,15,17</sup>. After dissolution of a globular inclusion (type I), only a hole remains which is likely to repassivate because of its openness. Type II attack of a multiphase oxide-sulphide inclusion however can lead to the formation of a small crevice in which repassivation is impeded because of enhanced local acidification and/or a potential drop (this phenomenon will be further discussed in 2.3).

The effect of the shape of the inclusions was demonstrated by Scotto<sup>17</sup>. He performed experiments on longitudinal and transverse sections of rolled steel rods. The transverse sections were more reactive because of the unfavourable geometry of the cavities formed upon dissolution of inclusions.

## **2.3 Stabilization of pit growth**

### **2.3.1 Introduction**

The dissolution of a (sulphide) inclusion will not have a serious effect if a passive film is formed again on the newly exposed metal surface. But if the local conditions are such that repassivation is impeded, the attack proceeds and does cause serious damage. The electrode potential and local composition of the electrolyte, especially the pH, determine whether or not a passive film can be formed again. In figure 2.2 a hypothetical situation is

shown of a steel in an electrolyte solution. The steel is covered for the larger part with a passive film. When the passive film is lacking at a certain spot, like C in figure 2.2, the potential drop across the passive layer and phase boundaries (A-B, potential profile I) must be compensated for because no considerable potential differences can exist between A and C and between B and E. A high anodic current at D results from potential profile II. The oxidation causes a new oxide film to be formed, which again protects the metal against further attack.

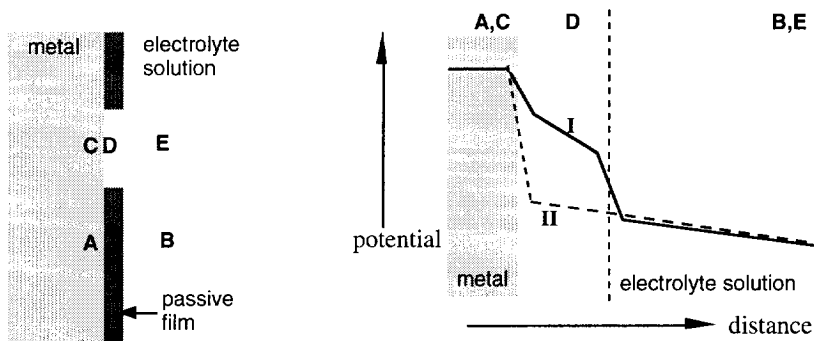


Figure 2.2. Schematic representation of a locally active metal and potential profiles. Negligible potential differences between A and C and between B and E.

If there is a barrier between C and E which provides the potential drop, an oxide film can not be formed and the surface will remain active. A barrier can consist of a physical crevice, causing a high ohmic resistance, or a salt film.

If the local electrolyte, at D, is such that an oxide film is not stable, for example a low pH, then the surface will also remain active. Another impediment to the formation of an oxide film is the presence of another adsorbed layer on the surface. Especially sulphide layers which can be formed under some conditions, have been mentioned in this respect.

It has been suggested that dissolution products from manganese sulphide inclusions, like sulphur, sulphides and thiosulphate, play an important role in the transition from pit initiation to propagation. This is not surprising as these compounds are known to aggravate localized corrosion when present in the environment. In this section several theories will be surveyed. First, attention is given to the effects of anions on pitting. Then the theories on

the role of dissolution products from sulphide inclusions and, finally, some general theories on propagation of localized corrosion are discussed.

### **2.3.2 The influence of anions**

Before the influence of anions on the stabilization of pit growth is discussed, a short introduction on halide ions has to be given. Halide ions are required to initiate pitting (and crevice) corrosion of stainless steel, although there have been some reports of initiation in thiosulphate solutions without halide ions<sup>18,19</sup>. Chloride is the most important and frequently studied anion. Szklarska-Smialowska<sup>20</sup> reviewed the numerous theories on the role of chloride. She concluded that "there are three primary reasons for the specific effect of chloride ions: (1) the ability to form complexes with cations and hydroxides; (2) the ability to increase the activity of hydrogen ions in the pit electrolyte; and (3) the ability to form a salt layer on the pit bottom at low pH". Oxide film formation is thus prevented. The initiation has been described by her as follows. At sites of imperfections in the metal surface, the passage of ions through the oxide film is rendered more facile, the adsorption of chloride is more pronounced at these sites and an aggressive environment due to hydrolysis is formed. The locally acidic solution first attacks the oxide film and then the metal itself.

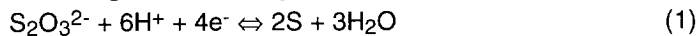
The presence of other anions in addition to chloride alters the pitting susceptibility. Most anions are known to inhibit pitting, but some, especially sulphur compounds, are known to enhance pitting attack. In literature, these effects are not explained explicitly in terms of possible influence on the attack of inclusions. The inhibiting effect is mostly explained by the competitive effect of the anions with chloride at the surface or during migration to the anodic site. In the former view, the chloride concentration at the surface is reduced to below a critical level needed to break down the passive film. For example, the inhibiting effect of sulphate<sup>21</sup>, perchlorate<sup>21</sup> and chromate<sup>22,23</sup> has been explained by such competitive adsorption. In the latter view, the accumulation of chloride anions at the anode is decreased, restricting local acidification. Garner<sup>24</sup>

used this view to explain the inhibiting effect of sulphate in chloride solutions on pitting corrosion of stainless steel.

It is well-known that thiosulphate ( $S_2O_3^{2-}$ ) in (very) low concentrations enhances pitting and crevice corrosion<sup>18,24,25</sup>. Sulphide<sup>26,27</sup> ( $S^{2-}$ ), tetrathionate<sup>27</sup> ( $S_4O_6^{2-}$ ) and thiocyanate<sup>27</sup> ( $SCN^-$ ) also enhance pitting. But bisulphite<sup>18,24</sup> ( $HSO_3^-$ ), sulphate<sup>24,28-30</sup> and also high concentrations of thiosulphate<sup>24,27</sup> increase the resistance to pitting. The effect of thiosulphate has been investigated most frequently, because of its aggressive behaviour often encountered in the paper industry, and because it is sometimes believed to be formed when manganese sulphide inclusions dissolve, whereupon thiosulphate would play an important role in hindering repassivation. The proposed mechanisms for the effect of thiosulphate will be surveyed next.

From stress corrosion cracking experiments, Horowitz<sup>31</sup> found evidence for adsorption of thiosulphate, and also tetrathionate, in various solutions. He measured increased anodic dissolution in the active-passive region of voltammetric scans, and attributed this to adsorption of the compounds which catalysed metal oxidation.

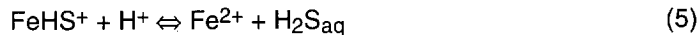
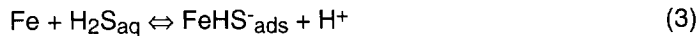
It has been suggested<sup>24</sup> that thiosulphate in crevices or pits is reduced at the metal surface to sulphur according to reaction 1:



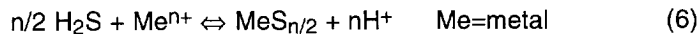
This reaction is possibly followed by a reduction of sulphur to (hydrogen) sulphide according to reaction 2<sup>25</sup>:



Hydrogen sulphide catalyses the metal dissolution<sup>20,25,26</sup>, for example as proposed in reactions 3 to 5:



A metal sulphide film can be formed<sup>25</sup> according to reaction 6:



The inhibiting effect of high concentrations of thiosulphate has been explained<sup>24</sup> with reactions 7 and 8:



Thiosulphate disproportionates in acid solutions to sulphur and bisulphite. Bisulphite buffers the solution and thus hinders pit growth. The inhibiting effect has also been explained with reaction 1: thiosulphate reduction increases the pH thereby hampering pit growth<sup>27</sup>.

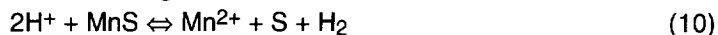
### 2.3.3 Dissolution products from manganese sulphide inclusions

A lot of research has been aimed at clarifying the dissolution process of manganese sulphide inclusions, because the reaction products could play a key role in preventing repassivation of the bare metal surface. One of the reasons to believe so is that sulphur is frequently found at (former) inclusion sites and in their vicinity after exposure of a steel to neutral or acidic sodium chloride solutions<sup>8,12,13,15,32</sup>.

It has often been suggested that thiosulphate results from anodic dissolution of manganese sulphide inclusions, according to reaction 9:



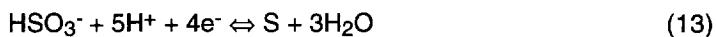
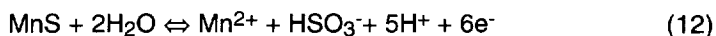
After a critical concentration of thiosulphate and chloride is reached, the metal adjoining the inclusion is activated<sup>12,33</sup>. Sulphur is released, after local acidification, by the acid dissolution of (the remainder of) the sulphide inclusion according to reaction 10:



Others have suggested that sulphur is directly formed by anodic oxidation of manganese sulphide<sup>9</sup>, according to reaction 11.



Sulphur might also result from reduction, outside the pit, of sulphite which was formed by oxidation of manganese sulphide<sup>13</sup> like in reactions 12 and 13:



Szklarska-Smialowska<sup>34</sup> suggested that hydrogen sulphide is released upon dissolution of manganese sulphide (and also iron and calcium sulphide) according to reaction 14:



Hydrogen sulphide, after adsorption, catalyses anodic dissolution of the metal like in reaction 3-5.

Recently Stewart<sup>10</sup> showed a correlation to exist between the manganese sulphide inclusion size and the lifetime of unstable pits. In his view a minimum pit size is necessary to supply enough sulphur to stabilize pit growth. For Ni- and Fe-based alloys it has been shown<sup>35-38</sup> that a sufficient surface coverage of sulphur accelerates anodic dissolution of the metal and can prevent repassivation. Molybdenum in stainless steel and nickel causes desorption of sulphur, probably by formation of molybdenum sulphide ( $\text{MoS}_2$ )<sup>35,39,40</sup>. This would account for the well-known beneficial effect of molybdenum on the pitting resistance.

Several investigators found corrosion products covering the small pit or crevice. A cap of an iron oxide on the crevice mouth and the sulphur contaminated area<sup>13</sup> and a cap of  $\text{Al}(\text{OH})_3$  on pits initiated at a complex oxide inclusion<sup>41</sup> have been reported. The covers enhance local acidification. Baker<sup>42</sup> proposed that pit growth is stabilized by the precipitation of  $\text{MnCl}_2$  on the exposed steel surface after dissolution of manganese sulphide inclusions. Size and geometry of the manganese sulphide inclusions determine the probability of salt film formation.

The number of proposed reactions to explain for the dissolution process of manganese sulphide inclusions indicates that either different mechanisms are possible (under slightly different conditions) or/and that these processes are very difficult to study.

#### **2.3.4 General stabilization theories**

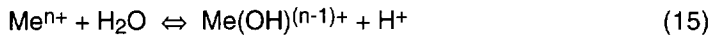
Theories of stabilizing mechanisms either emphasize the ohmic potential drops within pits (or crevices)<sup>43,44</sup> or emphasize the compositional changes of the electrolyte within pits (or crevices)<sup>45-53</sup>.

The necessity of a certain potential drop in order to stabilize localized corrosion is the essence of the theory developed by Pickering<sup>43,44</sup>. Localized corrosion is stabilized when the electrode potential in the cavity is less oxidizing than the Flade potential. To maintain an active surface, a potential drop in the pit or crevice is required. The potential drop can be provided by gas bubbles, crevices, corrosion products filling the cavity



and/or a remaining film of passivated metal covering most of the cavity. The theory has been supported by experiments on iron. It has not often been used by other investigators to explain results of experiments with stainless steels.

Many investigators defined some kind of critical situation which must be realized in order to stabilize pit growth in stainless steels. Galvele<sup>45,46</sup> considered localized acidification to be the main driving force. The acidification is caused by hydrolysis equilibria like:



which follow the anodic reaction



The concentrations in the pit solution are a function of the pit depth  $x$  and the current density  $i$  circulating through the pit. Pitting proceeds when a critical  $x \cdot i$  value is exceeded. Similarly, Sato<sup>47</sup> argued that the stability of growing pits is determined by the build-up of ions in the pit electrolyte. The critical concentration of the pit electrolyte is proportional to the product of pit dissolution current density  $i_{\text{pit}}$  and pit size  $r_{\text{pit}}$ . The critical (minimum)  $r_{\text{pit}}$  for stability is a function of  $i_{\text{pit}}$  and thus of the electrode potential. At relative anodic potentials the stability of pits is controlled by the concentration of aggressive anions (chloride). An anion contaminated oxide or salt film hinders repassivation. This situation results in hemispherical brightening pits. At relative cathodic potentials the stability of pits is ruled by the pH. This results in etching pits, characterized by crystallographically defined surface segments.

According to Beck<sup>48,49</sup>, a thin (nm) anhydrous halide salt layer precipitates within fractions of a second after pit nucleation and stabilizes pit growth. Pits can die upon convection of the solution or water permeation of the layer. Hemispherical brightening pits are formed at high applied potentials or after precipitation of an additional hydrous salt layer. Crystallographic pits are formed if only the anhydrous layer is present.

The dissolution rates of a metal in a solution of its dissolution products, simulating the situation in a pit, have been found to be influenced by the concentration of the dissolution products<sup>50-53</sup>. When the concentration of corrosion products falls below saturation, the dissolution rate increases, as is illustrated in figure 2.3. The concentration decrease is thus corrected. This behaviour accounts for stabilization of pit growth. Only at lower

concentrations the current falls rapidly if the concentration is reduced further, and pit repassivation becomes possible. Isaacs<sup>50,51</sup> further emphasizes the role of the passive oxide layer in reaching this state. The local concentration can increase because a pit is covered by the remaining passive oxide layer. This layer is undermined by the pitting process, and ruptures when the pit reaches a specific size, possibly enhanced by osmotic pressure. The properties of the film determine the moment of rupture and thus play a key role. Pits continue to grow only when the potential, and therefore the pitting current density, is sufficiently high to maintain the critical concentration without the cover film.

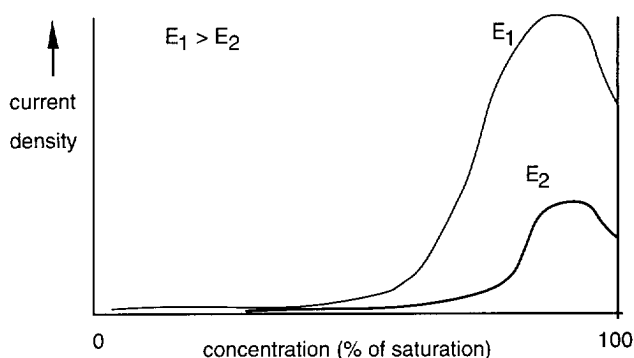


*Figure 2.3. The variation of the anodic current density as a function of the concentration of dissolved corrosion products near the surface (schematic).*

Frankel<sup>54</sup>, Pistorius<sup>55</sup> and Williams<sup>56</sup> adopted above mentioned theories to explain the transition from metastable pitting to stable pit growth. Metastable indicates that pit growth is only temporary. Metastable pitting is reflected by a current spike measured at a potential in the passive region of the stainless steel. When certain critical factors are exceeded, the pit does not repassivate and the metastable pit has become a stable pit. According to Frankel<sup>54</sup>, initial pit growth is controlled largely by the ohmic resistance of a porous cover over the pit. Metastable pits repassivate after rupture of the cover, but if the cover remains intact for a period long enough to allow for salt film precipitation on the pit surface, pit growth is stabilized. A strong passive layer acting as a cover will thus promote pitting, as opposed

to a weak or stressed layer. According to Pistorius<sup>55</sup>, for a pit to become stable, the product of the pit radius and its dissolution current density must reach a critical value: the pit stability product. Before this product is reached, the metastable pit needs a perforated cover to hinder diffusion. The growth rate of pits is controlled by diffusion of the metal cations. Williams<sup>56</sup> proposes similar mechanisms. A critical concentration of dissolved metal salts, expressed as a percentage of the saturation value, must be exceeded. Until then, a micropit can grow only in an occluded zone. The value of the exchange current density must be sufficiently large to obtain stability. Thiosulphate, or sulphur (compounds) formed when sulphide inclusions dissolve, enhances the dissolution rate and thus increases the chance for a metastable pit to become stable. Molybdenum decreases the current density and thus decreases this chance.

## 2.4 References

- 1 A.J. Sedriks, in *Advances in Localized Corrosion (NACE-9)*, ed. H.S. Isaacs, U. Bertocci, J. Kruger and S. Smialowska, NACE, Houston, USA (1990) 253-262.
- 2 J.W. Oldfield, *Corrosion* **46** (1990) 574-581.
- 3 G. Riedel, C. Voigt, H. Werner, M. Günzel and K.-P. Erkel, *Werkst. Korros.* **37** (1986) 519-525.
- 4 K.-J. Blom, *CORROSION/82*, Paper 87, NACE, Houston, USA (1982).
- 5 G. Hultquist, S. Zakipour and C. Leygraf, in *Passivity of Metals and Semiconductors*, ed. M. Froment, Elsevier Science Publishers B.V., Amsterdam, The Netherlands (1983) 399-404.
- 6 M.A. Barbosa, *Corros. Sci.* **23** (1983) 1293-1305.
- 7 M.A. Barbosa, A. Garrido, A. Campilho and I. Sutherland, *Corros. Sci.* **32** (1991) 179-184.
- 8 G.S. Eklund, *J. Electrochem. Soc.* **121** (1974) 467-473.
- 9 G. Wranglén, *Corros. Sci.* **14** (1974) 331-349.
- 10 J. Stewart and D.E. Williams, *Corros. Sci.* **33** (1992) 457-474.
- 11 G. Daufin, J. Pagetti, J.P. Labbe and F. Michel, *Corrosion* **41** (1985) 533-539.
- 12 R. Ke and R. Alkire, *J. Electrochem. Soc.* **139** (1992) 1573-1580.
- 13 J.E. Castle and R. Ke, *Corros. Sci.* **30** (1990) 409-428.
- 14 S.C. Srivastava and M.B. Ives, *Corrosion* **45** (1989) 488-493.

- 15 M.B. Ives and S.C. Srivastava, in *Advances in Localized Corrosion (NACE-9)*, ed. H.S. Isaacs, U. Bertocci, J. Kruger and S. Smialowska, NACE, Houston, USA (1990) 295-302.
- 16 R.D. Knutsen and A. Ball, *Corrosion* **47** (1991) 359-368.
- 17 V. Scotto, G. Ventura and E. Traverso, *Corros. Sci.* **19** (1979) 237-250.
- 18 R.C. Newman, W.P. Wong, H. Ezuber and A. Garner, *Corrosion* **45** (1989) 282-287.
- 19 A. Garner, *Corrosion* **41** (1985) 587-591.
- 20 Z. Szklarska-Smialowska, *Pitting Corrosion of Metals*, NACE, Houston, USA (1986).
- 21 H.C. Brookes and F.J. Graham, *Corrosion* **45** (1989) 287-293.
- 22 C. Lemaitre, B. Baroux and G. Beranger, *Werkst. Korros.* **40** (1989) 229-236.
- 23 E. McCafferty, *J. Electrochem. Soc.* **137** (1990) 3731-3737.
- 24 A. Garner and R.C. Newman, *CORROSION/91*, paper 186, NACE, Houston, USA (1991).
- 25 D. Tromans and L. Frederick, *Corrosion* **40** (1984) 633-639.
- 26 P. Süry, *Corros. Sci.* **16** (1976) 879-901.
- 27 R.C. Newman, H.S. Isaacs and B. Alman, *Corrosion* **38** (1982) 261-265.
- 28 M. Barbosa and J.C. Scully, *Corros. Sci.* **22** (1982) 1025-1036.
- 29 H. Ezuber, A.J. Betts and R.C. Newman, *Materials Science Forum* **44&45** (1989) 247-258.
- 30 P.C. Pistorius and G.T. Burstein, *Corros. Sci.* **33** (1992) 1885-1897.
- 31 H.H. Horowitz, *J. Electrochem. Soc.* **132** (1985) 2064-2071.
- 32 A.R.J. Kucernak, R. Peat and D.E. Williams, *J. Electrochem. Soc.* **139** (1992) 2337-2340.
- 33 S.E. Lott and R.C. Alkire, *J. Electrochem. Soc.* **136** (1989) 973-979.
- 34 Z. Szklarska-Smialowska and E. Lunarska, *Werkst. Korros.* **32** (1991) 478-485.
- 35 A. Elbiache and P. Marcus, *Corros. Sci.* **33** (1992) 261-269.
- 36 J. Oudar, *Br. Corros. J.* **25** (1990) 21-29.
- 37 P. Marcus, A. Teissier and J. Oudar, *Corros. Sci.* **24** (1984) 259-268.
- 38 P. Marcus and H. Talah, *Corros. Sci.* **29** (1989) 455-463.
- 39 P. Marcus and M. Moscatelli, *J. Electrochem. Soc.* **136** (1989) 1634-1637.
- 40 P. Marcus, *J. Chim. Phys.* **88** (1991) 1697-1711.
- 41 M.A. Baker and J.E. Castle, *Corros. Sci.* **33** (1992) 1295-1312.
- 42 M.A. Baker and J.E. Castle, *Corros. Sci.* **34** (1993) 667-682.
- 43 H.W. Pickering, *Corrosion* **42** (1986) 125-140.

- 44 H.W. Pickering, *Corros. Sci.* **29** (1989) 325-341.
- 45 J.R. Galvele, *J. Electrochem. Soc.* **123** (1976) 464-474.
- 46 J.R. Galvele, in *Critical Factors in Localized Corrosion*, ed. G.S. Frankel and R.C. Newman, The Electrochemical Society, Inc., Pennington, USA (1992) 94-108.
- 47 N. Sato, *J. Electrochem. Soc.* **129** (1982) 260-264.
- 48 T.R. Beck and R.C. Alkire, *J. Electrochem. Soc.* **126** (1979) 1662-1666.
- 49 T.R. Beck, in *Advances in Localized Corrosion (NACE-9)*, ed. H.S. Isaacs, U. Bertocci, J. Kruger and S. Smialowska, NACE, Houston, USA (1990) 85-91.
- 50 H.S. Isaacs and G. Kissel, *J. Electrochem. Soc.* **119** (1972) 1628-1632.
- 51 H.S. Isaacs, *Corros. Sci.* **29** (1989) 313-323.
- 52 T. Hakkarainen, in *Advances in Localized Corrosion (NACE-9)*, ed. H.S. Isaacs, U. Bertocci, J. Kruger and S. Smialowska, NACE, Houston, USA (1990) 277-282.
- 53 T. Hakkarainen, in *Corrosion Chemistry within Pits, Crevices and Cracks*, Ed. A. Turnbull, HMSO, London, UK (1987), 17-26.
- 54 G.S. Frankel, L. Stockert, F. Hunkeler and H. Böhni, *Corrosion* **43** (1987) 429-436.
- 55 P.C. Pistorius and G.T. Burstein, *Phil. Trans. R. Soc. Lond. A* **341** (1992) 531-559.
- 56 D.E. Williams, J. Stewart and P.H. Balkwill, in *Critical Factors in Localized Corrosion*, ed. G.S. Frankel and R.C. Newman, The Electrochemical Society, Inc., Pennington, USA (1992) 36-64.

# THE MEANING OF CURRENT SPIKES

## 3.1 Introduction

Investigations on pitting corrosion of stainless steels are mostly performed by application of electrochemical techniques. Quantities such as the pitting (pit nucleation) potential, the repassivation (protection) potential, the repassivation time, the induction time or the critical pitting temperature can be determined<sup>1</sup>, for example for comparative studies. The most popular of these quantities is the pitting potential,  $E_p$  or  $E_{np}$ , which can be defined as the potential above which pits nucleate and develop<sup>1</sup>. However, the value of the pitting potential depends on the method of determination and the experimental circumstances like the scan rate, solution agitation, the composition of the electrolyte solution and the surface condition of the metal. But even pitting potentials measured under similar conditions on stainless steels cover a certain potential region. The determination and the usefulness of 'the' pitting potential are still being discussed in literature<sup>2-6</sup>.

In order to gain more insight in pitting corrosion mechanisms, the separate processes involved in pitting can be studied adequately by electrochemical methods such as measuring current or potential noise, *current spikes* or *impedance characteristics* and also by surface analytical techniques. To study pitting of commercial, non homogeneous, stainless steels, potentiostatic measurements of current spikes occurring in the passive region can be appropriate. A number of studies on these spikes (also termed current fluctuations, noise, pulses, transients, events, peaks or transient spikes) has recently been published<sup>7-17</sup>. The current of the

measured spikes varies from microamperes down to picoamperes. The larger of these (nano- to microamperes) are associated with film breakdown or pit initiation at inclusions, temporary pit growth and repassivation. The shape of the spikes is characterized by a gradual increase of the current followed by an abrupt fall down to the level of the passive current. This phenomenon is now commonly called metastable pitting, as opposed to stable pitting which is characterized by an on-going increase of the current. The smaller (picoampere regime) events are measured on microelectrodes<sup>14,16</sup>. The shape of these spikes is the mirror image of the larger spikes: a fast increase followed by a slow decrease of the current. The origin of these spikes is not clear.

This chapter deals with studies on pitting corrosion of stainless steels AISI 304 and 316\*. Current-potential curves are compared with current spikes (nanoampere regime) measurements. Current spikes are related to macroscopic pitting events on the one hand, and manganese sulphide inclusions on the other hand. Furthermore, the influence of various electrolyte solutions is studied. The investigations enable a more detailed description of pit initiation.

## 3.2 Experimental

### *Materials*

The composition of the commercial stainless steels that were studied is given in table 3.1.

	Cr	Ni	Mo	C	Si	P	Mn	S
ss 304	17.5	8.8	0.26	0.070	0.60	0.340	1.65	0.024
ss 316	17.1	10.6	2.53	0.033	0.63	0.029	1.41	0.025

*Table 3.1 Composition of the investigated steels (wt.%), balance of iron.*

---

\* Henceforth these steels will be denoted as ss (Stainless Steel) 304 and ss 316.

### *Test cell*

All experiments were performed in Avesta cells<sup>18</sup> in order to avoid crevice corrosion during the measurements. A schematic picture is given in figure 3.1. The cell was used with some minor modifications. The bottom plate was constructed from glass reinforced teflon which enabled better machining to obtain a smooth surface at the sample mounting site. For special experiments with a video camera focussed on the sample surface, the top of the cell and the inner cell wall were removed and the outer cell wall was replaced with a cylinder of 3 cm height. Water was supplied to the cell with a peristaltic pump (Gilson Minipuls 3). The cell enabled testing of plate-like samples (3 cm x 3 cm) with an exposed area of 0.78 cm<sup>2</sup>.

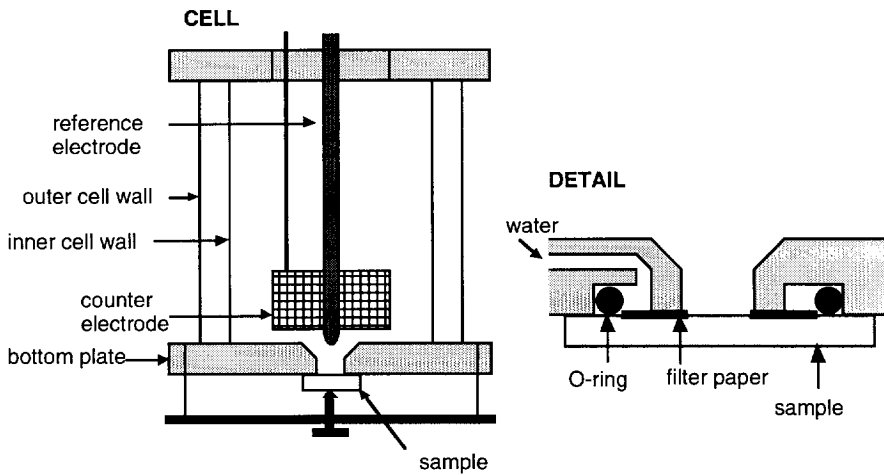


*Figure 3.1. The Avesta cell.*

### *Current-potential curves*

An ECO PGSTAT20 and an ECO Autolab with a personal computer (Olivetti M250) were used for measuring current-potential curves. The curves were measured in aerated 0.1 M NaCl at ambient temperature with a scan rate of 1 mV/s from the open circuit potential (OCP) in anodic direction. Samples were ground with silicon carbide paper to P1200 grit surface finish.



### *Camera observations*

A video camera (Canon Canovision EX Hi8, Canon EOS 100 mm macrolens, Canon Life-Size converter ES) was placed above the modified Avesta cell. Perpendicular incident illumination of the sample, polished with 3  $\mu\text{m}$  diamond paste, was adequate. A magnification of 60 times and a lateral resolution of about 20  $\mu\text{m}$  were obtained. For the potential control the same equipment was used as for recording the current-potential curves.

### *Current spikes*

The experimental set-up for the for the measurement of current spikes is sketched in figure 3.2. A photograph has been added to the sketch. A battery-operated potentiostat (Jaissle 1002T-NC) was used for the potential control. An isolation amplifier with a clock, designed by the Electronic Service Department, Delft University of Technology, connected the potentiostat to a personal computer (HP Vectra 286/12 with an analog/digital converter board Metrabyte DAS16). The clock enabled sampling with the exact frequency of the mains electricity supply, which reduced 50 Hz noise in the measured signal. The cell was placed inside a Faraday cage for further reduction of noise. Computer programs for the data acquisition and analysis were written in Asyst (Asyst Software Technologies). More details on the programs can be found in appendix B. The detection limit for spikes depended on the settings of the potentiostat and could be as low as 5 nA.

Current spikes were measured during anodic polarization at various potentials for 205 minutes at ambient temperature in aerated 0.1 M NaCl solution, unless stated otherwise. Polarization was started a few minutes after addition of the electrolyte solution. The number of spikes was determined from the current measurement between 10 minutes and 205 minutes after polarization. All the samples were ground to grit P1200 at least one day before the measurement.

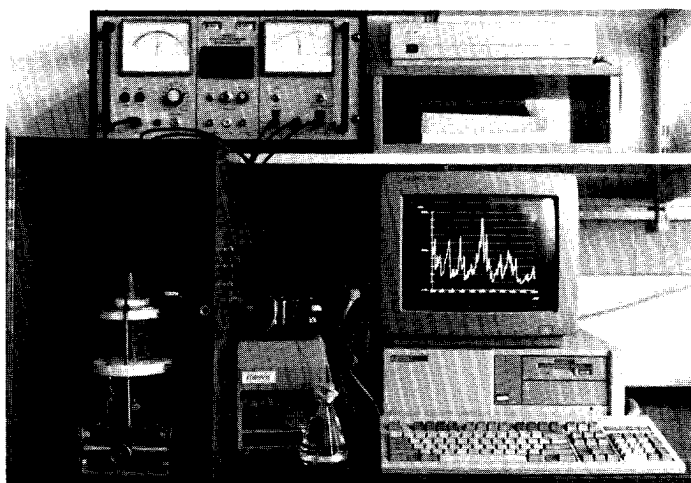
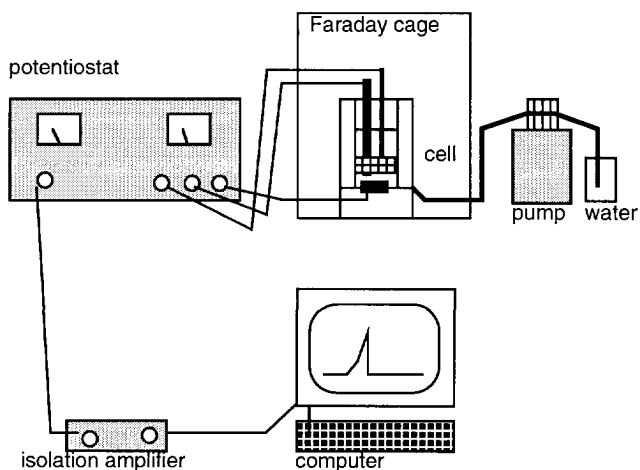


*Figure 3.2. The experimental set-up for the current spikes measurements, sketch and photograph.*

### *Surface analyses*

*Electron Probe Micro Analysis / Scanning Electron Microscopy (EPMA/SEM).* A Jeol JXA 733 electronprobe X-ray microanalyser equipped with four wave-length dispersive spectrometers and an energy

dispersive spectrometer, fully automated with Tracor Northern TN5500 and TN5600 systems, was used to determine the size and composition of the inclusions in the stainless steel specimens. The analyses were performed with a 12 keV, 2 nA electron beam. An inverse backscattered electron signal was used to recognize the inclusions. A total area of 1 mm<sup>2</sup> of each specimen, polished down to 1 µm diamond paste and ultrasonically cleaned in 2-propanol, was analysed with a magnification of 2000x. The following elements were considered: Mg, Al, Si, S, P, Cl, Ca, Ti, Cr, Mn, Fe, Ni, Cu and Na.

*Scanning Auger Microscopy (SAM)*. Additional composition analyses of inclusions were performed with a PHI 4300 scanning Auger microprobe (Perkin-Elmer), using a 10 keV, 20 or 40 nA electron beam. Specimen were prepared as described above. Prior to the analyses, surfaces were cleaned by sputtering with a 3.5 keV Ar<sup>+</sup> scanning beam during 10 minutes. Sulphide inclusions were found by acquiring a sulphur Auger map.

### **3.3 Results and discussion**

#### **3.3.1 Current-potential curves and current spikes**

The current-potential curves of ss 304 and 316 were measured and are shown as figure 3.3 and 3.4. None of the curves showed an active-passive transition, except the curves of freshly ground ss 304 surfaces. The typical current rise attributed to pitting corrosion starts at about 300 mV/SCE for ss 304. The curves are jagged due to current fluctuations. These fluctuations however are only significant after the active-passive transition, as can be seen in the detail of the current-potential curve, figure 3.3b. The curves of ss 316, see figure 3.4, show large current fluctuations.

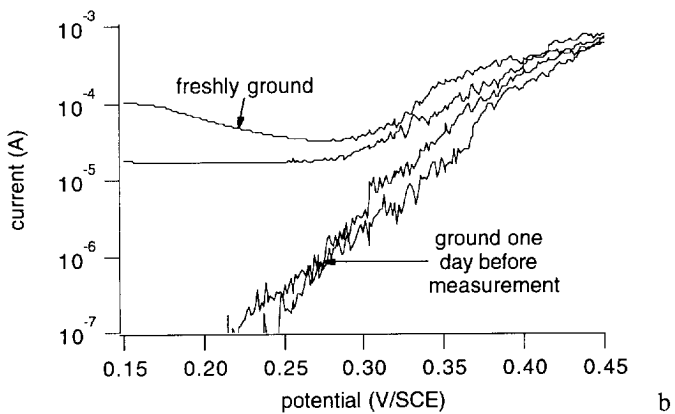
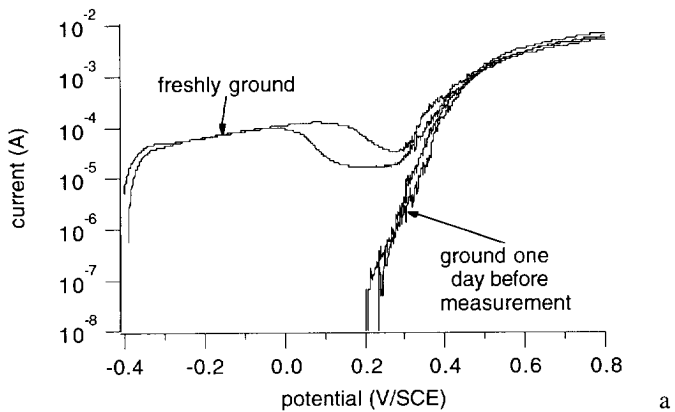


Figure 3.3. (a) Current-potential curves of ss 304; (b) detail of the curves.

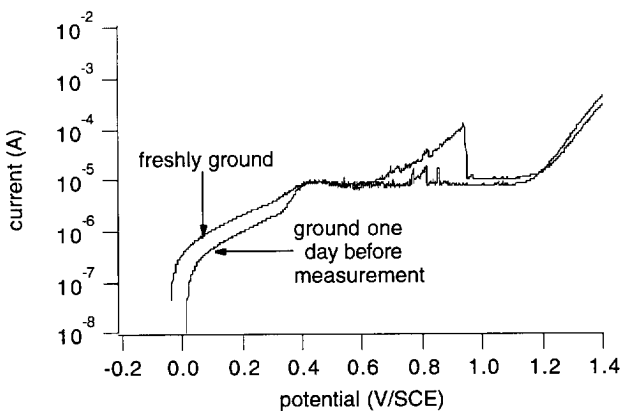


Figure 3.4. Current-potential curves of ss 316.

The current fluctuations visible in the passive regions of the current-potential curves were studied in more detail in potentiostatic experiments. The fluctuations then appear as spikes and will be named accordingly. Current spikes were measured on ss 304 and 316 at various potentials. Typical current-time curves for ss 316 at two potentials are shown in figure 3.5. Some examples of spikes are given in figure 3.6 and 3.7. A spike is characterized by a relatively slow, gradual increase of the current, often followed by a short peak, after which the current always falls back fast to the level of the passive current. The features of every spike were determined as is indicated in figure 3.8. The results of duplicate measurements on ss 304 and 316 at various potentials are summarized in table 3.2. Data on the charge related to each of the spikes, for ss 304 measured at three potentials, were used to construct figure 3.9. The cumulative number of spikes related with less than a certain amount of charge is plotted as a function of that charge. The frequency of spikes always decreased during a measurement, as is illustrated in figure 3.10. In figure 3.11 the current spikes of ss 304 and ss 316 measured at the same potential, 250 mV/SCE, are compared.

Light microscopy examinations could not reveal any differences between surfaces before and after the measurement of current spikes.

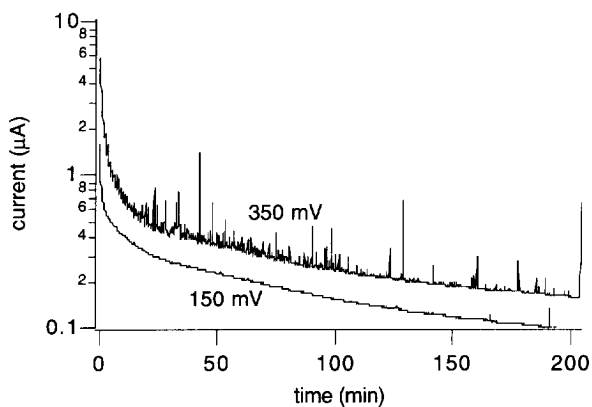


Figure 3.5. Typical current-time curves for ss 316 at 150 and 350 mV/SCE in 0.1M NaCl.

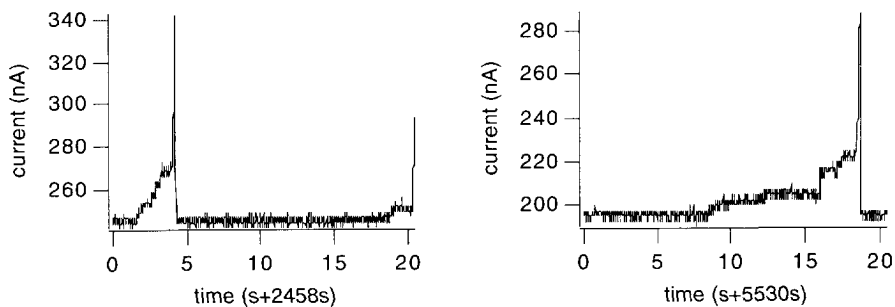


Figure 3.6. Examples of current spikes,  $ss$  304, 250 mV/SCE.

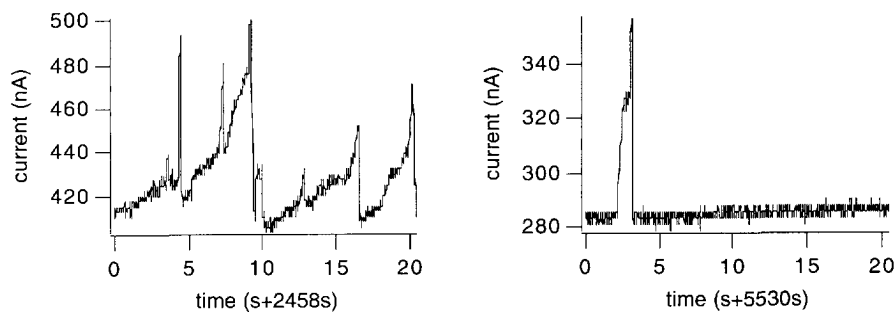


Figure 3.7. Examples of current spikes,  $ss$  316, 350 mV/SCE.

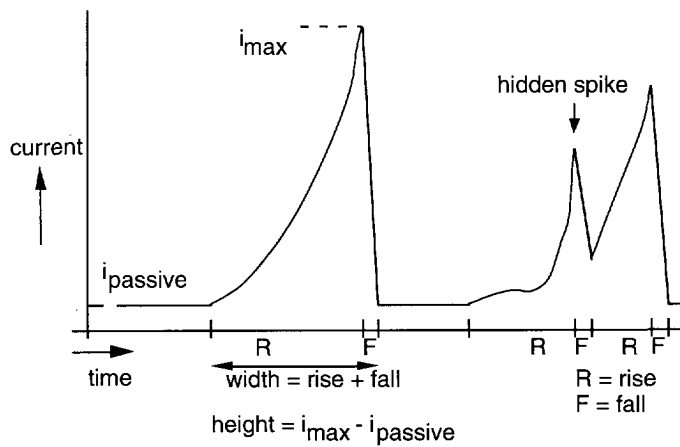


Figure 3.8. Scheme for spike characterization.

	pot. mV/ SCE	number incl.	width (s)	rise (s)	fall (s)	height (nA)	number excl.	width (s)	height (s)
304	50	170	2.4	1.9	0.43	39	170	2.4	39
		57	3.0	2.7	0.33	53	57	3.0	53
	150	502	1.5	1.4	0.18	75	490	1.6	73
		774	1.6	1.4	0.19	76	738	1.7	74
	250	3089	1.2	1.0	0.11	230	1771	2.0	202
		3204	1.2	1.1	0.11	208	2037	1.9	193
316	150	10	3.8	3.6	0.22	50	10	3.8	50
		43	3.9	3.7	0.20	42	42	4.0	41
	250	492	1.9	1.6	0.29	59	489	1.9	58
		342	3.6	3.3	0.31	169	335	3.7	139
	350	1785	1.4	1.2	0.24	103	1510	1.7	94
		1658	2.1	1.8	0.33	288	1351	2.6	173

*Table 3.2. Number of current spikes inclusive or exclusive hidden spikes and the average of the width, rise, fall and height of the spikes, ss 304 (50, 150, 250 mV/SCE) and ss 316 (150, 250, 350 mV/SCE), measurements in duplicate.*

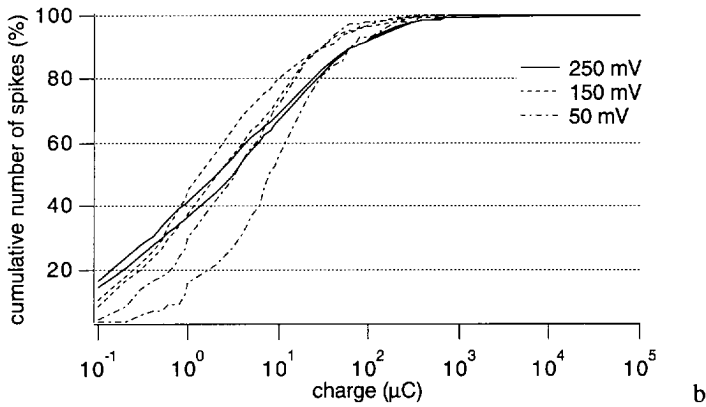
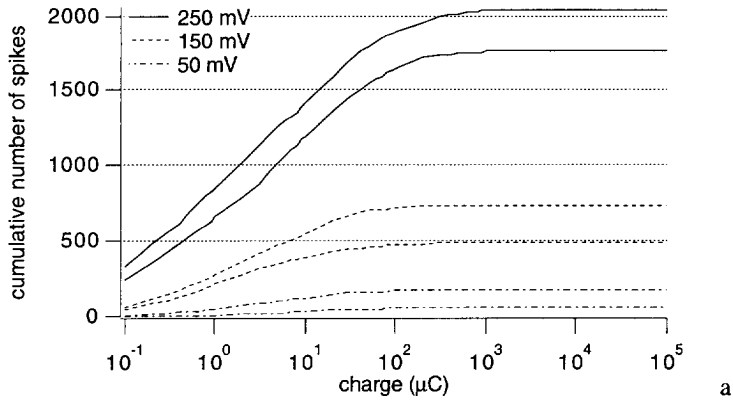


Figure 3.9. Cumulative number of spikes as a function of the charge for ss 304 measured at 50, 150 and 250 mV/SCE.

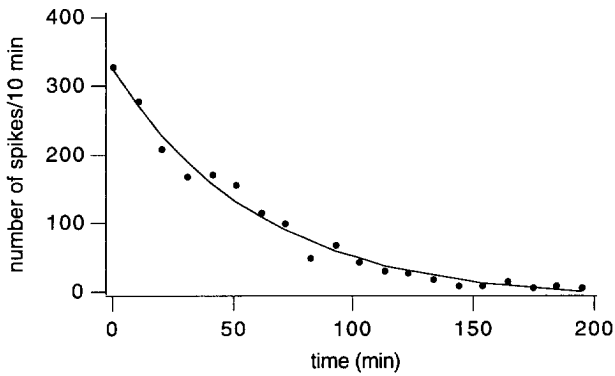


Figure 3.10. Frequency of spikes, ss 316, 350 mV/SCE.



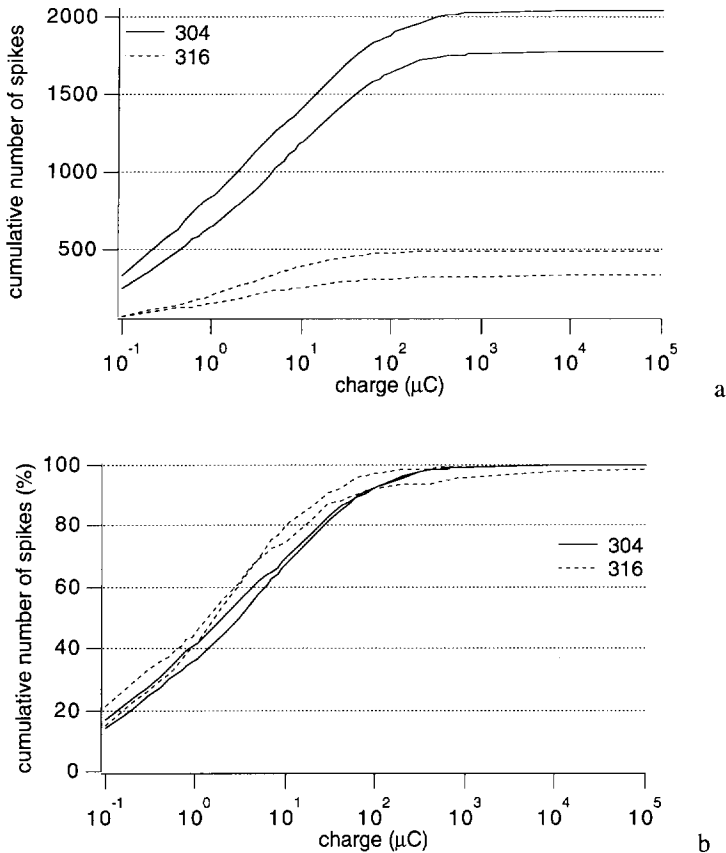


Figure 3.11. Comparison of current spikes of ss 304 and 316 measured at 250 mV/SCE.

Although there is a certain amount of scatter in the number of spikes determined in duplicate experiments, it is clear that the number of spikes is a function of the potential (table 3.2, figure 3.5 and 3.9a). More spikes are measured as the polarization potential is increased (as long as there is no stable pitting, i.e. an on-going increase of the current). Apparently, more sites are activated at higher potentials. The shape of the spikes is also affected by the potential; especially the average height increases as the potential increases (table 3.2). This is comparable to a step measurement

when an active surface is polarized to an anodic potential in the passive region; the higher this potential the higher the initial current. The amount of charge involved in one event is however hardly affected by the potential, see figure 3.9b.

The number of spikes is related to the type of steel. Stainless steel 304 shows more spikes at the same potential than ss 316, but the size of the spikes does not differ much when measurements performed at the same potential are compared, see figure 3.11. In one of the two measurements on ss 316 some very large spikes occur. This phenomenon was also observed in the current-potential curves. Large current fluctuations which appeared at random gave the curves the jagged appearance.

It has been suggested in literature that the current spikes are related to manganese sulphide inclusions in the stainless steels. This can partly explain the results shown above. Each spike would represent the phenomena related to the dissolution of a manganese sulphide inclusion. However, the number of sulphide inclusions in a stainless steel surface is reported<sup>19-21</sup> to be hundreds or even thousands per mm<sup>2</sup>. As the numbers of spikes mentioned in this section (up to a few thousand per measurement) are related to an exposed surface area of 78 mm<sup>2</sup>, obviously not all inclusions lying at the surface cause a spike. Moreover, because the frequency of spikes decreases, the passive film is believed to play a role in the process. From the current-potential curves of ss 304 it was already concluded that the state of the passive film is of importance in the development of significant current fluctuations i.e. current spikes. More information is needed on the inclusions in the steels in order to explain the differences between ss 304 and ss 316. Various aspects concerning the inclusions will be discussed in the following section.

### **3.3.2 Current spikes and manganese sulphide inclusions**

#### *Pickling*

A simple test to further investigate the relationship between current spikes and manganese sulphide inclusions, consists of measuring spikes after pickling the stainless steel. Pickling is known to remove manganese sulphide inclusions from the surface<sup>22-24</sup>. The surface of a ss 316 sample

was pickled by immersion in 20% HNO<sub>3</sub> / 5% HF for four minutes at ambient temperature before current spikes were measured. As was expected, this treatment markedly reduced the number of spikes, see figure 3.12 (to be compared with figure 3.5). During this measurement, 19 large spikes were counted with an average width of 8.8 s and an average height of 587 nA.

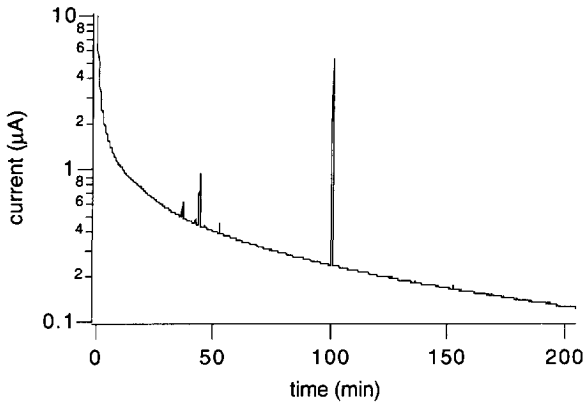


Figure 3.12. Current-time profile measured after pickling the surface, ss 316, 350 mV/SCE, 0.1 M NaCl.

#### Surface analyses

The relation between current spikes and inclusions was studied in more detail by examination of the surfaces with SEM and EPMA. The inclusions were counted and their size and composition were determined. After the characterization, the samples were shortly polished again with 1 µm diamond paste and exposed to 0.1 M NaCl for 205 minutes at 250 mV/SCE (ss 304) or 350 mV/SCE (ss 316). The current spikes were measured during the exposure. Afterwards the surfaces were analysed again. Some inclusions were analysed in more detail with SAM.

Three types of inclusions were distinguished (see table 3.3):

- discrete manganese sulphide inclusions;
- oxides of iron and/or chromium;
- inclusions with silicon, aluminium, calcium, titanium, manganese and/or sulphur.

The number of inclusions containing a certain element was determined, see table 3.4. Other elements than the ones mentioned were not found. The surface of the exposed ss 316 sample was analysed twice, E1 and E2 in table 3.3. In the first analysis (E1), a part of the surface that was badly attacked along a large inclusion was included. This caused a large number of particles to be recognized by the analysis program. The number of small iron/chromium particles was very sensitive to the settings of the equipment which had to be adjusted prior to each analysis. This (partly) accounts for the differences between the various measurements ('316', '316E1' and '316E2' in table 3.3). Moreover, irregularities in the surface could be misinterpreted by the analysis program as iron-chromium particles. These 'particles' will therefore be left out in further discussions.

	304	304E	316	316E1	316E2
MnS	729	13	587	94	0
FeCr	1066	1194	2127	2981	775
complex	533	439	543	1014	178

Table 3.3. Number of inclusions per mm<sup>2</sup> in the surfaces of ss 304 and 316 determined before and after exposure (E). The ss 316 sample was analysed twice after exposure (E1 and E2).

		304	304E	316	316E1
S		749	49	679	105
	A (μm <sup>2</sup> )	1.3	1.3	0.4	0.1
Mn		869	381	478	76
	A (μm <sup>2</sup> )	1.2	0.3	0.4	0.1
Si		168	219	226	336
	A (μm <sup>2</sup> )	0.2	0.4	1.5	0.9
Ca		1	2	226	287
	A (μm <sup>2</sup> )	3.0	0.7	1.7	1.0
Ti		0	1	466	636
	A (μm <sup>2</sup> )		1.2	0.7	0.4
Al		1	7	17	18
	A (μm <sup>2</sup> )	0.5	2.9	10	9

Table 3.4. Number of inclusions per mm<sup>2</sup> with S, Mn, Si, Ca, Ti and Al and their average size (A), determined before and after exposure (E).

	potential mV /SCE	number excl. hidden /78mm <sup>2</sup>	average width (s)	average height (s)	number /mm <sup>2</sup>
ss 304	250	985	2.6	181	12.6
ss 316	350	702	1.8	101	9.0

Table 3.5. Current spikes measured on polished surfaces (1  $\mu\text{m}$  diamond paste) between the surface analyses of ss 304 and ss 316.

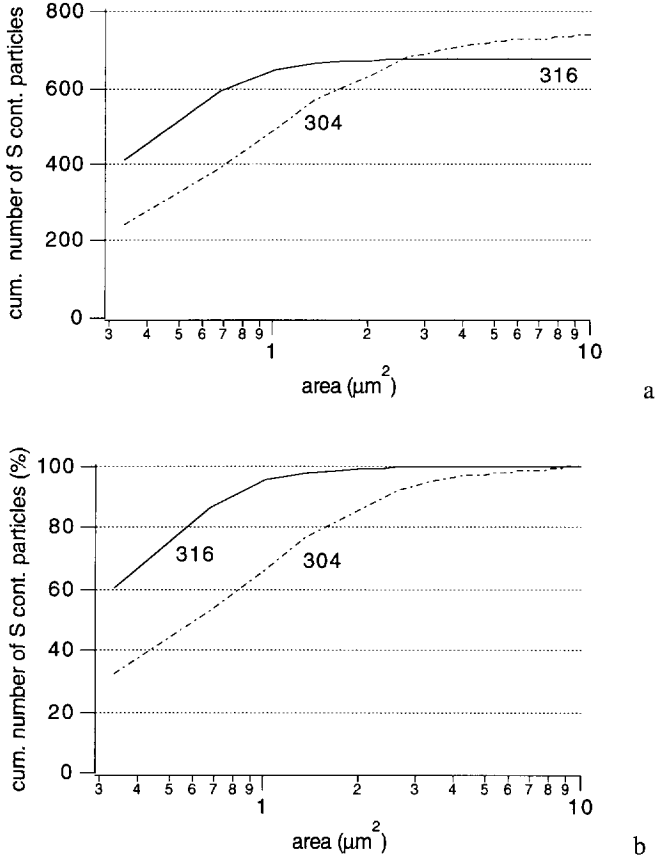


Figure 3.13. Area of the cross-sections of sulphur containing inclusions in ss 304 and ss 316, data from surface analyses.

The sulphur in the studied alloys was found mainly in separate manganese sulphide inclusions: 729 out of 749 and 587 out of 679 particles for ss 304 and 316 respectively, see table 3.3 and 3.4. The number of manganese sulphide particles was drastically reduced after the exposure. However, the number of current spikes measured, 9-13/mm<sup>2</sup>, table 3.5, was much lower than the number of inclusions that dissolved, 500-700/mm<sup>2</sup>. So dissolution of most of the sulphide inclusions lying at the surface did not result in a (measurable) spike.

Whether or not the dissolution of an inclusion leads to a spike could possibly be determined by:

1. the size of the inclusion;
2. the geometry.

The distribution of the size of the inclusions could give further clues. From surface analyses data on the size of the sulphur containing particles in ss 304 and 316, figure 3.13 was constructed. The cumulative number of particles with an area smaller than a certain size is plotted as a function of that area. In the analysis of the ss 304 surface, 25 sulphur-containing particles with a surface area larger than 10 μm<sup>2</sup> were found. These are not included in figure 3.13. It shows (figure 3.13a) that the numbers of sulphur containing particles for both steels do not differ very much, but the particles in ss 304 are considerably larger than the ones found in the ss 316 surface (figure 3.13b).

Histograms constructed from the same data as used for figure 3.13 are shown in figure 3.14. They indicate again that small inclusions outnumber the larger inclusions. The actual distribution of the size of inclusions is however somewhat obscured because the inclusions are sliced at random upon preparation of the surface. For the critical evaluation, a sphere is defined which is sliced a number of times. Slicing the sphere at a certain fraction of the radius results in a surface area of the cross-section that is calculated as  $\pi \cdot r^2 \cdot (1-x^2)$ , where  $x$  ( $0 < x < 1$ ) is the fraction of radius  $r$  determined from the centre of the sphere, see figure 3.15a. In figure 3.15b a histogram is shown that was constructed from the areas calculated from 256 cross-sections, divided in 30 groups for the histogram. Comparing this histogram with the experimental data of figure 3.14, it is clear that the small inclusions in the steel must by far outnumber the larger inclusions in order to obtain distributions like the ones shown in figure 3.14. Statements

on the inclusions will however always be qualitative, as the density as a function of the size is not known. Moreover, the inclusions are not spherical and each inclusion has a different geometry.

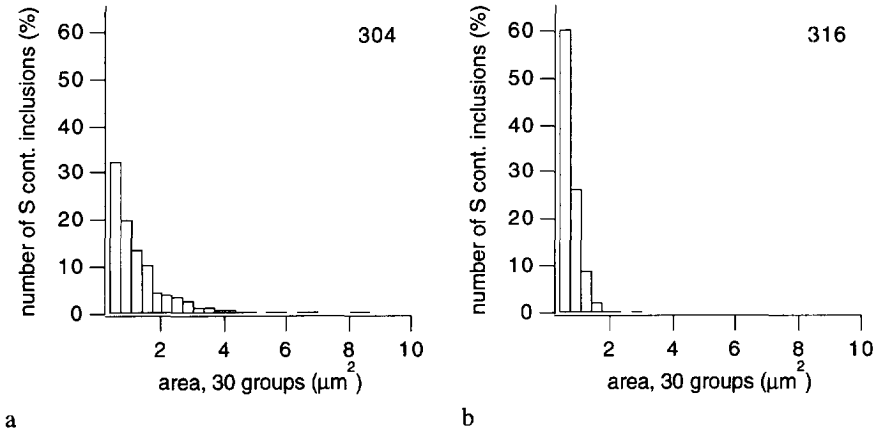


Figure 3.14. Area distributions for the manganese sulphide particles found in ss 304 and ss 316.

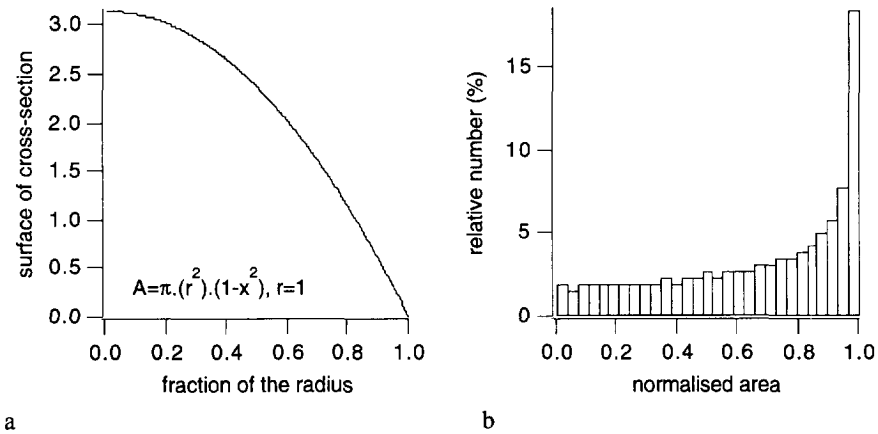
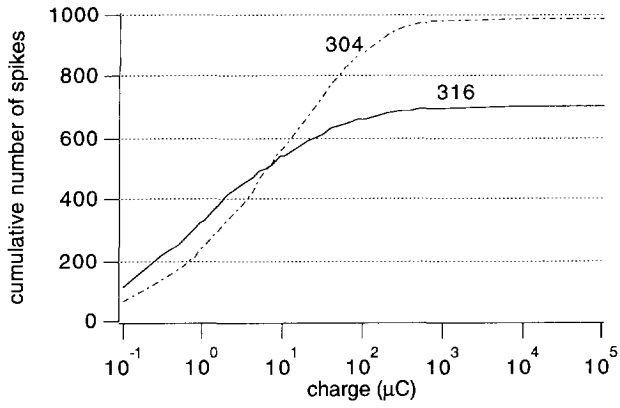


Figure 3.15. Illustration of the expected distribution of surface areas at random cross-sections of a sphere.

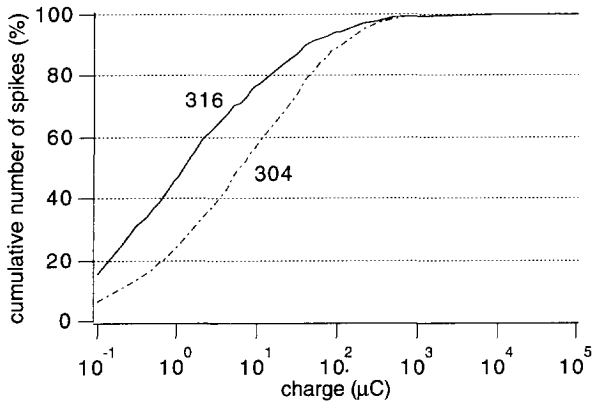
The charge associated with a spike can in principle originate from oxidation of manganese sulphide (e.g.  $\text{MnS} \rightarrow \text{Mn}^{2+} + \text{S} + 2\text{e}^-$ ) or from oxidation of the steel matrix. One coulomb would dissolve  $11 \cdot 10^7 \mu\text{m}^3$  MnS (molar mass 87, density  $3.99 \text{ g/cm}^3$ , 2 electrons/mole), or  $3 \cdot 10^7 \mu\text{m}^3$  stainless steel<sup>13,17</sup>. A large manganese sulphide inclusion, which would have a maximum surface area at cross-section of  $10 \mu\text{m}^2$  (compare figure 3.13), would need only  $0.21 \mu\text{C}$ . In figure 3.16 the cumulative number of spikes with a certain charge is plotted as a function of that charge. It shows that the charge accompanying the spikes is generally much higher than necessary to dissolve even very large inclusions. It must therefore be concluded that most of the charge of a spike originates from oxidation of the steel matrix. The charge calculated from the spikes can be hundreds of microcoulombs. It would be unlikely that all this is needed for repassivation only. The repassivation is therefore probably hindered for longer or shorter times.

In figure 3.17 an attacked site in ss 316 is shown. The long side of the (former) elliptical inclusion(s) in figure 3.17 probably did not lie exactly parallel to the surface, but somewhat penetrated in the metal. An occluded cell was realized because the passive layer was undermined, as can be seen from the presence of a cover over the right part of the attacked site. Other studies of inclusions with SAM and EPMA confirmed that the particles were usually elliptically shaped. This can be seen in figure 3.18, a sulphur map of the surface of ss 316, which shows that sulphur containing inclusions are present as stringers. Rolling of the steel in the production process causes this phenomenon.





a



b

Figure 3.16. Cumulative number of spikes as a function of the charge.

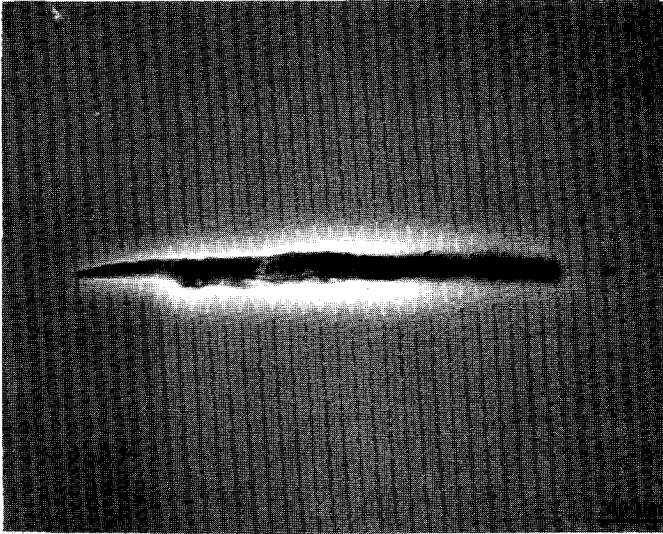


*Figure 3.17. Attacked spot at the surface of ss 316.*

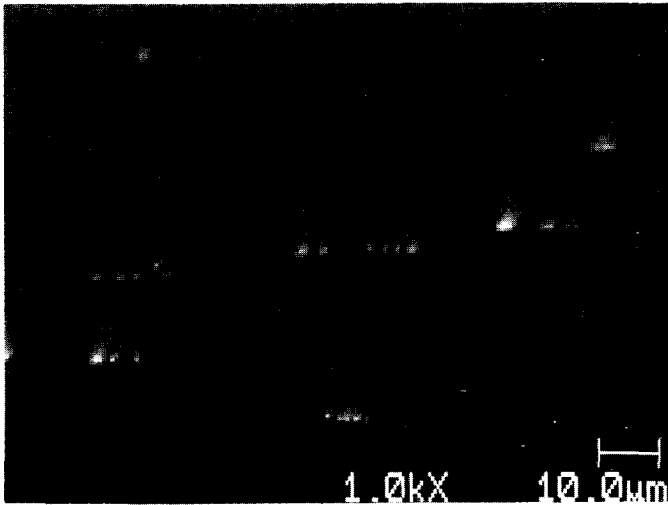


*Figure 3.18. Sulphur map taken from the surface of ss 316.*

### *Discussion*

The experiments have shown that only a fraction of the inclusions in a stainless steels surface generates spikes upon dissolution. Stainless steel 304 differs from ss 316 both in composition (molybdenum content) and in size of inclusions. As it was concluded that most of the charge originates from metal dissolution, the overall composition will certainly play an important role. However, it was demonstrated (figure 3.11) that at the same potential, the charge accompanying a spike does not differ very much comparing ss 304 and ss 316. It has been argued in literature<sup>19,20</sup>, see also chapter 2, that dissolution products from manganese sulphide inclusions, particularly thiosulphate or sulphur, would enhance the anodic dissolution of the steel. In such a process, adsorption of the dissolution compounds is important, and therefore the ratio of surface and volume. The larger a (spherical) particle, the more of a dissolution product can be adsorbed because the volume (determining the amount of product available for adsorption) increases proportional to  $r^3$  and the surface area to  $r^2$ . At a certain potential, a number of sites is activated, starting with the dissolution of an inclusion larger than a certain critical size. As the sulphide inclusions in ss 316 are smaller, less sites are activated at a certain potential. This effect could possibly be enhanced if the presence of molybdenum as an alloying element would require even larger sulphide inclusions for activation. If the suggestion that depletion of dissolution products from sulphide inclusions determines the lifetime of a spike is indeed valid, than, as larger inclusions are involved in the activation of ss 316 at similar potentials, the corresponding spikes are not expected to be smaller than the spikes for ss 304, in spite of the better repassivation ability of ss 316. This research could not reveal further details on the possible dissolution products.

After pickling of a sample, only a few spikes were measured, but these spikes were large (average width and height of 8.8 s and 587 nA, to be compared with for example 2.6 s and 173 nA for a not pickled surface, see table 3.2). The spikes appeared at random during the measurement. As pickling removed the inclusions lying at the surface, the spikes can be expected to have originated from inclusions which were initially covered by a passive layer and a thin metal layer. During exposure, the passive layer 'moves inwards' proportional to the passive current, due to the continues dissolution and formation (by oxidation) of the layer. At

inclusion sites the passive film formation can not be optimal and eventually the inclusion will get exposed to the solution and dissolve. The number of new inclusions to get exposed is difficult to calculate, as the number of particles as a function of the size is not known. Only a rough estimate can be made. For spherical particles of uniform diameter and present with a certain density, the number of new inclusions per hour can be calculated according to:

$$D \cdot (I_p \cdot k) \cdot 3600/d$$

where  $D$  is the number of inclusions determined in a cross-section ( $\text{cm}^2$ ),  $I_p$  is the passive current density ( $\text{C}/\text{cm}^2$ ),  $k = 3 \cdot 10^{-5} \text{ cm}^3/\text{C}$ , and  $d$  is the diameter (cm) of the inclusions. Thus with  $I_p = 0.4 \mu\text{A}/\text{cm}^2$  (figure 3.12),  $d = 0.4 \mu\text{m}$  and  $D = 587/\text{mm}^2$  (table 3.3 and 3.4), 63 particles come out each hour per  $\text{cm}^2$ . If only the larger inclusions are of importance, this number is an overestimate of the generation rate of new pit initiation sites ( $D$  is smaller and  $d$  is larger for larger inclusions). Considering the dimensions of the passive film (nanometer) and the size of inclusions (micrometer), an occluded cell is readily formed when a just exposed inclusion starts dissolving. When the passive film is able to keep the cell covered for a while, and the oxide layer formed by pickling<sup>23,24</sup> is expected to be able to do so, the situation can easily aggravate in the occluded cell. This accounts for the large spikes observed after pickling. Comparison of the current-time profiles of pickled (figure 3.12) and not pickled (figure 3.5) surfaces reveals furthermore that the inclusions lying at the surface of the latter are not instantaneously removed by exposure and polarization in salt solutions, because in that case the profiles would be similar. Apparently it takes some time for inclusions to start dissolving after exposure, even if they lie at the surface.

Substantial differences were found in numbers of spikes between ground (table 3.2) and polished (table 3.5) surfaces. Increasing surface roughness will increase the number of inclusions which lie at the surface because of the increase of surface area. Moreover, the extent to which sites are occluded will also increase because of the roughness. This means that inclusions of such a size that they would dissolve without prolonged dissolution of the surrounding steel on polished samples, can cause a spike on ground specimens because prolonged dissolution is enabled in occluded regions. This aspect will be further discussed in chapter 5.

The number of spikes also depends on the polarization potential. Increasing anodic potentials increase the numbers of spikes measured. At increasing potentials more sites are activated. While at a lower potential an inclusion would just dissolve and the surrounding metal would repassivate, at higher potentials the dissolution of the same inclusion is followed by prolonged attack. Neighbouring inclusions (in a stringer) might be reached before the spot repassivates, aggravating the localized attack, especially when dissolution products from manganese sulphide inclusions catalyse the metal dissolution.

The shape of the spikes can be explained in accordance with Pistorius<sup>17</sup>. He argued that the sharp current increases are caused by partial ruptures of the cover of the pit. The size of the perforation is increased or new holes are created with each rupture, allowing more rapid diffusion of cations from the pit interior and thus a larger current. After a major rupture of the cover, the pit anolyte can be diluted to such an extent that the pit repassivates. This causes the final sharp current increase prior to repassivation. In addition to this it can be argued that sharp current increases or 'hidden spikes' can be caused when a near sulphide particle in a stringer is reached and an opening is created from this inclusion to the bulk solution. This process can be illustrated with figure 3.19, representing a schematic drawing of a steel surface. Attack starting at particle B in this figure can proceed towards particle C. A breakthrough above this particle would accelerate the anodic dissolution processes.

Summarizing it can be concluded that spikes are only generated through dissolution of the larger inclusions at the surface and new inclusions which come out, followed by an attack of the surrounding steel matrix. These spots represent possible initiation sites for pitting. The chance that dissolution of an inclusion actually generates a spike is determined by factors which can cause prolonged local dissolution, such as the size and geometry of soluble inclusions, the properties of the passive layer, the roughness of the surface and the polarization potential.

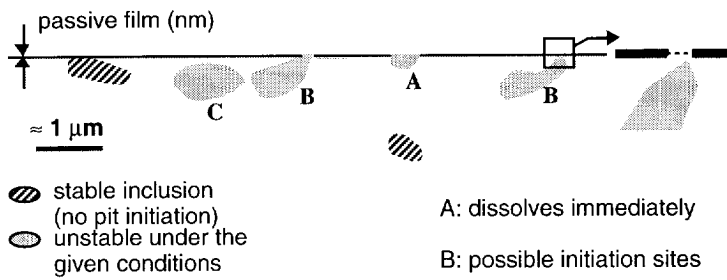


Figure 3.19. Schematic representation of pit initiation sites in a stainless steel surface.

### 3.3.3 The influence of anions

So far it can be concluded that current spikes represent unsuccessful pit initiation events. A manganese sulphide particle, or any other particle that can dissolve under the given circumstances, is a possible initiation site when an occluded cell is formed upon dissolution. The chance that local attack is prolonged is influenced by a number of factors, among which the polarization potential. It will very likely be also influenced by the composition of the bulk solution because the composition affects the rate at which the chloride ion concentration and the pH change. The more aggressive the solution, the higher the chance that attack after dissolution of an inclusion will proceed. This concept has been verified by studying the effect of pH, chloride concentration, thiosulphate and, as a reference, acetate, on current spikes of ss 316 measured at 350 mV/SCE.

Increasing the pH from about 5.4 (the pH of the unbuffered 0.1 M NaCl solution) to pH 10.3, with NaOH, resulted in a gradual decrease of the number of spikes, see figure 3.20 (to be compared with figure 3.5). Apparently the inclusions do not dissolve or (slow) dissolution of the inclusions is followed by fast repassivation of the freshly exposed bare metal. There are indeed reports on manganese sulphide being stable at high pH values<sup>25</sup> and on decreased dissolution rates<sup>26</sup> of manganese sulphide inclusions at high pH values.

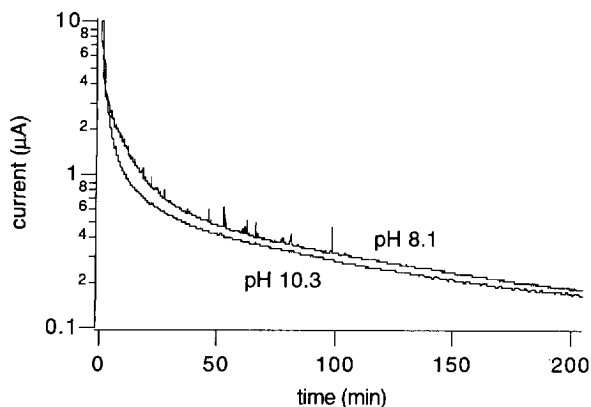


Figure 3.20. The effect of pH, ss 316, 350 mV/SCE, 0.1 M NaCl, to be compared with figure 3.5.

No clear relation was found between the chloride concentration (0.05, 0.1 and 0.5 M) and the number or size of spikes measured in the corresponding solutions, but the frequency of spikes was affected. Compared with the measurements in 0.1 M NaCl, the frequency of spikes in 0.5 M NaCl is initially higher and decreases faster, see figure 3.21. Low concentrations of thiosulphate had the same effect on the frequency, as is also indicated in figure 3.21. The current-time curve shown in figure 3.22 additionally demonstrates this effect for 0.001 M thiosulphate in 0.1 M NaCl. The effect on the total number of spikes for a range of thiosulphate concentrations is given in figure 3.23a. The numbers of spikes are however not very accurate because the first 10 minutes are always left out when counting the spikes (in figure 3.22 it can be seen that it will be difficult to determine this number). A similar diagram was constructed for acetate at two chloride concentrations, figure 3.23b. In chloride free thiosulphate solutions no spikes were detected.

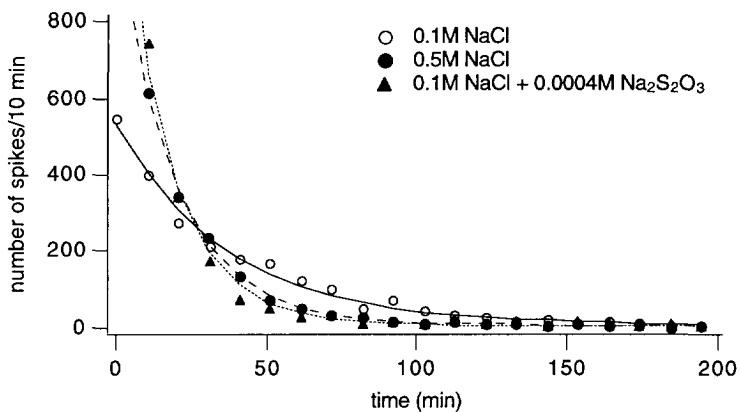


Figure 3.21. The effect of increasing the chloride concentration or adding thiosulphate to 0.1 M NaCl on the frequency of spikes (hidden included), ss 316, 350 mV/SCE.

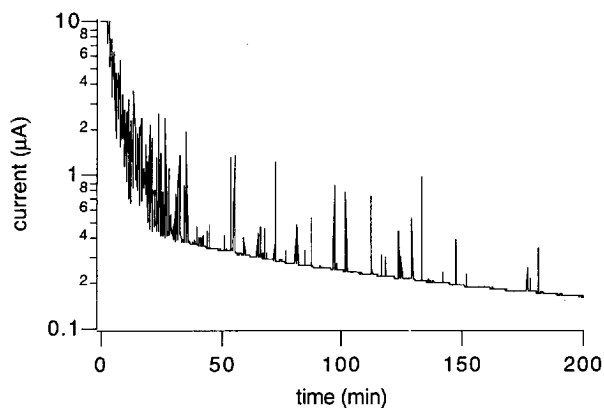


Figure 3.22. Current-time profile, ss 316, 0.1 M NaCl + 0.001 M Na<sub>2</sub>S<sub>2</sub>O<sub>3</sub>, 350 mV/SCE, to be compared with figure 3.5.



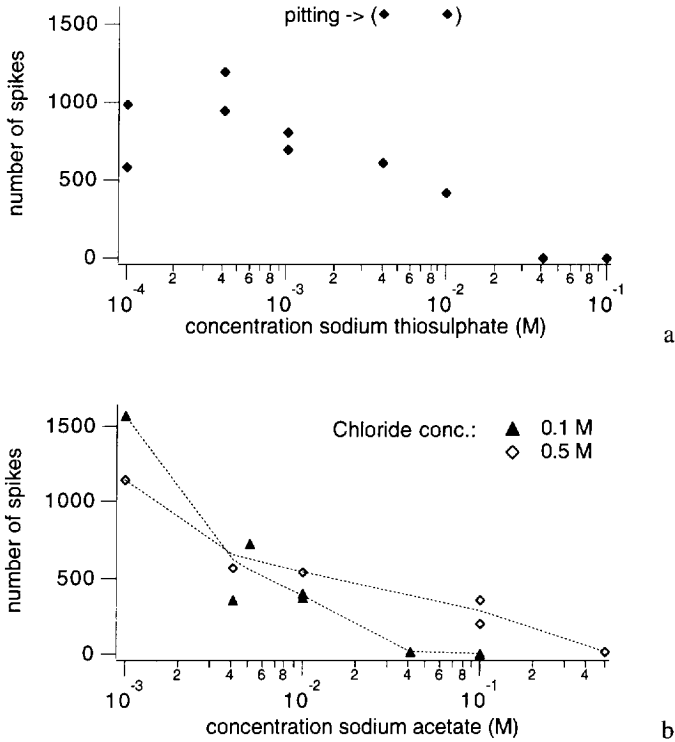


Figure 3.23. (a) The effect of various sodium thiosulphate additions to 0.1 M NaCl and (b) sodium acetate additions to 0.1 or 0.5 M NaCl on the total number of spikes, ss 316, 350 mV/SCE.

The initially high current and high frequency of spikes observed in 0.5 M NaCl and in dilute thiosulphate solutions indicate that localized attack in the beginning of the measurements is aggravated compared with the situation in 0.1 M NaCl. More possible initiation sites are removed shortly after the anodic polarisation is started. This leaves less initiation sites for the continuation of the exposure, which explains the decrease to lower frequencies of spikes. Towards the end of the measurements, the inclusions which 'come out' become more and more important, and the frequency of spikes will be determined to an increasing extent by this process. Therefore the frequencies become similar (0-10 spikes per 10 minutes).

At 0.01 M and 0.004 M thiosulphate stable pits were formed in one of the two measurements performed for both concentrations, see figure

3.23a. When the thiosulphate concentration approaches the concentration of the chloride ions the spikes disappear. This effect looks like the effect of acetate shown in figure 3.23b. The influence of acetate depends on the chloride concentration. At the higher chloride concentration more acetate is needed to suppress the spikes. This indicates a competitive effect between chloride and acetate. The phenomena can be explained if it is assumed that sulphide inclusions can not dissolve when the relative concentration of chloride falls below a certain level. Whether this is caused by acetate or thiosulphate does not make any difference. But if the thiosulphate is just too low to completely inhibit the dissolution of inclusions, it will accelerate local attack at spots where bare metal is exposed, possibly due to complexing action of thiosulphate with metal cations. In figure 3.24 it can be seen that the spikes indeed are somewhat larger when they are generated in thiosulphate solutions. However, it should be remembered that the important spikes seen in the beginning of each measurement also lack in this figure, which might obscure the issue.

It is also possible, and maybe more plausible, to explain the results with the buffering action of both thiosulphate (see section 2.3.2) and acetate. In case of thiosulphate there must be a competition between enhancement of dissolution rates (dominating at low concentrations) and buffering of the local solution (dominating at high concentrations).

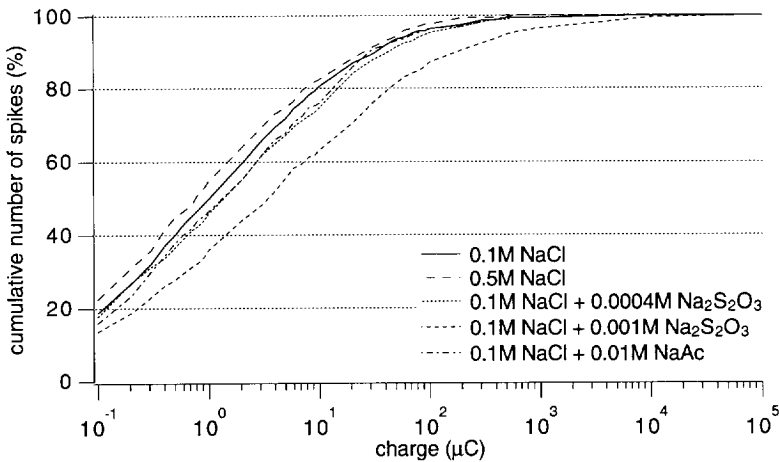


Figure 3.24. The effect of anions on the charge related to spikes.

### 3.3.4 The relation between spikes and pitting

In order to relate the current spikes to pitting corrosion, experiments were performed at higher anodic potentials during which the development of pits could be observed with a video camera. Polished ss 304 and ss 316 samples were polarized from the OCP to 500 mV/SCE and 850 mV/SCE respectively. On the ss 304 surface the generation of pits which keep growing and pits which die after a short while were both seen after polarization had started. The process is illustrated with the photographs, taken from the video recordings, shown in figure 3.25. The arrows indicate some pits which grew for a limited time only.

The pit generation rate for ss 316, deduced from the video recordings, was very high, 100-200 pits/cm<sup>2</sup>min. All the pits repassivated, although in a few experiments, under the same conditions, some stable pits formed. The visible development of a pit took 10 to 25 s which corresponded with the time scale of the large current spikes, measured simultaneously, see figure 3.26. Examination of the specimens afterwards by light microscopy revealed that the repassivated pits were hemispherical and had a diameter up to 50 μm and a depth of about 15 μm.

The nucleation frequency of pits decreased during an experiment, but was higher again after a quick and short potential excursion to 0 mV/SCE.

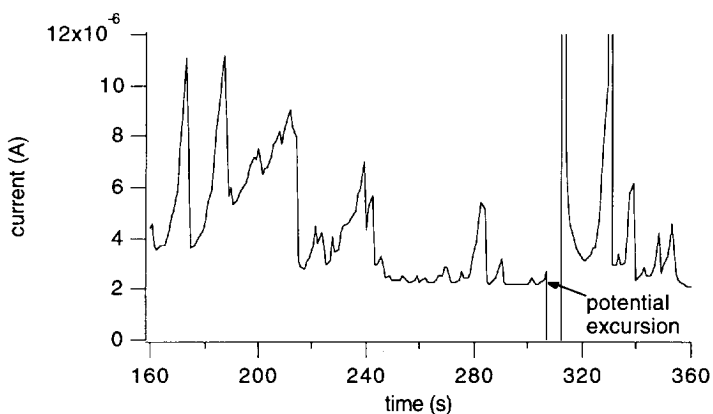


Figure 3.26. Large current spikes (ss 316, 850 mV/SCE, recorded with simultaneous camera observation).

The experiments show that large current spikes with essentially the same shape as those measured at lower potentials, characterized by a slow current increase followed by a fast current decrease, correspond with the development of macroscopically visible pits. The stable pit growth which was observed always for ss 304 specimens and only occasionally for ss 316 specimens, can be considered as the end of a chain; the unsuccessful pitting events with corresponding small current spikes at low potentials scale up at increasing anodic potentials to larger pits and larger current spikes and eventually stable pits.

The hemispherical brightening appearance of the repassivated pits of ss 316 indicates that the growth was controlled by a salt film<sup>27</sup>, see also section 2.3.4. The fact that repassivation takes place indicates that at a certain moment the current is not sufficient any more to maintain the necessary concentrations near the pit surface. Because of the increasing radius of the hemispherical pit, an increasing current is necessary to sustain pit growth<sup>13,28</sup>. At a certain radius, this requirement can not be met any more. The stable pits of ss 304 were found to be covered by remnants of the passive layer, see figure 3.27. Apparently, the oxide was able to keep the pits largely covered at this potential, which hindered repassivation. A picture of the attacked surface of ss 304 is shown in figure 3.28. Apart from the large attacked region, attack at stringers can be seen very well.

Figure 3.25. Photographs taken from the video recordings, ss 304, 500 mV/SCE, 0.1 M NaCl. The time (s) is indicated at the right bottom. Rotate the book.

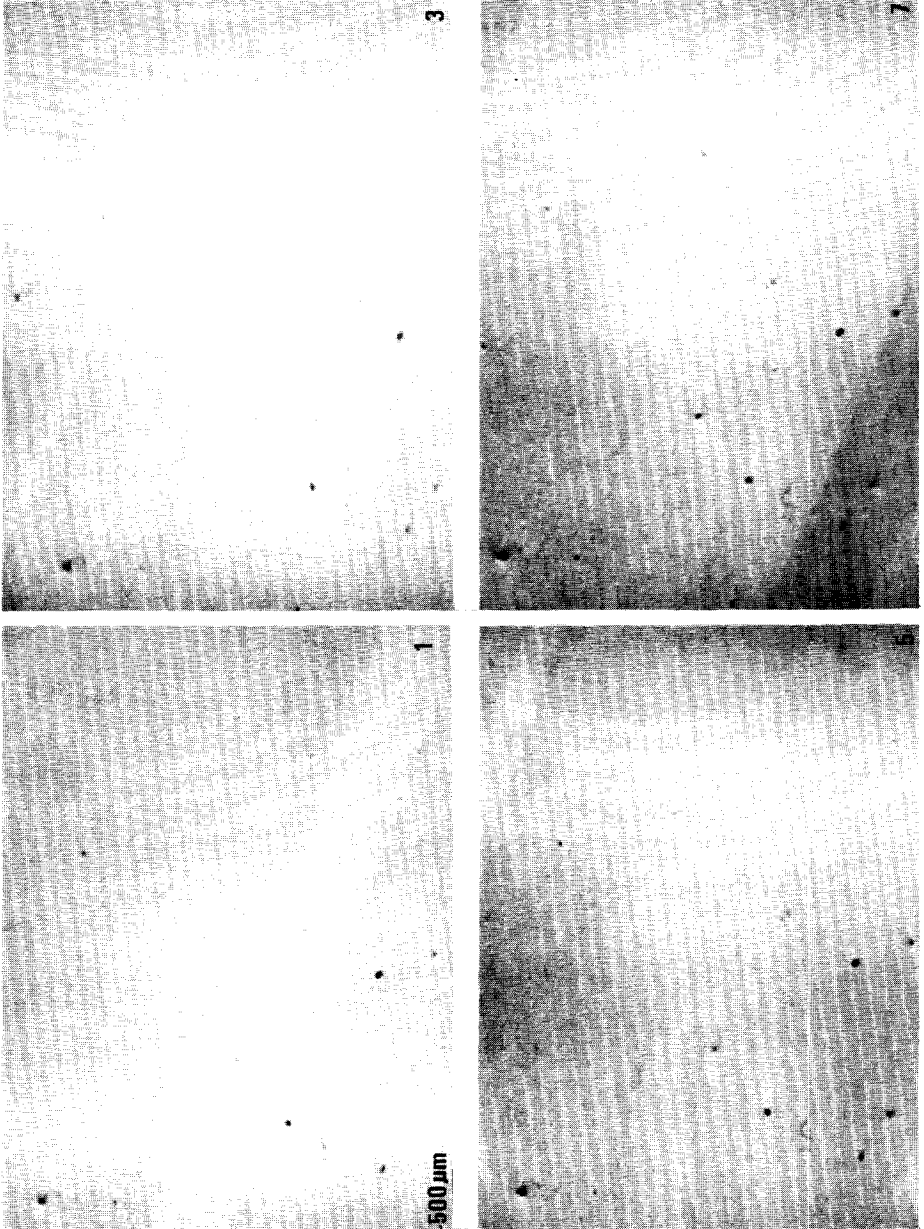


Figure 3.25. -continue

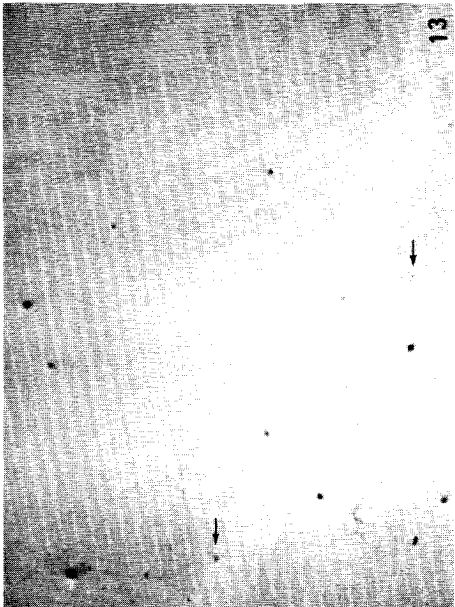
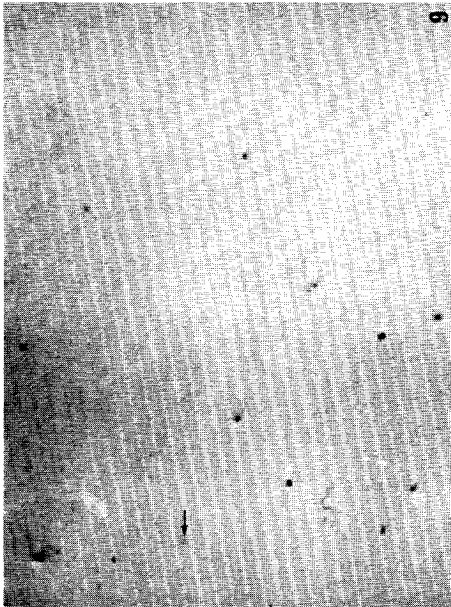
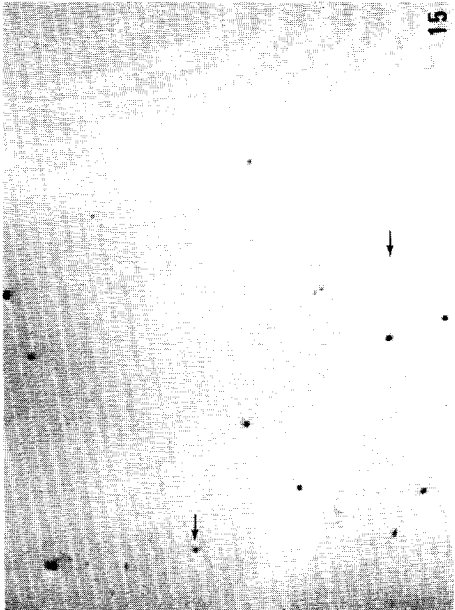
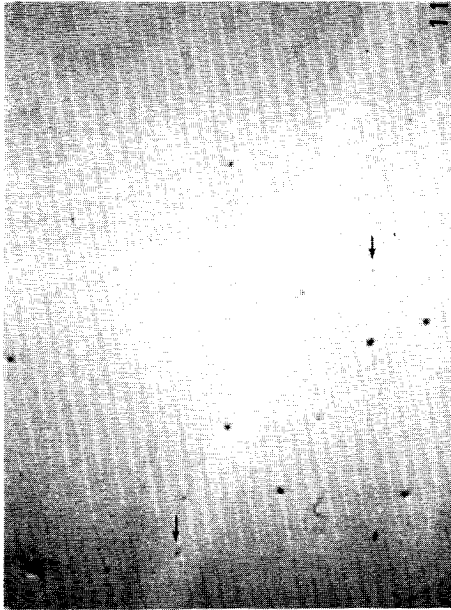


Figure 3.25. -continue

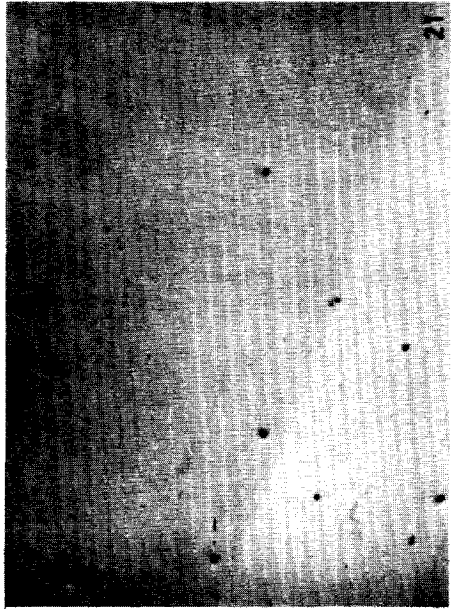
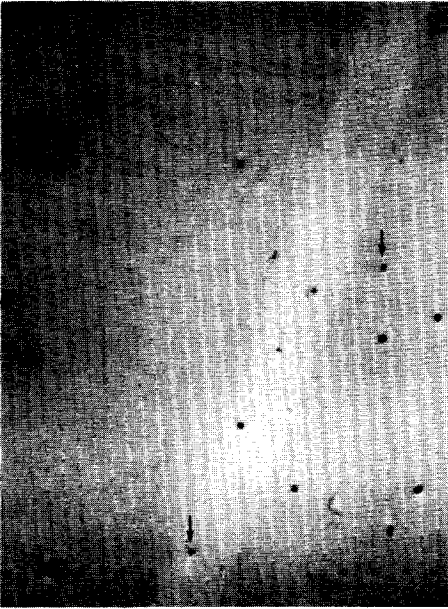
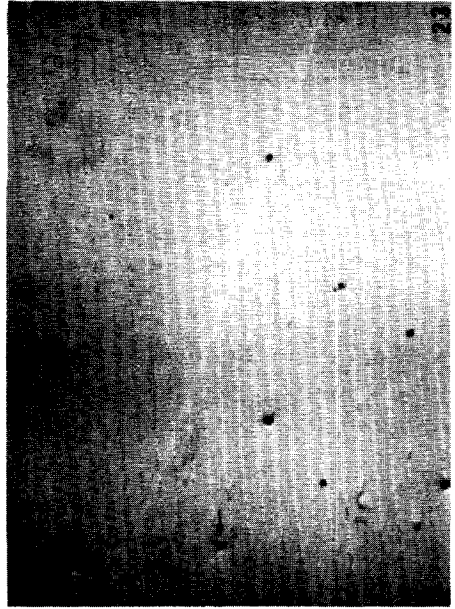
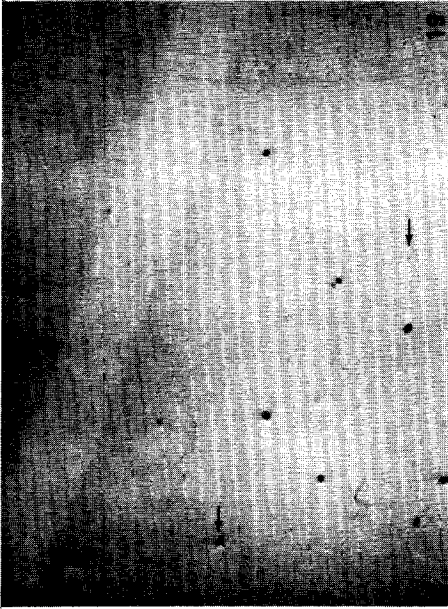
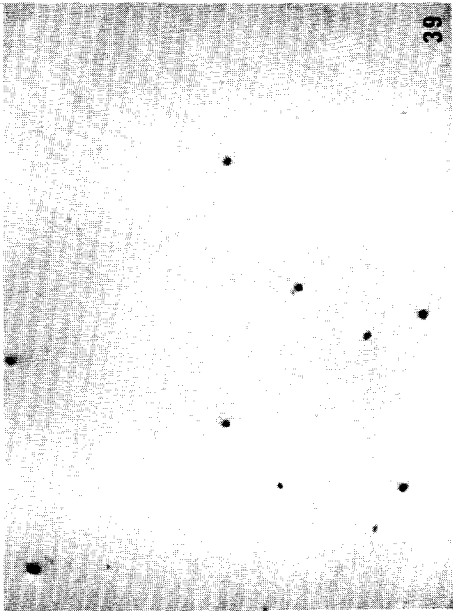
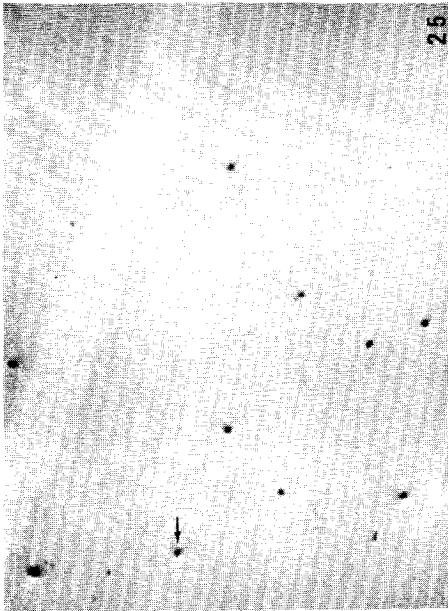
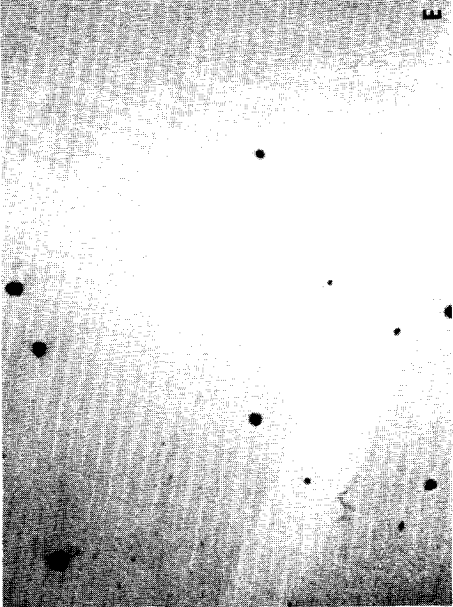
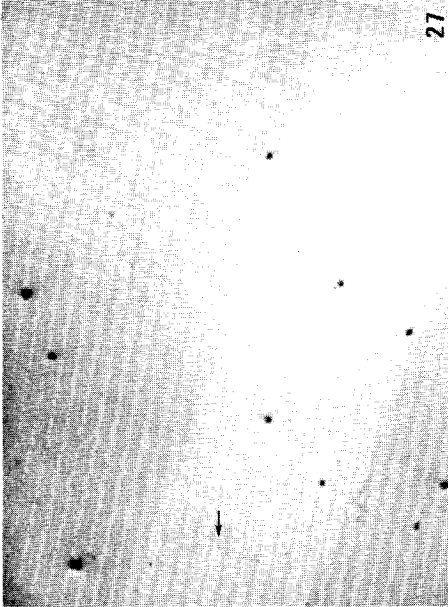
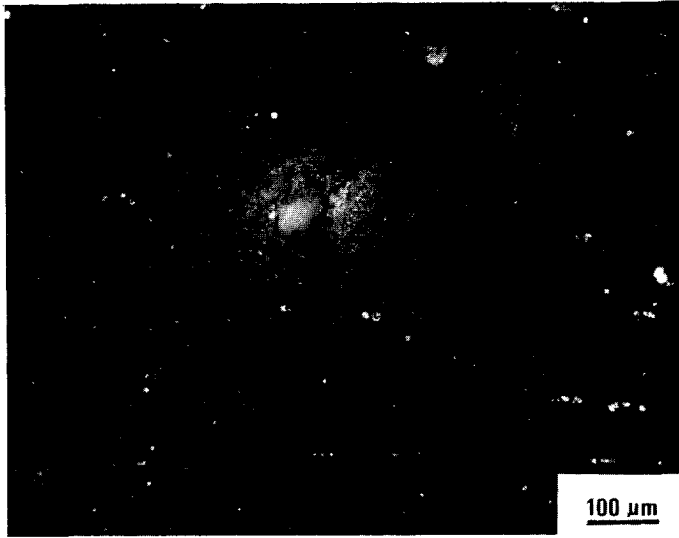


Figure 3.25. -continue.





The cathodic potential excursion resulted in an increased nucleation frequency. This could mean that the passive film was locally less protecting after this treatment due to depassivation which allowed attack of otherwise at that moment unattacked inclusions.



*Figure 3.27. Stable pit , largely covered, initiated in ss 304 at 500 mV/SCE in 0.1 M NaCl solution.*

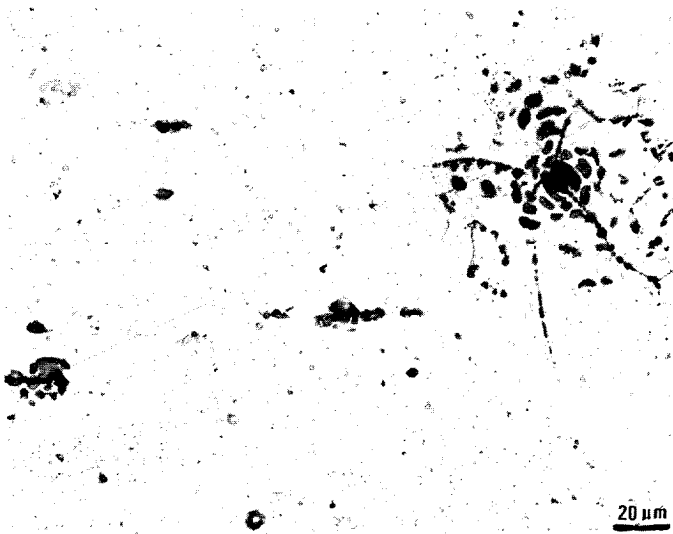


*Figure 3.28. Stainless steel 304, exposed in 0.1 M NaCl solution, 500 mV/SCE*

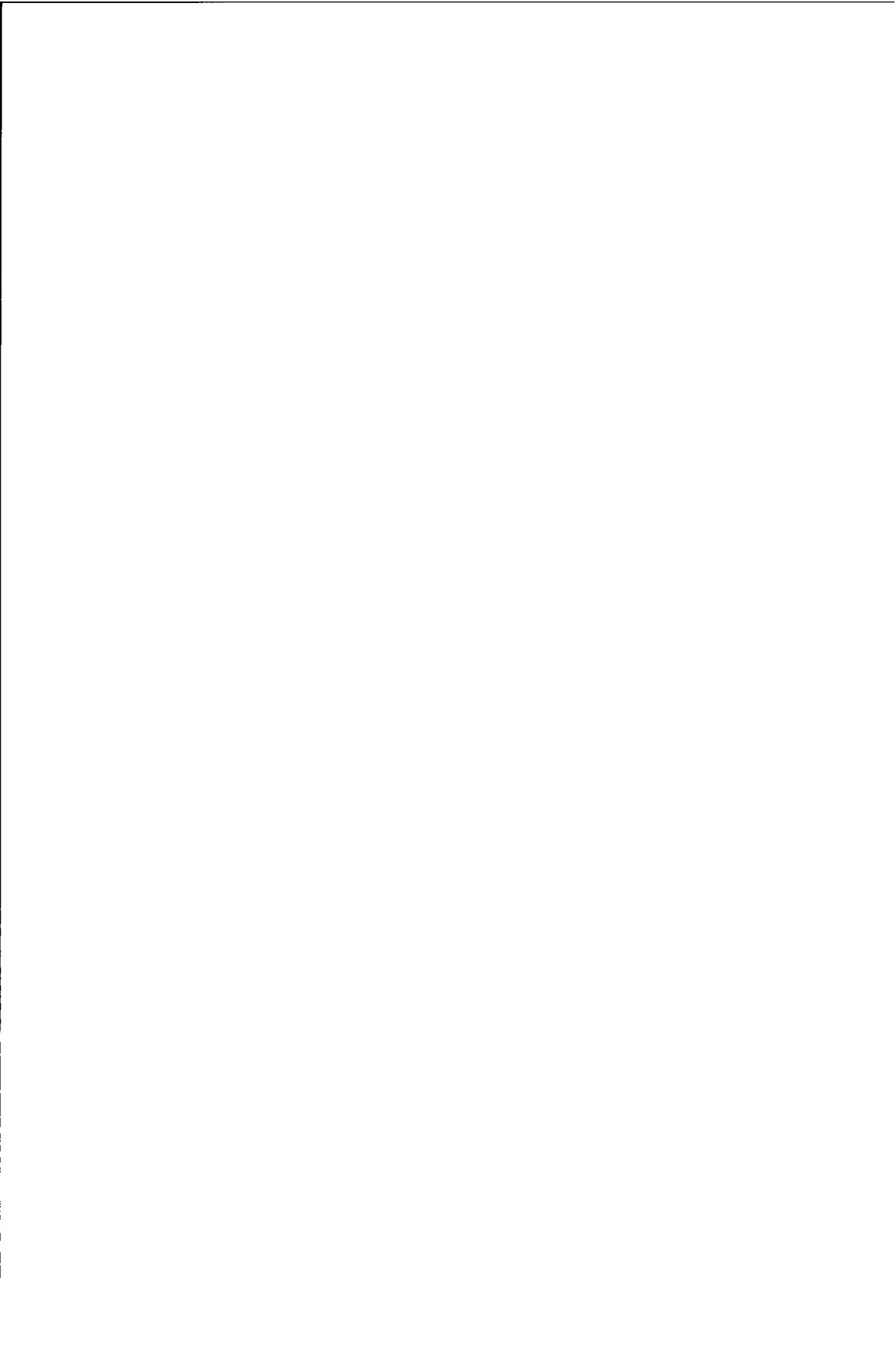
### 3.4 Conclusions

Current spikes have been related to manganese sulphide particles present in large amounts in the investigated stainless steels 304 and 316. The larger of these soluble inclusions at the surface and the inclusions lying just below the surface can cause spikes. The dissolution of just the inclusion can not be registered. It has to be followed by attack of the surrounding steel before the event is measured as a current spike. The chance for prolonged attack is influenced by the size of the inclusions, the geometry, the properties of the passive layer, the polarisation potential and the electrolyte composition. Current spikes are unsuccessful pit initiation events. The number of spikes and their size can be considered as a measure for the susceptibility of the steel to pitting.

### 3.5 References

- 1 Z. Szklarska-Smialowska, Pitting Corrosion of Metals, NACE, Houston, USA (1986).
- 2 B.E. Wilde, *Corrosion* **28** (1972) 283-291.
- 3 F.L. Laque, *Mater. Perform.* **22** (1983) 34-36.
- 4 N.G. Thompson and B.C. Syrett, *Corrosion* **48** (1992) 649-659.
- 5 L. Soria and E.J. Herrera, *La Metallurgia Italiana* **83** (1991) 1017-1021.
- 6 P. Eskelinen, O. Forsén, H. Hänninen, J. Onnela and S. Yläsaari, *Materials Science Forum* **111-112** (1992) 515-524.
- 7 H. Böhni and L. Stockert, *Werkst. Korros.* **40** (1989) 63-70.
- 8 M. Keddam, M. Krarti and C. Pallotta, *Corrosion* **43** (1987) 454-458.
- 9 W.M. Carroll and M.B. Howley, *Corros. Sci.* **30** (1990) 643-655.
- 10 H. Ezuber, A.J. Betts and R.C. Newman, *Materials Science Forum* **44&45** (1989) 247-258.
- 11 U. Bertocci, M. Koike, S. Leigh, F. Qiu and G. Yang, *J. Electrochem. Soc.* **133** (1986) 1782-1786.
- 12 Y. Miyata, T. Handa and H. Takazawa, *Corros. Sci.* **31** (1990) 465-470.

- 13 D.E. Williams, J. Stewart and P.H. Balkwill, in *Critical Factors in Localized Corrosion*, ed. G.S. Frankel and R.C. Newman, The Electrochemical Society, Inc., Pennington, USA (1992) 36-64.
- 14 A.M. Riley, D.B. Wells and D.E. Williams, *Corros. Sci.* **32** (1991) 307-1313.
- 15 T. Tsuru and M. Sakairi, *Corros. Engineering* **39** (1990) 401-409.
- 16 G.T. Burstein and S.P. Mattin, *Phil. Magazine Letters* **66** (1992) 127-131.
- 17 P.C. Pistorius and G.T. Burstein, *Phil. Trans. R. Soc. Lond. A* **341** (1992) 531-559.
- 18 R. Qvarfort, *Corros. Sci.* **28** (1988) 135-140.
- 19 J. Stewart and D.E. Williams, *Corros. Sci.* **33** (1992) 457-474.
- 20 R. Ke and R. Alkire, *J. Electrochem. Soc.* **139** (1992) 1573-1580.
- 21 G. Daufin, J. Pagetti, J.P. Labbe and F. Michel, *Corrosion* **41** (1985) 533-539.
- 22 W.M. Carroll and T.G. Walsh, *Corros. Sci.* **29** (1989) 1205-1214.
- 23 G. Hultquist, S. Zakipour and C. Leygraf, in *Passivity of Metals and Semiconductors*, ed. M. Froment, Elsevier Science Publ. B.V., Amsterdam, The Netherlands (1983) 399-404.
- 24 M.A. Barbosa, A. Garrido, A. Campilho and I. Sutherland, *Corros. Sci.* **32** (1991) 179-184.
- 25 G.S. Eklund, *J. Electrochem. Soc.* **121** (1974) 467-473.
- 26 J.E. Castle and R. Ke, *Corros. Sci.* **30** (1990) 409-428.
- 27 N. Sato, *J. Electrochem. Soc.* **129** (1982) 260-264.
- 28 H.S. Isaacs, *Corros. Sci.* **29** (1989) 313-323.



## COMPARISON OF 6 STAINLESS STEELS

### 4.1 Introduction

Ranking of stainless steels by the pitting potential, the Pitting Resistance Equivalent (PRE) or Critical Pitting Temperature (CPT) is rather common practice. The pitting potential, already discussed in the previous chapters, is hardly used for highly alloyed molybdenum containing stainless steels because most of these alloys do not pit under the test conditions at ambient temperature. The PRE is a factor calculated from the composition (chromium, molybdenum and nitrogen content) of the alloy and used as a rough estimate of the pitting resistance<sup>1</sup>. The critical pitting temperature is the lowest temperature at which pitting initiation occurs on the test specimen during an anodic polarization scan<sup>2</sup>. All these quantities reveal little, if nothing, on the actual pitting events on the surface. In the previous chapter current spikes have been identified as unsuccessful pitting events related to the dissolution of inclusions. It was proposed that the number and size of the spikes indicate the chance for localized corrosion. Current spikes measurements could be an appropriate method for investigations on pitting corrosion of highly alloyed stainless steels.

This chapter is a report of some investigations on highly alloyed molybdenum containing stainless steels with a ranging susceptibility to pitting corrosion. The following steels were studied (trade names): 316, 316L, 317L, 34LN, SAN(ICRO)28 and 254 SMO. More information on the designations and applications of these steels is given in appendix A. In several reports the stainless steels have been compared with respect to their

pitting resistance. In paper mill bleach plant environment, ss SAN28 and especially ss 254 SMO proved to be superior to ss 316 and 317L; they showed much less pitting damage<sup>3</sup>. The current-time profiles for ss 316 and SAN28 have been discussed in two papers by Carroll<sup>4,5</sup>. The profiles for SAN28 measured in 0.5 M NaCl were smooth, even when the pH was lowered or the potential was increased to +300 mV/SCE, whereas the profiles of ss 316 showed a lot of current spikes. Ranking by the PRE<sup>1</sup>, calculated as

$$\text{PRE} = \text{Cr} + 3.0 * \text{Mo} + 12.8 * \text{N}$$

where Cr, Mo and N stand for the weight percentages of the respective alloying elements in the steels (table 4.1), results in the following order: 316L < 316 < 317L < 34LN < SAN28 < 254 SMO. Ranking of the steels according to the critical pitting temperature (CPT) of the steels 316 (L), 317L, 17-14-4LN (34LN) and 254SMO also resulted in the order 316 < 317L < 34LN < 254SMO<sup>1,2</sup>. Summarizing, the following ranking can be established: 316L < 316 < 317L < 34LN < SAN28 < 254SMO.

In order to investigate the role of inclusions in localized corrosion processes of the mentioned stainless steels, current spikes were measured, current-potential curves were recorded and the inclusions were characterized by surface analytical techniques. The results are discussed in this chapter. The merits of current spikes measurements with respect to the assessment of the susceptibility to pitting of highly alloyed stainless steels are to become clear.

## 4.2 Experimental

The current-potential curves were measured in 0.1 M NaCl, at ambient temperature, with a scan rate of 1 mV/s from the open circuit potential (OCP) in anodic direction. The current spikes were measured at 350 mV/SCE, after grinding the surfaces with SiC paper P1200 grit, for 205 minutes in 0.1 M NaCl at ambient temperature. The number of spikes occurring between 10 and 205 minutes after the start of the experiment, was determined. The surfaces of the alloys were examined with SEM/EPMA, and some inclusions were examined in more detail with

SAM. Further details on the equipment and procedures can be found in chapter 3.

The investigated alloys\*, denoted by their trade names, are listed in table 4.1. The magnesium, aluminium, calcium, titanium and vanadium content were determined by Inductive Coupled Plasma - Optic Emission Spectrometry (ICP-OES) techniques after dissolution of the steels in Aqua regia.

	316L	316	317L	34LN	SAN28	254SMO
Cr	17.4	17.1	18.3	16.3	27.2	20.0
Ni	11.1	10.6	14.0	13.5	31.1	17.9
Mo	2.28	2.53	3.13	4.50	3.47	6.07
C	0.016	0.033	0.017	0.002	0.014	0.011
Mn	1.48	1.41	1.63	1.75	1.76	0.53
S	0.021	0.025	0.011	0.002	0.003	0.001
Si	0.49	0.63	0.59	0.48	0.41	0.33
P	0.035	0.029	0.026	0.023	0.020	0.020
N	0.052	0.062	0.072	0.146	0.062	0.204
Cu	0.62	0.49	0.28	0.15	0.98	0.69
Mg	0.001	0.001	0.003	0.001	0.007	0.001
Al	0.017	0.022	0.021	0.032	0.047	0.050
Ca	0.001	0.003	0.012	0.002	<0.001	0.001
Ti	<0.005	0.014	<0.005	<0.005	<0.005	<0.005
V	0.054	0.050	0.050	0.057	0.061	0.045

Table 4.1. The stainless steels and their composition (wt.%), balance of iron.

## 4.3 Results and discussion

### 4.3.1 Current-potential curves

The current-potential curves of all the stainless steel specimens are shown in figure 4.1. Two curves of each steel are given, one was measured immediately after grinding, the other was measured one day after the sample preparation.

\* The steels were kindly supplied by Avesta Sheffield and Shell Billiton Research.



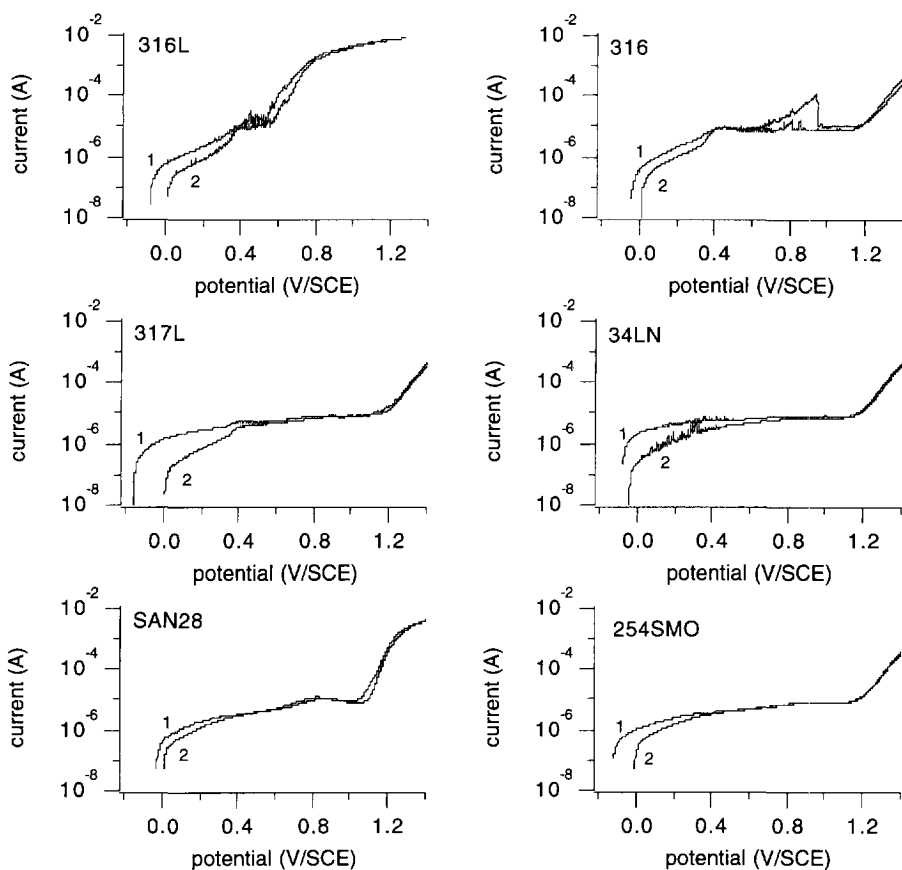


Figure 4.1. Current-potential curves of 316L, 316, 317L, 34LN, SAN28 and 254 SMO, recorded with a scan rate of 1 mV/s from the OCP in 0.1 M NaCl at ambient temperature, samples were ground the same day (1) or the day before (2).

Four of the steels, ss 317L, 34LN, SAN28 and 254 SMO, stay passive up to the transpassive region during the measurement. The curves of one of the type 316 steels, ss 316L, shows a distinct current increase at about 0.6 V/SCE, indicating the onset of pitting corrosion. Pits were clearly visible on the exposed surface. The curves of ss 316 show large current fluctuations. Current fluctuations, appearing in a different potential regime, can also be seen on the curves of ss 34LN. Small current fluctuations were also found on the curves of 317L, although they are not visible in figure 4.1. The OCP of freshly ground specimens is always more

cathodic than the OCP of specimen ground one day earlier. However, the curves coincide from about 0.4 V/SCE on, except for ss 316L. The freshly ground specimen of this steel seems to pit at a slightly more cathodic potential than the specimen ground earlier.

The current-potential curves indicate that ss 316L is most sensitive to pitting under these conditions, followed by ss 316. No distinction with respect to the pitting susceptibility can be made between the other four steels on the basis of these curves.

### 4.3.2 Current spikes

The current spikes were measured in duplicate on all the specimens. One current-time curve for each specimen is shown in figure 4.2. Plots of the cumulative number of spikes, absolute and relative, as a function of the charge related to the spikes are shown in figure 4.3. The numbers of spikes are compared in figure 4.4. More details on the shape of the spikes are listed in table 4.2. In general, no major differences were found between the shape of the individual spikes measured for the different alloys.

The difference observed before between the current-potential curves of ss 316L and 316 (figure 4.1) manifests itself now by a difference in number of spikes. Moreover, a ranking on this basis (figure 4.3.a and 4.4) can be made for all the alloys and results in the order: 316L < 316 < 317L < 34LN < SAN28 < 254SMO, which is similar to the ranking based on various reports concerning the pitting resistance discussed in the introduction of this chapter.

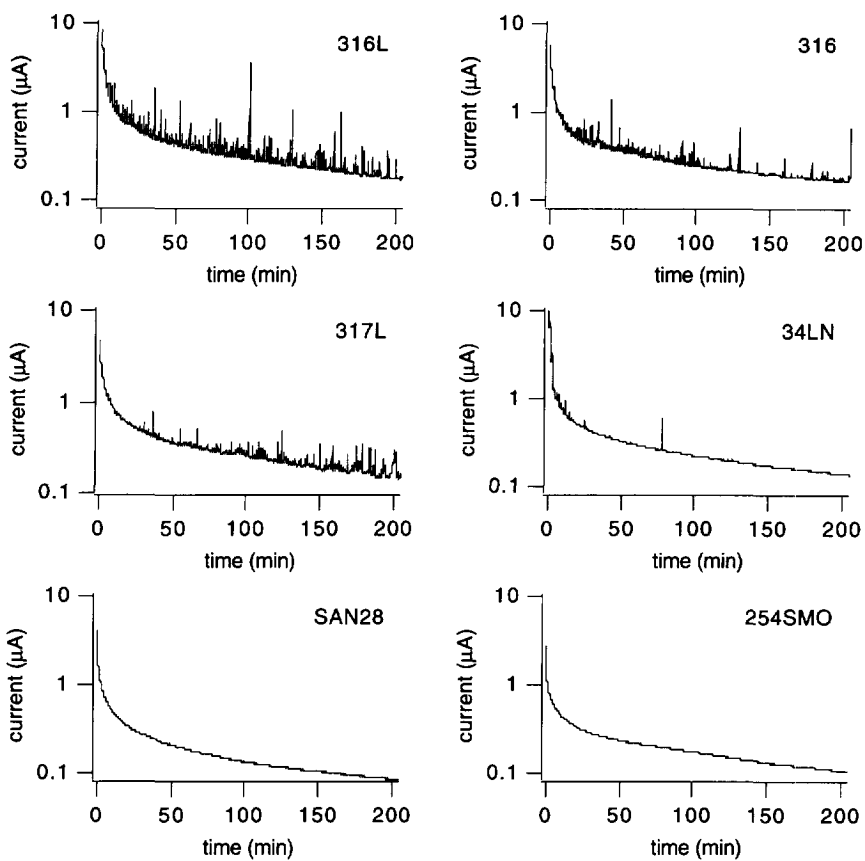
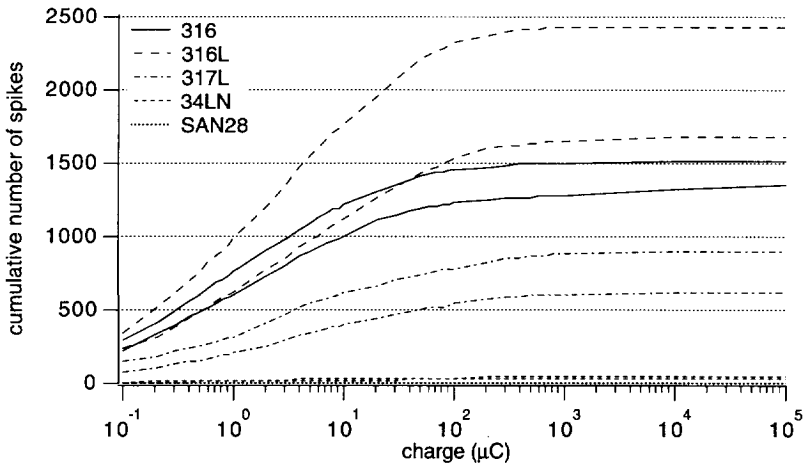
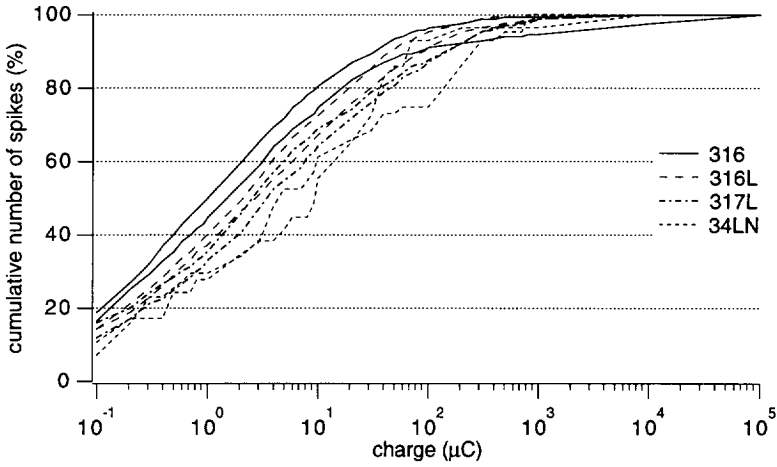


Figure 4.2. Current-time profiles of 316L, 316, 317L, 34LN, SAN28 and 254SMO, measured at 350 mV/SCE in 0.1 M NaCl.



a



b

Figure 4.3. Cumulative number of spikes of ss 316L, 316, 317L, 34LN and SAN28 plotted as a function of the charge, spikes measured at 350 mV/SCE in 0.1 M NaCl. In 4.3b the results of ss SAN28 have been omitted because only a few spikes were measured for this alloy.

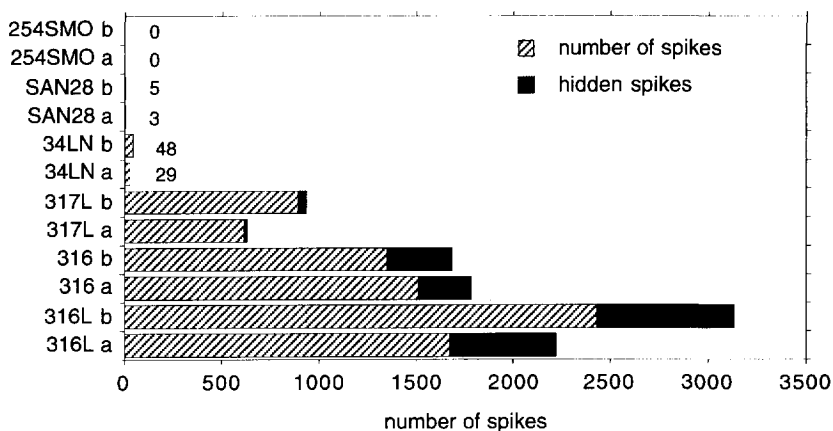


Figure 4.4. Comparison of the number of spikes for 6 stainless steels.

	number of spikes	average width (s)	average height (nA)
316L	1674	2.3	160
	2430	1.8	126
316	1510	1.7	94
	1351	2.6	173
317L	574	3.1	82
	893	3.2	75
34LN	29	2.7	96
	44	3.2	137
SAN28	3	1.2	34
	5	1.2	38
254 SMO	0		
	0		

Table 4.2. Results of spikes measurements at 350 mV/SCE, 0.1 M NaCl.

Apart from differences in the numbers of spikes for the various alloys, other differences can be seen as well. Relatively more large spikes, with respect to the charge, were measured for ss 316L, 317L and 34LN as compared with ss 316, see figure 4.3b. The extra contribution to the

charge related to the spikes of ss 317L and 34LN mainly results from a prolonged lifetime of the spikes, not from an increase in the height of the spikes, see table 4.2. This can be caused by differences in dimensions of the inclusions in these alloys, or by an increased stability of the passive films formed by ss 317L and 34LN, which can keep occluded cell conditions for longer times. The results will be further evaluated in the next section, after discussion of the analyses of the inclusions in the various steels.

### 4.3.3 Surface analyses

The inclusions in the stainless steel specimens were analysed before and after exposure to 0.1 M NaCl, 205 minutes at 350 mV/SCE during which the current spikes were measured. The samples were polished down to one micron diamond paste before the first analysis, and were shortly polished again before exposure.

In table 4.3 and 4.4 the results from the surface analyses before exposure are given. Manganese sulphide inclusions were recognized as such in ss 316L, 316 and 317L. Comparing table 4.3 and 4.4 it can be seen that most of the particles containing sulphur (335/mm<sup>2</sup> in ss 316L, 679/mm<sup>2</sup> in ss 316 and 757/mm<sup>2</sup> in ss 317L) are manganese sulphide inclusions (291/mm<sup>2</sup>, 587/mm<sup>2</sup> and 749/mm<sup>2</sup> respectively). In ss 34LN, SAN28 and 254 SMO also some sulphur containing particles were found (75/mm<sup>2</sup>, 6/mm<sup>2</sup> and 19/mm<sup>2</sup> respectively) but no discrete manganese sulphide particles were identified. In ss 34LN sulphur was mainly associated with manganese and aluminium, calcium, silicon and/or titanium. In ss SAN28 and 254 SMO no manganese was detected in any of the particles. Sulphur was found in combination with magnesium, aluminium, silicon, calcium and/or titanium. It has to be noted that all the steels contain some vanadium which can not be distinguished from titanium in the EPMA.

The size of inclusions is related to the constituting elements, see table 4.4. Aluminium containing inclusions as well as silicon and calcium containing inclusions were generally large. Manganese sulphide particles and other inclusions with manganese and/or titanium were generally small.

	316L	316	317L	34LN	SAN28	254SMO
MnS	291	587	749	0	0	0
complex	54	543	452	210	101	106

Table 4.3. Number of inclusions per mm<sup>2</sup>, MnS = discrete manganese sulphide particle, complex = particle with Al, Si, Ca, Ti, Mg, Mn and/or S.

	316L	316	317L	34LN	SAN28	254SMO
S	335	679	757	75	6	19
A (µm <sup>2</sup> )	0.9	0.4	0.4	3.5	3.1	0.3
Mn	275	478	748	23	0	0
A (µm <sup>2</sup> )	0.5	0.4	0.5	4.1		
Al	25	17	1	24	0	1
A (µm <sup>2</sup> )	3.1	10	5.8	1.4		0.5
Si	45	226	211	30	0	7
A (µm <sup>2</sup> )	5.6	1.5	1.0	4.4		6
Ca	61	226	199	76	5	32
A (µm <sup>2</sup> )	4.6	1.7	1.0	4.1	2.9	0.2
Ti	3	466	84	13	2	107
A (µm <sup>2</sup> )	0.6	0.7	1.2	0.5	0.5	0.3
Mg					81	5
A (µm <sup>2</sup> )					0.8	0.8

Table 4.4. Number of inclusions per mm<sup>2</sup> which contain the specified element, and the average area of the inclusions.

The analyses made before and after exposure were compared and the differences between the numbers of the various types of inclusions determined, see table 4.5 The effect of exposure is most pronounced in the reduction of the sulphur and manganese containing particles in all the specimen except for ss SAN28 and 254 SMO. Often more titanium containing particles were recognized after exposure. A possible explanation for the apparent increase is that the surrounding of particles dissolves thereby uncovering insoluble titanium compounds. A similar

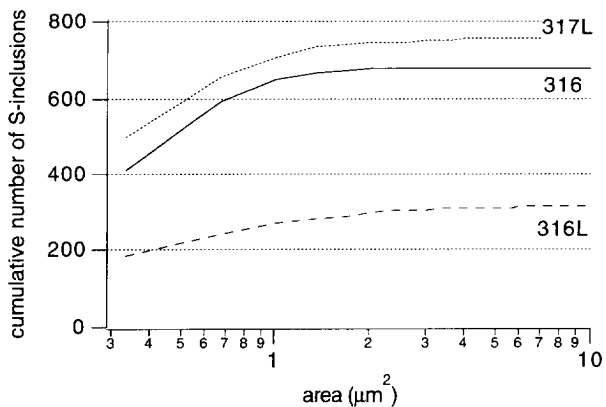
explanation can be given for the larger number of complex inclusions identified for ss 316 after exposure.

	316L	316	317L	34LN	SAN28	254SMO
$\Delta$ MnS	-270	-493	-690	-	-	-
$\Delta$ complex	+3	+471	-11	-104	-43	+15
$\Delta$ S	-291	-676	-680	-63	+1	-7
$\Delta$ Mn	-257	-402	-639	-20	-	-
$\Delta$ Al	+19	+1	0	0	+3	0
$\Delta$ Si	+15	+110	-6	-4	+30	-3
$\Delta$ Ca	-26	+61	-8	-31	+11	-8
$\Delta$ Ti	+4	+170	+40	+5	0	+1
$\Delta$ Mg	-	-	-	-	-70	-4

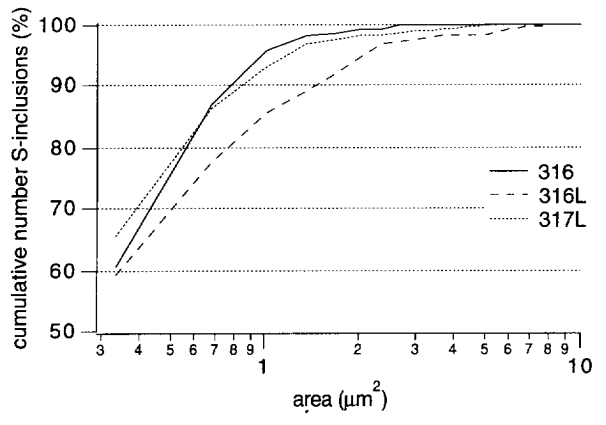
Table 4.5. Effect of exposure (0.1 M NaCl, 350 mV/SCE, 205 minutes) on the number of inclusions per mm<sup>2</sup>.  $\Delta$  = (situation after - situation before exposure).

The reduction in the number of complex inclusions for ss 34LN and SAN28 is due to the dissolution of some of these inclusions, mainly sulphur containing inclusions for ss 34LN and magnesium containing inclusions for ss SAN28. The magnesium content of ss SAN28 was found to be relatively high, see table 4.1. Silicon was detected after exposure of this alloy, while it was not found before exposure. Further studies are needed to investigate the origin of these particles. In ss 254 SMO no particular type of inclusions seems to dissolve under the given circumstances.





a



b

Figure 4.5. Cumulative number of sulphur containing inclusions per  $\text{mm}^2$  plotted as a function of the area measured at the surface of the specimens.

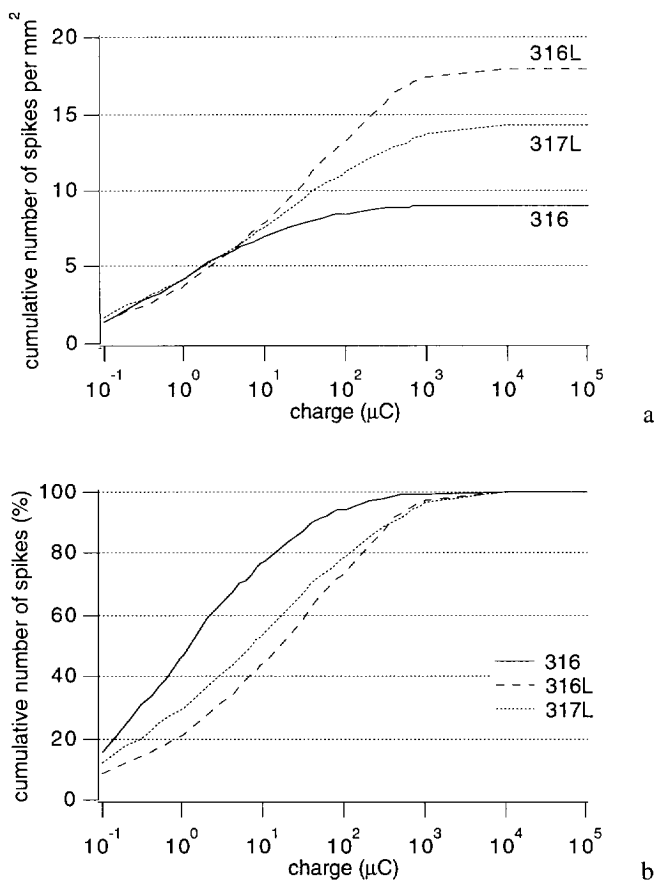


Figure 4.6. Cumulative number of spikes measured during exposure between surface analyses, plotted as a function of the charge.

In figure 4.5 the results of the area measurements of the sulphide particles are given for the alloys in which the majority of these particles was identified as manganese sulphide. The current spikes were measured during the exposure between the surface analyses. The results are shown in figure 4.6. In table 4.6 some data are put together: data on the spikes measured between the surface analyses, the spikes measured on the ground specimens (table 4.2), the number of dissolved manganese sulphide particles, the sulphur content of the alloys and the average size of the inclusions. The number of spikes measured on ground specimens (column

D) should be higher than the number measured on polished specimens (column A), as was discussed in chapter three. This does not hold for 317L. This might be coincidental because there is always a considerable scatter in the number of spikes measured.

	spikes number /mm <sup>2</sup>	average width (s)	average height (nA)	spikes number /mm <sup>2</sup> table4.2	$\Delta$ MnS number /mm <sup>2</sup>	S (wt.%)	S-incl. number /mm <sup>2</sup>	S-incl average area ( $\mu$ m <sup>2</sup> )
	A	B	C	D	E	F	G	H
316L	17.9	4.0	311	26.3	-270	0.021	335	0.9
316	9.0	1.8	101	18.3	-497	0.025	679	0.4
317L	14.2	4.5	112	7.1	-690	0.011	757	0.4
34LN	0.5	3.0	274	0.5	0	0.002	75	3.5
SAN28	0.05	0.8	58	0.05	0	0.003	6	3.1
254SMO	0	-	-	0	0	0.002	19	0.3

Table 4.6. Comparison of some data, column A, B and C: data on spikes measurements between surface analyses,  $\Delta$ MnS = difference in number of manganese sulphide inclusions found before and after exposure, S = sulphur content of the alloy, S-incl = sulphur containing inclusions. Exposure conditions: 0.1 M NaCl, 350 mV/SCE. Spikes were measured from 10 to 205 minutes after applying the anodic potential.

#### Comparing ss 316L, 316 and 317L.

For these steels manganese sulphide inclusions were identified as the most important unstable inclusions (table 4.5). Comparing figure 4.5a and 4.6a, and from table 4.6 column A and E, it can be seen that the number of manganese sulphide inclusions that dissolved is considerably larger than the number of spikes measured, similar to what was reported in the previous chapter. Most inclusions did not cause a measurable spike. Although more sulphide inclusions were found in ss 316 than in ss 316L, less spikes were measured on the former one. If only the very large inclusions cause a spike, then the number of spikes in ss 316L is not expected to be smaller than the number for ss 316 any more. For example, for ss 316L 15% of the cross-sections of sulphur containing inclusions was larger than 1  $\mu$ m<sup>2</sup> (figure 4.5b), that is 50 inclusions per mm<sup>2</sup>, while for ss 316 only 5%, that is 34 cross-sections of inclusions per mm<sup>2</sup> had a larger area. As the

contents of alloying elements are very similar for ss 316L and 316, see table 4.1, the differences in behaviour (the number and size of the current spikes and the shape of the current-potential curves) can be attributed to the difference in size of the manganese sulphide inclusions. As the charge of a spike originates for the larger part from oxidation of the metal matrix and not the inclusion itself, see chapter three, dissolution products, that is sulphur compounds derived from manganese sulphide inclusions, are likely to contribute to the difference. Of course, the size of the area which must passivate after dissolution of an inclusion is related the dimensions of the particle, and the size of the corresponding spike will be affected likewise.

No major differences exist between the inclusions in ss 316 and 317L (table 4.3-4.5, figure 4.5). Only slightly more large inclusions were found in ss 317L. More spikes were measured for ss 317L during exposure between the surface analyses, but this does not match the results obtained from ground surfaces, as was discussed before. However, in all the current spikes measurements the lifetime of the spikes for ss 317L was longer than for and ss 316, see table 4.2 and 4.6. The difference is more likely caused by an improved ability of the passive layer of ss 317L, compared with ss 316, to keep occluded cell conditions, than by the small differences in the dimensions of inclusions. The chromium, nickel and molybdenum content of ss 317L are considerably higher than for ss 316. In the current-time curves of ss 317 (figure 4.2) it can be seen that the spikes evolving towards the end of the measurement become broader. This is in accordance with the idea that for a more stable passive film (after it has been polarized for a while at a potential in the passive region) the spikes are larger. Later on in a measurement the inclusions lying just below the surface become more important compared with the sliced inclusions, and the role of the passive film will be of increasing importance. This also explains the generation of large spikes at a pickled surface, reported in the previous chapter.

#### *The steels 34LN, SAN28 and 254 SMO.*

These steels differ from the other three alloys in the sulphur content, which is very low, and the resulting lack of discrete manganese sulphide inclusions. In ss 34LN sulphur was found in combination with manganese and various other elements. In ss SAN28 and 254 SMO the combination of sulphur and manganese was not found at all. Only a few spikes were

measured on the ss 34LN and SAN28 specimens, none were measured on ss 254 SMO (figure 4.4). This would indicate that in the former two alloys some inclusions are soluble under the given circumstances. For ss 34LN it is a sulphur containing component, see table 4.5, which dissolved completely because the number of complex particles found after exposure ( $106/\text{mm}^2$ ) was significantly lower than the number found before exposure ( $210/\text{mm}^2$ ). The spikes are relatively large (figure 4.3, table 4.2 and 4.6), which could be caused by the size of the sulphur containing inclusions in this alloy (table 4.4), or by the good ability of the passive layer to keep occluded cells covered, similar to the situation for ss 317L.

In ss SAN28, magnesium containing particles were found which apparently could dissolve during exposure, see table 4.4 and 4.5. But only a few small spikes were measured, maybe because no hazardous dissolution products were formed when the inclusion dissolved as opposed to the dissolution of manganese sulphide, or because this alloy is able to repassivate fast due to the exceptionally high nickel and chromium content (table 4.1) and because of the small size of the magnesium inclusions (table 4.4). One particle was investigated in detail with SAM, the line scan is shown in figure 4.7. In this homogeneous and relatively large particle not only magnesium and calcium but also sulphur is present. Although the surface was cleaned by sputtering before analyses, it is remarkable to find an oxide layer on the surrounding metal which has been formed in spite of the high vacuum.

No spikes were measured on the ss 254 SMO specimen, and also no obvious changes were seen in the number of inclusions in this steel. So the relatively few and small inclusions seem to be stable under the given exposure conditions.

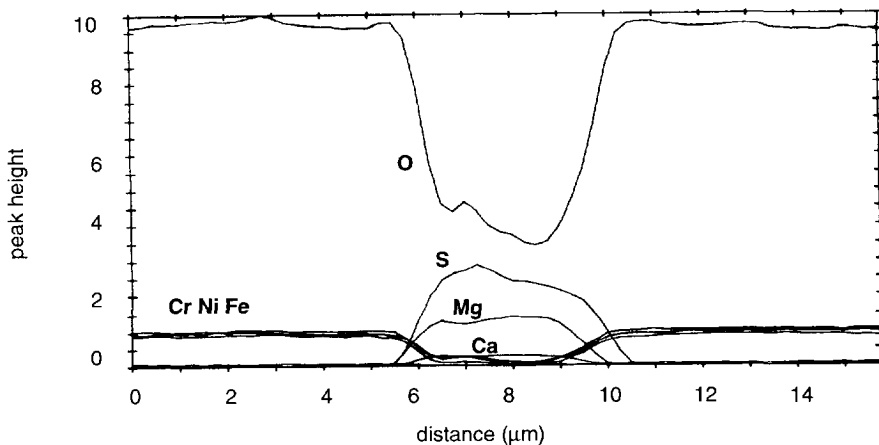


Figure 4.7. Line scan (SAM) of a particle found in ss SAN28.

#### 4.4 Conclusions

The relative pitting resistance of the investigated high alloyed molybdenum containing stainless steels can not be determined from the current-potential curves measured in 0.1 M NaCl solution at ambient temperature. However, obvious differences in the number and size of spikes can be measured under these circumstances in potentiostatic tests at 350 mV/SCE. These data can be used to indicate the susceptibility to pitting corrosion of these alloys. The ranking determined by the number of spikes corresponds with the ranking established by other methods. Again, the chance of damage due to localized corrosion of highly alloyed stainless steels is reflected in the number and size of the current spikes.

High resistance to pitting corrosion is primarily determined by the number and size of sulphur containing inclusions in the steels. In alloys with a relatively high sulphur content (> 0.011 %) the larger part of these inclusions was identified as manganese sulphide inclusions. But even in alloys with a very low sulphur content (< 0.003 %) sulphur was found in inclusions of complex compositions. In 34LN these large inclusions were soluble, and spikes could be measured. In SAN28, an alloy with a

relatively high magnesium content (0.007 %), small magnesium containing particles seemed to be soluble, but no considerable local activation was measured. In ss 254 SMO the inclusions were small and did not dissolve under the given conditions, and no spikes could be measured.

The high pitting resistance of ss 34LN, SAN28 and 254SMO appears to be mainly due to the very low sulphur content, and thus the absence of (manganese) sulphide inclusions. The improved repassivation rates will certainly contribute, but there are strong indications that the quality of the passive layer also plays an unfavourable role of importance. The more stable the film is, in acid environments for example, the longer it can delay repassivation after local activation by keeping local cells occluded for longer times.

#### 4.5 References

- 1 E. Alfonsson and R. Qvarfort, *Materials Science Forum* **111-112** (1992) 483-492.
- 2 P.-E. Arnvig and R.M. Davison, Paper to be presented at 12'th Int. Corrosion Congress, September 1993, Houston, USA.
- 3 R.M. Davison, T. DeBold and M.J. Johnson, in *Metals Handbook Ninth Edition*, Vol 13, Corrosion, American Society for Metals, Metals Park, Ohio, USA (1987).
- 4 W.M. Carroll and T.G. Walsh, *Corrosion Science*, **29** (1989) 1205-1214.
- 5 W.M. Carroll and M.B. Howley, *Corrosion Science*, **30** (1990) 643-655.

# THE EFFECT OF SURFACE DEFORMATION

## 5.1 Introduction

In this chapter the effects of (surface) deformation by rolling and micropeening, a type of shot peening, on pitting corrosion will be discussed. Shot peening is a surface treatment for metallic surfaces which is performed by hammering with a specifically chosen type of shot. Shot type and size depend on the alloy treated and the impact on the surface to be obtained. The treatment is applied for various purposes, for example to improve mechanical or corrosion properties, to reduce porosity, to form a piece of metalwork, or to change adherence properties. Peening with glass beads was performed for the first time in 1960<sup>1</sup>. Micropeening is a trade name for a shot peening process by which a surface is cold worked with a jet of glass beads of a chosen uniform diameter under well controlled operating conditions (micropeening should not cause any metal removal).

Upon peening, the metal surface yields but is restrained by the underlying material, resulting in a residual compressive stress in a surface layer up to a few hundred micrometers in thickness. This stress is the most important but not the only result of peening. The surface hardness increases, the surface roughness changes, phase transformations can be induced and grain boundaries are broken<sup>2</sup>.

The changes induced by peening influence the mechanical properties. Especially the fatigue, wear and erosion resistance improve under most peening conditions<sup>2-5</sup>. The corrosion properties are also influenced by peening. The effect of peening on stress corrosion cracking, hydrogen



embrittlement and pitting corrosion of austenitic stainless steels is scarcely discussed in literature. The resistance to stress corrosion cracking of ss 304 is generally believed to improve by peening<sup>6-8</sup>. In constant strain rate studies at high temperature however, shot peening (with ceramic shot) was found to accelerate stress corrosion cracking, which was explained by a reduced ductility in a thin surface layer<sup>8</sup>. Peening, with ceramic microballs, was found to be detrimental to the hydrogen embrittlement susceptibility of ss 304<sup>9</sup>. The effect was related to the phase transformation induced by peening. An increased passive current density, increased pit density (number of pits per unit surface area) and a cathodic shift of the pitting potential (the potential corresponding with a current of 10  $\mu\text{A}/\text{cm}^2$ ) were found by Werner<sup>10</sup> after shot peening CrNi(Mo) steels with several types of shot and testing in 0.05 M  $\text{H}_2\text{SO}_4$  + 0.1 M NaCl at 25°C. The results were explained by a rise in the number of crystalline defects. Martensite was formed by the peening process, but the extent to which martensite was formed was not reflected in the extent to which the pitting potential was shifted for the differently treated specimens. Martensite formation was therefore not held responsible for the observed changes in pitting behaviour.

Cold deformation by rolling of stainless steels also causes residual compressive stress<sup>11</sup>. Stefec<sup>12</sup> reported that with increasing cold deformation of CrNiMo steel the number of pits, the current density and the total area of pits increased (potentiostatic tests in 0.1 M NaCl at 30°C). An increased pit density after cold deformation by rolling of CrNi steel was also reported by Randak<sup>13</sup>, but the pitting potential was found to be not affected. The pits nucleated at the martensite which was formed by the cold deformation.

Two interesting papers deal with the effect of cold deformation on the corrosion behaviour of amorphous NiFeCrPB<sup>14</sup> and FeNiCrPB<sup>15</sup> alloys in NaCl. Deformation affected neither the passive corrosion current density nor the pitting corrosion resistance. However, severe cold rolling resulted in cracks at the surface where crevice corrosion or pitting was observed.

Cold deformation of commercial stainless steels can result in breakage of inclusions<sup>16,17</sup>. The crevices thus formed can act as initiation sites for localized corrosion.

In a review on the cold work effects, Szklarska-Smialowska<sup>18</sup> concluded that the influence of cold work on pitting is complex. Studies have yielded contradictory results. It seemed however that cold work often results in an increase of the pit density and sometimes results in a lower pitting potential.

This chapter deals with the pitting behaviour of micropeened and (extra) cold rolled austenitic stainless steels. Current-potential curves and current spikes measurements are used to assess the effects of cold deformation on the pitting corrosion susceptibility.

## 5.2 Experimental

Specimens of ss 304, 316 and 254 SMO were micropeened and specimens of ss 316 were rolled. For each experiment half of the number of specimens prepared was deformed while the other half was used as blanks. The samples were tested not earlier than one day after the surface preparation. Grinding was performed semi-automatically (Struers Rotapol-2 / Struers Pedemat sample holder) with SiC paper grit P220, as opposed to the manually grinding of the samples used in the experiments described in the previous chapters.

Micropeening\* was manually performed, first with the nozzle at an angle of 45° at a distance of 25 ± 4 cm from the surface, a pressure of 2.3 atm and a glass bead diameter of 90 to 150 µm. After this pretreatment, a final treatment with the nozzle at 90° at a distance of 25 ± 4 cm, a pressure of 2.0 atm and glass bead diameter of 100 to 200 µm was performed.

Some ss 316 samples were cold rolled up to a reduction of 25% of the thickness. The surfaces were ground after the rolling. Hardness profiles were measured on cross-sections of rolled and micropeened specimens. The surface roughness was determined (Perthen Perth-O-Meter and Perth-O-Graph) for polished, ground and micropeened specimens of ss 316.

The current-potential curves of all the samples were recorded with a scan rate of 1 mV/s from the OCP in anodic direction, in 0.1 M NaCl at ambient temperature. The current spikes were measured at 150 mV/SCE

---

\* Micropeening was kindly performed by *Corrosie Technisch Bureau* CTB, Pernis.

for ss 304, 250 mV/SCE for ss 316 and 550 mV/SCE for 254SMO, in 0.1 M NaCl at ambient temperature.

For all the experiments an Avesta cell was used. For further experimental details on the measurements of current-potential curves, current spikes, the Avesta cell and the composition of ss 304 and 316, see chapter three. The composition of ss 254SMO is given in chapter four. All experiments were performed in duplicate or triplicate, except for the measurements on ss 254 SMO.

### **5.3 Results**

#### **5.3.1 Current-potential curves**

The current-potential curves were recorded on three ss 304 specimens with a polished surface (3  $\mu\text{m}$  diamond paste) and three identically polished specimens which were micropeened afterwards. The curves are shown, from 0 to 0.5 V/SCE, in figure 5.1. The OCP of the micropeened specimens is lower than the OCP of the unpeened ones. The current (per 78  $\text{mm}^2$ ) measured on the micropeened samples is higher at all potentials. The current increase representing the onset of pitting starts at about 0.3 V for the polished samples and at 0.15-0.20 V for the micropeened ones. Pitting of the micropeened specimens thus starts about 100 millivolts more cathodic under these circumstances.

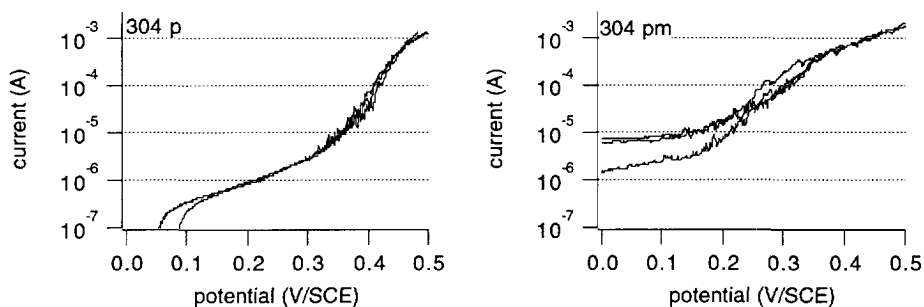


Figure 5.1. Part of the current-potential curves of ss 304 measured (in triplicate) after polishing (p) and micropeening (pm) the surface.

The current-potential curves of ss 316, recorded after polishing (3  $\mu\text{m}$  diamond paste), grinding (grit P220) and after micropeening the polished or ground surfaces were recorded and are shown, from 0.2 to 1.2 V/SCE, in figure 5.2. Although the curves are difficult to interpret because of the large current fluctuations and big differences especially in the potential region from 0.7 to 1.2 V/SCE, some general characteristics can be noticed. Upon anodic polarization of the polished (p) samples, figure 5.2a, two of the three samples show a considerable current increase at about 0.65 V, the third sample showed a marked current increase only at 1.1 V. The curves of the ground (g), polished and micropeened (pm), ground and micropeened (gm) and rolled (rg) specimens, figure 5.2b-e, are similar in some respects. They all show a current plateau from 0.4 V to the moment of the major current increase, mostly at 0.6-0.8 V, and a generally higher current at all potentials compared with the curves of the polished samples. The current at the plateaus of the rolled and micropeened specimens is higher than for the ground specimens. The curves measured for the micropeened specimens, figure 5.2c and 5.2d, are similar despite the different treatment before micropeening. The curves of the rolled specimens show more disturbing current fluctuations than the curves of the ground specimens, but less than the micropeened specimens. The major current increase for the ground specimens takes place between 0.7 and 1.2 V, for the micropeened specimens between 0.6 and 0.7 V and for the rolled specimens at 0.65 and 0.75 V. Micropeening of polished ss 254

SMO, see figure 5.3, led to an increased current density at all potentials as well, but not to current fluctuations.

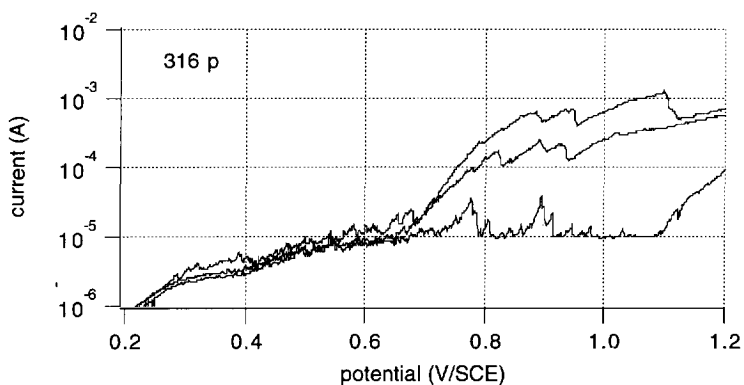


Figure 5.2a

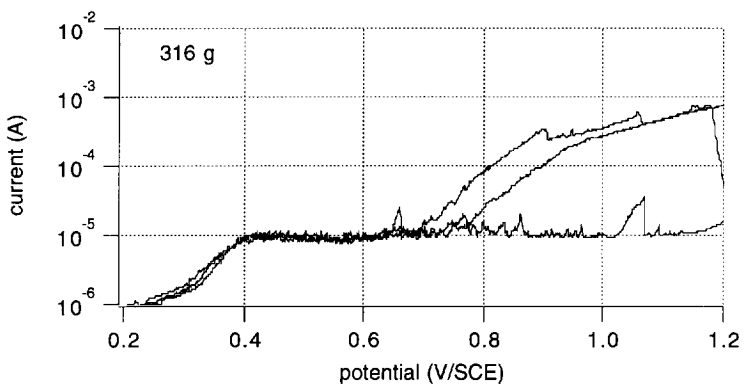


Figure 5.2b

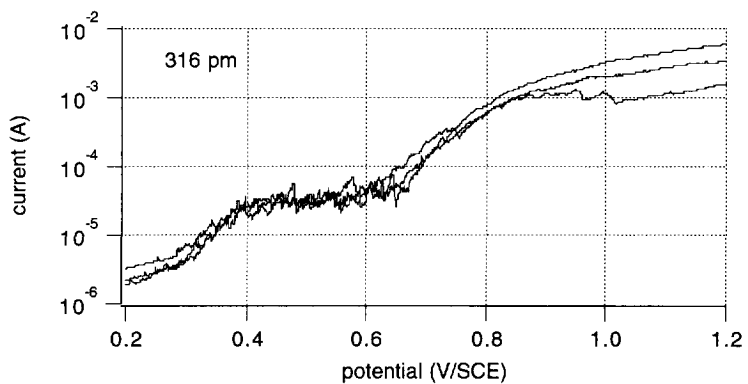


Figure 5.2c

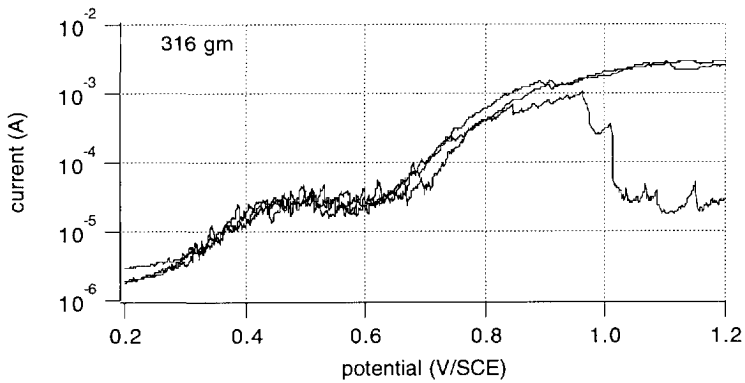


Figure 5.2d

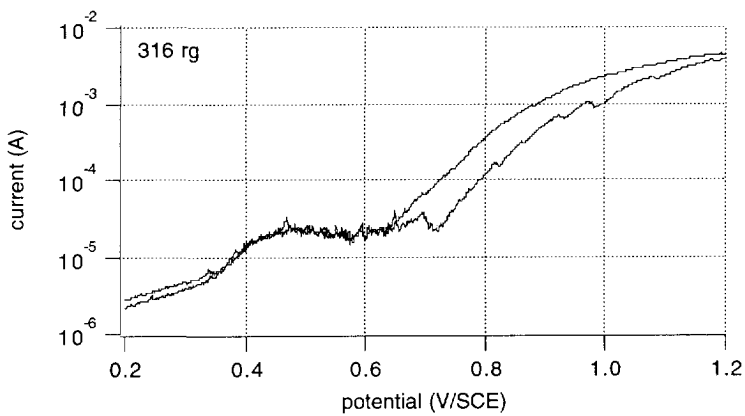


Figure 5.2e

Figure 5.2a-e. Part of the current-potential curves of ss 316, measured after polishing (p), grinding (g), micropeening (pm and gm) and rolling (rg) the surface.

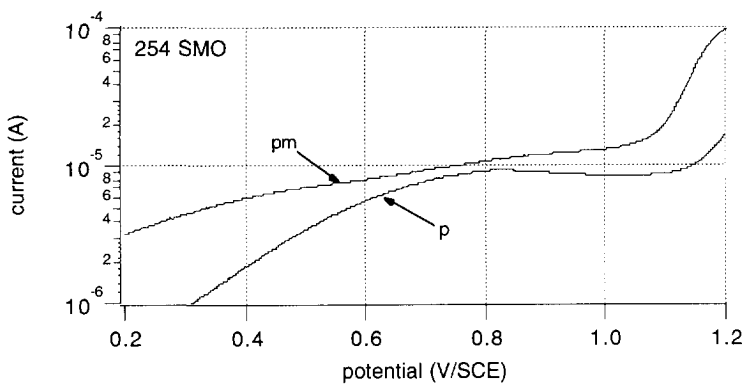


Figure 5.3. Part of the current-potential curve of polished (p) and micropeened (pm) 254 SMO.

The charge accompanying the polarization was calculated from the curves, from the start of the measurement up to 0.5 V, 0.8 V, 1.0 V and 1.2 V, see table 5.1. The considerable scatter is reflected again. But it is still clear that more charge is related to the curves of the micropeened and rolled ss 316 specimens compared with the polished and ground ones. For ss 304 and 254 SMO polarization of the micropeened specimens is related with more charge than polarization of polished specimens as well.

		Q (mC) OCP-0.5 V	Q (mC) OCP-0.8 V	Q (mC) OCP-1.0 V	Q (mC) OCP-1.2 V
304 p	1	56			
	2	56			
	3	80			
304 p m	1	160			
	2	160			
	3	151			
316 p	1	1.2	15	117	273
	2	1.0	4.3	7	12
	3	0.9	9.2	44	124
316 g	1	1.6	4.9	30	128
	2	1.6	4.8	7	10
	3	1.6	7.4	56	155
316 p m	1	5.6	57	260	490
	2	4.4	48	323	866
	3	5.0	57	451	1363
316 g m	1	4.2	43	305	770
	2	3.5	34	158	167
	3	4.1	30	264	784
316 rg	1	3.4	26	269	955
	2	3.2	13	121	619
254SMO p	1	0.5	2.4	4.2	6.1
254SMO p m	1	2.0	4.6	7.0	13.9

Table 5.1. The charge associated with the current-potential curves of polished (p), ground (g), micropeened (pm and gm) and rolled (rg) surfaces, calculated from the OCP to 0.5 V, 0.8 V, 1.0 V and 1.2 V.

### 5.3.2 Current spikes

Current spikes were measured at 150 mV/SCE (ss 304), 250 mV/SCE (ss 316) or 550 mV/SCE (ss 254SMO). Typical current-time curves are given in figure 5.4. The curves of the polished samples all show an inexplicable current increase shortly after the beginning of the measurements. The results of the current spikes measurements are listed in table 5.2. In figure 5.5 some details of the curves of ss 316 are shown. In figure 5.6 the differently treated specimens of ss 316 are compared with respect to the charge related to the spikes. Grinding, rolling and micropeening results in more spikes compared with polishing, see table 5.2 and figure 5.6a, but the size of the spikes is smallest for the ground specimens, see figure 5.6b. Surprisingly, some spikes were also found upon testing ss 254 SMO with a micropeened surface. These small spikes showed typically a fast current increase and decrease, see figure 5.7.

	potential (mV/SCE)	number of spikes	average width (s)	average height (nA)
304 p	150	80	2.0	86
304 pm	150	1423	2.9	186
316 p	250	160	5.4	158
316 g	250	1250	1.6	61
316 pm	250	1032	4.0	134
316 gm	250	938	4.0	138
316 r	250	1635	2.1	66
254 SMO p	550	0		
254 SMO pm	550	15	1.1	72

*Table 5.2. Results of the current spikes measurements of ss 304, ss 316 and ss 254 SMO, average of three experiments except for 254SMO (one measurement) and 316rg and 316g (two measurements).*



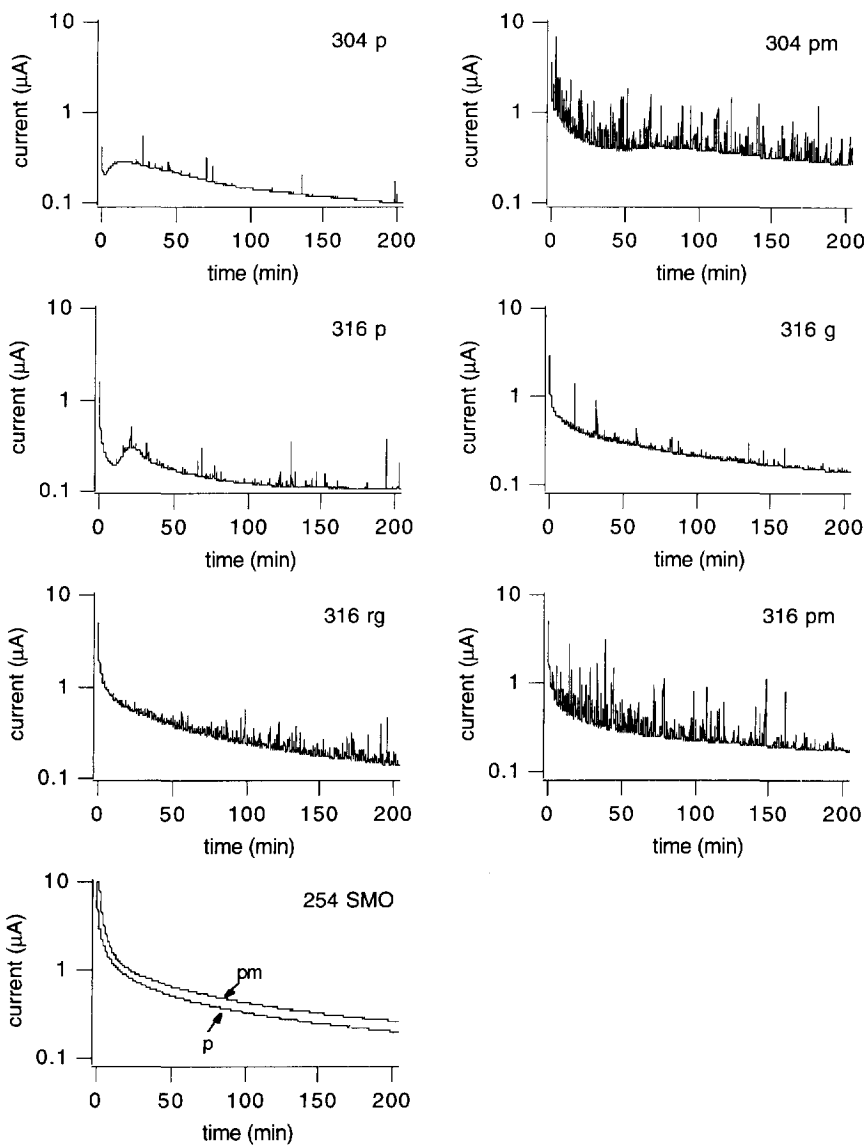


Figure 5.4. Typical current-time curves for ss 304 (150 mV/SCE), ss 316 (250 mV/SCE) and ss 254SMO (550 mV/SCE) measured after grinding (g), polishing (p), micropeening (m) or rolling (rg).

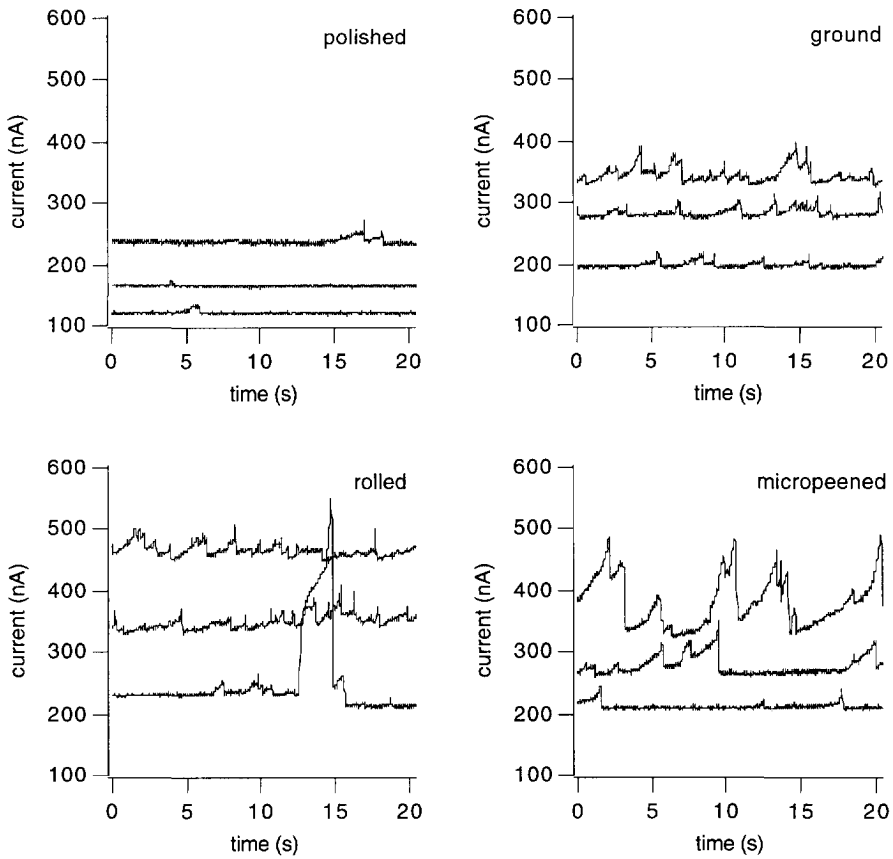
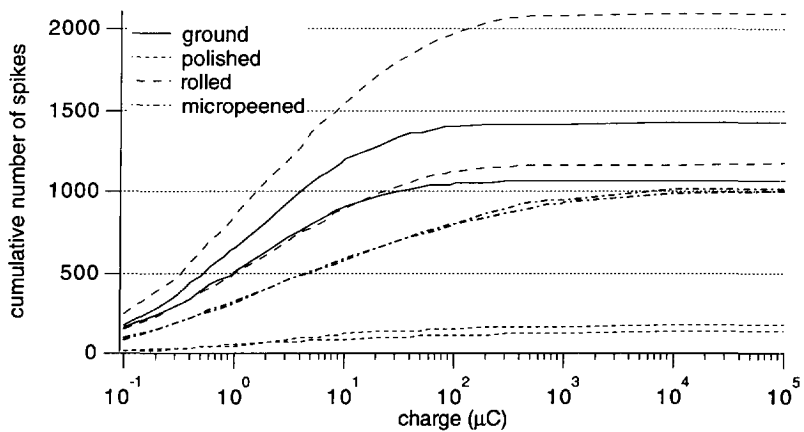
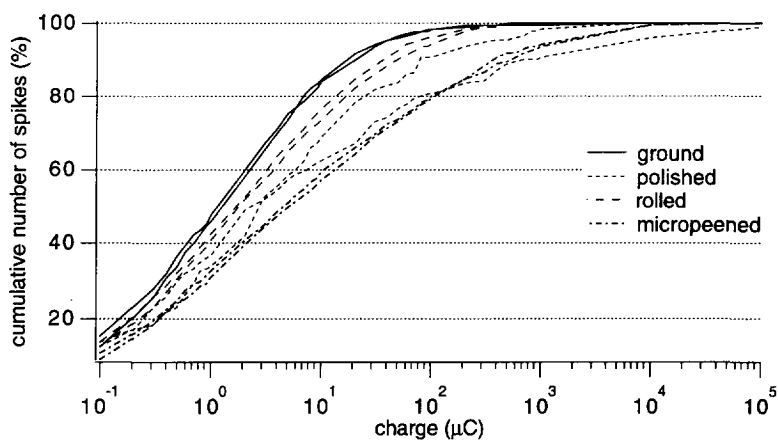


Figure 5.5. Parts of the current-time profiles of ss 316 polished, ground, rolled and micropeened. The curves represent the current after 30 minutes (top curve), 50 minutes (middle curve) and 100 minutes (bottom curve) measured from the moment the potential was applied.



a



b

Figure 5.6. Cumulative number of spikes as a function of the charge for ss 316 polished, ground, rolled and micropeened specimens, 250 mV/SCE.

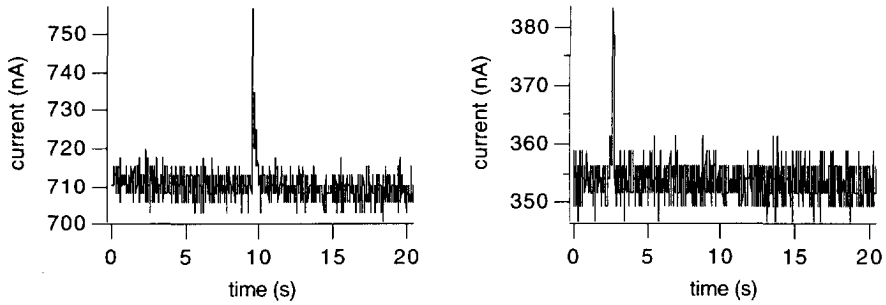


Figure 5.7. Two typical spikes from micropeened ss 254 SMO, 550 mV/SCE.

The hardness was measured across a cross-section of a rolled and a micropeened specimen, see figure 5.8. Rolling had resulted in an increased hardness which is approximately constant throughout the sample. The micropeened specimen had a surface layer of about 200  $\mu\text{m}$  with an increased hardness. The surface roughness of the polished, ground and micropeened specimens was determined and is shown in figure 5.9. It should be noticed that the vertical scale for the polished and ground surfaces differs from the scale used for the micropeened surface. Finally, scanning electron microscopic pictures of the ground and micropeened surface of ss 316 are shown in figure 5.10 and 5.11.

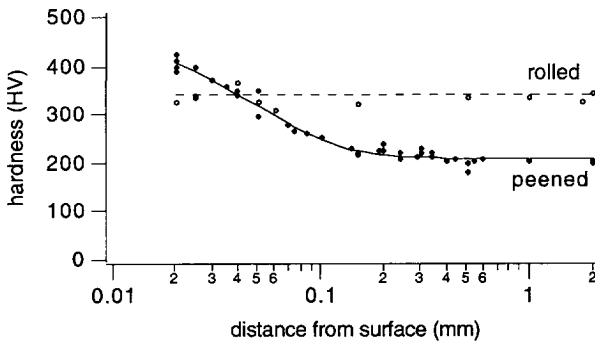


Figure 5.8. The hardness measured on a cross-section of micropeened and rolled ss 316 specimens.

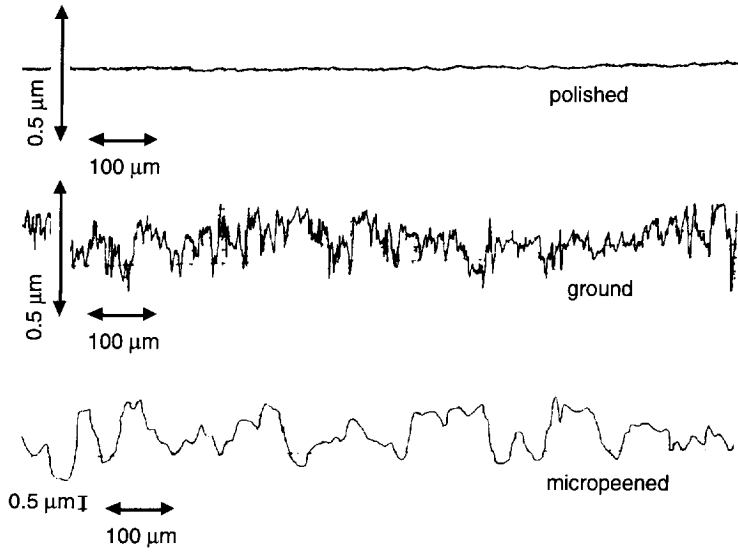
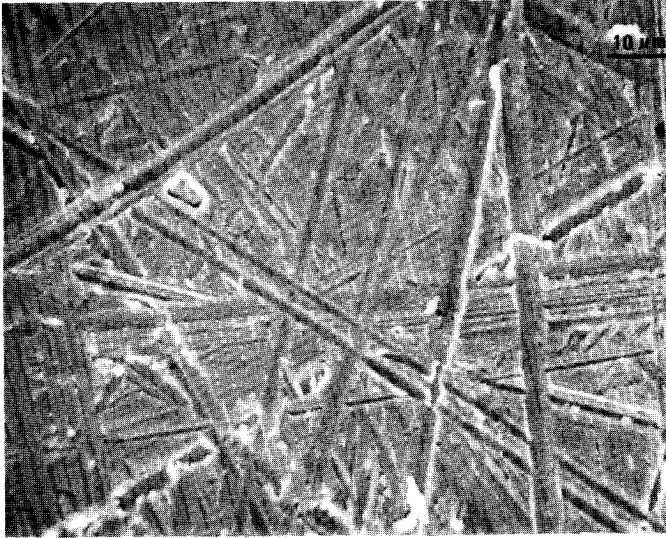


Figure 5.9. Surface roughness of polished, ground and micropeened samples of ss 316.



*Figure 5.10. The surface of ss 316 after grinding.*



*Figure 5.11. The surface of ss 316 after polishing and subsequent micropeening.*

## 5.4 Discussion

For ss 304 the current-potential curves, figure 5.1, show that micropeening causes the major current increase to occur at more cathodic values, which can be interpreted as an increase of the susceptibility to pitting. More charge is associated with the curves of the micropeened specimens, see table 5.1, indicating more metal loss during polarization. The current spikes measurements, see figure 5.4 and table 5.2, show that micropeening of a polished surface drastically increases the number of spikes, from 80 to 1423. Also the passive current at this potential (150 mV/SCE) is increased by micropeening. The spikes from micropeened surfaces have a longer average lifetime (2.9 s compared with 2.0 s) and higher current peaks (186 nA compared with 86 nA). All the measurements indicate that micropeening of a polished ss 304 surface increases the susceptibility to localized corrosion under these test conditions.

The current-potential curves of ss 316, figure 5.2, show large current fluctuations. In some experiments, figure 5.2a and 5.2b, a specimen surface remains passive during the measurement, but in most cases a current increase between 0.6 and 0.8 V/SCE indicates stable pitting. This potential differs only slightly for the curves of polished, ground, micropeened and rolled samples. The appearance of the curves is related to the treatment of the sample. The curves of ground, micropeened and rolled specimens, figure 5.2b-e, show a region where the current is almost independent of the potential, about 0.4 to 0.6 V. The current level is higher for rolled and micropeened specimens compared with ground specimens. This is probably due to the extra stress present in rolled and micropeened specimens. Grinding is also known to cause a slightly stressed surface, which would explain the difference between polished samples on the one hand (no current plateau) and ground and micropeened samples on the other hand. But it remains unclear why such current plateaus exist. Further research is needed for clarification of this phenomenon.

The data in table 5.1 confirm once again the large differences between current-potential curves measured in triplicate or duplicate on similar surfaces of ss 316. But still it can be seen that the extra stress induced by

rolling or micropeening increases the charge related to the current-potential curves, when compared with the ground ss 316 specimen.

Similar to what was seen for ss 304, micropeening of polished ss 316 surfaces increases the number of spikes, from 160 to 1032, see figure 5.4, figure 5.5 and table 5.2. Compared with the ground surface however micropeening does not lead to an increase in the number of spikes.

The size of the spikes measured on the various ss 316 specimens shows clear differences. In figure 5.6 the results are shown for two measurements of each treatment. Figure 5.6b shows that the size of the spikes can be ranked as ground < rolled < polished < micropeened. The treatments influence different aspects of the spikes, see table 5.2. Compared with ground specimens, rolling increases mainly the average width, from 1.6 to 2.1 s, and hardly the height of the spikes, whereas polishing and micropeening increase both the width, from 1.6 to 5.4 and 4.0 s respectively, and the height, from 61 to 158 and 134/138 nA respectively. The comparable effects of micropeening and polishing can hardly be explained by a similar mechanism.

The lifetime of a spike is determined by the ability of the cover over an occluded cell to withstand rupture. Increasing the stress would promote rupture, as was suggested in literature<sup>19,20</sup>. Ground surfaces are more stressed than polished ones, which explains the increased width of the spikes in case of polished surfaces. Because during this time the extent to which the local solution is acidified is increased, and because a larger surface area has to repassivate in the end, the current peak after the major breakthrough of the cover over the occluded cell is higher on polished than on ground samples.

The lifetime of a spike would be expected to be even smaller in case of a highly stressed surface layer which results from the micropeening treatment compared with ground surfaces. But the spikes have a longer lifetime than the spikes which originated at ground surfaces. The morphology of the surfaces differs markedly, see figure 5.9, 5.10 and 5.11. The 'large scale' wave-like roughness of the micropeened surfaces can not be expected to be of importance in providing occluded regions for localized corrosion starting at inclusions of only several  $\mu\text{m}^3$ . However, the scanning electron microscopic pictures show a kind of roughness, obscured in figure 5.9, which could be of importance. A lot of small



crevices can be seen to exist. These crevices would provide occluded regions in which localized corrosion can continue for a while. A solid shell is provided and localized corrosion can proceed relatively long.

The increase of the number of spikes by micropeening compared with polished samples is due to the increase in this secondary surface roughness. Not only more inclusions lie at the surface because of the increased effective surface area, but also more occluded cells are provided *a priori* where localized dissolution, starting at (even small) inclusions, can proceed.

Rolling of the ss 316 specimens led to slightly larger spikes, see figure 5.6b. Especially the lifetime of the spikes is longer, but the current peaks also seem slightly higher. The increase in lifetime could be due to a more unfavourable geometry of the inclusions after rolling. The ductile manganese sulphide inclusions can be further elongated, giving possibly more unfavourable crevices upon attack.

The measurements on polished and micropeened ss 254 SMO specimens show again that the current increases because of a stressed surface layer. The few small spikes indicate that the surface is activated locally. Possibly some inclusions dissolve at this relatively high potential (550 mV/SCE) and current spikes are now visible because of the relatively high currents involved due to the stress in the surface or because of the well occluded regions provided by the surface treatment. Further research would be needed for clarification.

The pit density is not considered in this chapter because of the difficulty of identifying pits on the ground and especially the micropeened surfaces.

## 5.5 Conclusions

Micropeening a polished surface increases the number of sites where localized corrosion can be initiated, as demonstrated by a large increase of the number of current spikes. Pitting initiation starts at slightly more cathodic values in current-potential measurements.

Micropeening a ground surface does not increase the number of initiation sites but the extent of localized attack, as indicated by a marked increase of the size of the spikes. This could be caused by the crevices

which can be observed on the micropeened surfaces. They can provide the (solid) occluded region needed for localized attack to proceed for a while.

Additional rolling of ss 316 specimens results in a slightly increased size of current spikes.

Stress induced by rolling or micropeening leads always to larger current densities. The stress caused by grinding is beneficial because, compared with a polished surface, it decreases the size of the spikes. The stress promotes breakdown of the occluded cell cover and thus enhances repassivation after local activation.

## 5.6 References

- 1 G. Nachman, in Shot Peening, Proceedings of the Third International Conference on Shot Peening, Ed. H. Wohlfahrt *et.al.*, Deutsche Gesellschaft für Metallkunde, Oberursel, Germany (1987) 37-48.
- 2 P. O'Hara, *Trans. Inst. Metal Finish.*, **68** (1990) 87-91.
- 3 O. Clancy, J. Ponsonby, L. McCarthy and D. Taylor, *Surface Engineering* **3** (1987) 64-68.
- 4 H. Wohlfahrt, in Shot Peening, Proceedings of the Third International Conference on Shot Peening, Ed. H. Wohlfahrt *et.al.*, Deutsche Gesellschaft für Metallkunde, Oberursel, Germany (1987) 563-584.
- 5 A. Ebenau, O. Vöhringer and E. Macherauch, in *Shot Peening*, Proceedings of the Third International Conference on Shot Peening, Ed. H. Wohlfahrt *et.al.*, Deutsche Gesellschaft für Metallkunde, Oberursel, Germany (1987) 253-260.
- 6 K. Risch, in *Shot Peening*, Proceedings of the Third International Conference on Shot Peening, Ed. H. Wohlfahrt *et.al.*, Deutsche Gesellschaft für Metallkunde, Oberursel, Germany (1987) 141-148.
- 7 B. Gillespie, in *Shot Peening*, Proceedings of the Third International Conference on Shot Peening, Ed. H. Wohlfahrt *et.al.*, Deutsche Gesellschaft für Metallkunde, Oberursel, Germany (1987) 149-156.
- 8 M.J. Povich, *Corrosion* **34** (1978) 162-169.
- 9 A.M. Brass, J. Chêne, G. Anteri, J. Ovejero-garcia and L. Castex, *J. Mater. Sci.* **26** (1991) 4517-4526.
- 10 H. Werner, C. Voigt, G. Riedel, J. Müller and K. Feist, *Korrosion, Dresden* **22** (1991) 175-187.

- 11 K.H. Kloos and E. Macherauch, in *Shot Peening*, Proceedings of the Third International Conference on Shot Peening, Ed. H. Wohlfahrt et.al., Deutsche Gesellschaft für Metallkunde, Oberursel, Germany (1987) 3-28.
- 12 R. Stefec and F. Franz, *Corros.Sci.* **18** (1978) 161-168.
- 13 A. Randak and F.-W. Trautes, *Werkst. Korros.* **21** (1970) 97-109.
- 14 T.M. Devine, *J.Electrochem.Soc.* **124** (1977) 38-44.
- 15 R.B. Diegle, *Corrosion* **36** (1980) 362-368.
- 16 M.B. Ives and S.C. Srivastava, in *Advances in Localized Corrosion (NACE-9)*, ed. H.S. Isaacs, U. Bertocci, J. Kruger and S. Smialowska, NACE, Houston, USA (1990) 295-302.
- 17 S.C. Srivastava and M.B. Ives, *Corrosion* **45** (1989) 488-493.
- 18 Z. Szklarska-Smialowska, *Pitting Corrosion of Metals*, NACE, Houston, USA (1986).
- 19 G.S. Frankel, L. Stockert, F. Hunkeler, H. Böhni, *Corrosion* **43** (1987) 429-436.
- 20 H.S. Isaacs, G. Kissel, *J. Electrochem. Soc.* **119** (1972) 1628-1632.

# GENERAL CONCLUSIONS AND RECOMMENDATIONS

## 6.1 General conclusions

The investigations reported in this thesis have led to a better understanding of several aspects of localized corrosion of commercial stainless steels. The role of inclusions has become more clear and the complex effects of surface deformation are better understood. But still a lot of questions remain unanswered. Even more have been raised by this work, and they will be discussed in the next section. In this section the conclusions from the experimental chapters have been gathered and combined.

Localized attack starts at weak spots in the metal surface, which have been identified to be mainly manganese sulphide inclusions in ss 304, ss 316, ss 316L and ss 317L, all alloys with a relatively high sulphur content ( $> 0.011\%$ ). The sulphide inclusions dissolve readily under the given experimental circumstances. Dissolution of an inclusion is the first step of localized attack. In highly alloyed steels with low sulphur contents ( $< 0.003\%$ ) no separate manganese sulphide inclusions were found. In ss 254 SMO no soluble inclusions at all were identified, which will attribute to the excellent pitting resistance of this alloy. Although it has to be noted that minor local activation was detected on a micropeened surface. Relatively few soluble sulphur containing and magnesium containing inclusions were found in respectively ss 34LN and SAN28, and only occasionally local activation could be detected.

The dissolution of an inclusion itself can not be measured using the equipment developed for the measurement of current spikes. Only when

the dissolution of an inclusion is followed by attack of the surrounding metal a current spike can be registered. The number and the size of the current spikes reflect the number of sites where such prolonged attack takes place and the extent of the localized attack respectively. Upon increasing anodic polarization the spikes become larger until finally pits do not repassivate any more (stable pitting). The number and size of the current spikes are considered to reflect the pitting susceptibility of the steel.

A number of factors was found to influence the extent of localized attack. The factors will be dealt with successively.

*The potential.* The higher the applied potential, the more sites can be activated at the steel surface (chapter 3). The theory described by Pistorius<sup>1</sup> is suitable to explain the results. At high anodic potentials, hemispherical brightening pits are formed on ss 316, in accordance with the theory developed by Sato<sup>2</sup>.

*The size of the inclusion.* The more large manganese sulphide inclusions are present in a steel, the more sensitive it is for localized corrosion (chapter 3 and 4). It has been suggested<sup>3,4</sup> that sulphur (compounds), formed upon dissolution of manganese sulphide inclusions, catalyse dissolution of the steel matrix. This would explain the results.

*The composition of the inclusion.* Dissolution of an inclusion depends on its composition (chapter 3 and 4). Especially (manganese) sulphide inclusions, and maybe also magnesium containing inclusions, were found to dissolve readily under the experimental circumstances, 0.1 M NaCl and 350 mV/SCE. Stable inclusions do not cause spikes. Furthermore, dissolution products from manganese sulphide inclusions could promote further attack, as discussed before. The absence of such inclusions in some highly alloyed steels with a low sulphur content contributes to the good pitting resistance of these alloys.

*The geometry of the inclusion.* Inclusions were found to be elliptically shaped. Upon dissolution this can lead to undercutting of the passive film as is shown to occur (chapter 3). Unfavourable occluded cells are thus created.

*Neighbouring inclusions (stringers).* Sulphide inclusions were found to be present as stringers (chapter 3). Localized attack can proceed easily along such stringers.

*Alloying elements.* Compared with ss 316, larger spikes were measured on the higher alloyed steels 317L and 34LN (chapter 4). The oxide films of these steels remain intact for longer periods and therefore provide better covers for occluded cells. Local attack can get more severe. A similar reasoning explains why large spikes were measured on pickled surfaces (chapter 3). The results support the view of Isaacs<sup>5,6</sup> and Frankel<sup>7</sup> that the stability of the passive layer is of importance. Of course, the repassivation ability is improved with increasing contents of chromium, nickel and molybdenum. This reduces the chance for prolonged localized attack proportionally.

*The pH of the electrolyte solution.* Increasing the pH leads to a decrease in the number of activated sites (chapter 3). At sufficiently high pH values, inclusions do not dissolve any more or the freshly exposed metal repassivates immediately upon contact with the electrolyte solution, and initiation sites for localized attack are thus eliminated (chapter 3).

*The concentration of the chloride ions.* A higher chloride concentration increases the rate of attack. Critical situations are reached sooner, upon which attack proceeds (chapter 3).

*Inhibiting anions (acetate) in the electrolyte solution.* In the presence of acetate in addition to chloride ions, less sites are activated (chapter 3). The mechanism is unclear. It could be caused by buffering of the local electrolyte solution or by hinderance of the dissolution of inclusions (chapter 3).

*Catalysing anions in the electrolyte solution.* Thiosulphate in low concentrations catalyses dissolution of the steel, and increases the rate of localized attack compared with thiosulphate free solutions. The action resembles the action of an increased chloride concentration and can be explained accordingly. High concentrations of thiosulphate reduce the number of sites where localized attack proceeds, similar to the action of acetate (chapter 3).

*Stress.* Stress induces higher current densities. From comparison of ground and polished surfaces it was concluded that the stress due to grinding is beneficial because it enhances breakdown of the cover over occluded cells (chapter 5).

*The surface roughness.* The roughness resulting from grinding is detrimental as a ground surface provides more occluded regions for

localized attack than a polished surface. The 'large scale' roughness resulting from micropeneing does not provide such regions, but the small crevices formed in the process of peening do provide solid shells for localized attack.

The general view that 'critical concentrations' must be reached in order to get on-going attack (section 2.3.4) is a very suitable concept with which most of the phenomena described above can be qualitatively explained.

## **6.2 Recommendations**

The research was mainly a qualitative investigation of several aspects of pitting corrosion. This research project can be considered as a basis for further research work on localized corrosion. The results presented in this thesis offer several interesting leads for further studies.

The current spikes measurements proved to be adequate for this research. However, the spikes occurring immediately after applying the potential could not be analysed. By modification of the technique, namely a gradual increase of the potential from the OCP to the desired value, it should be possible to detect initial localized activation more accurately.

The detection limit for current spikes was about 5 nA, and for most measurements reported in this thesis, this was even not fully exploited. It is possible to detect smaller current spikes. With some modifications it should even be possible to measure current fluctuations in the pico-ampere regime. This offers new possibilities for further research.

The inclusions have been characterized as far as elemental composition is concerned, but the chemical state has not been elucidated. To do this is an almost impossible assignment, if all the types of inclusions in all the steels were to be studied. But more detailed investigations especially of exposed steels are necessary in order to gain more insight in the types of attack, possible dissolution products (sulphur) of soluble inclusions, salt films and occluded cell covers. At higher anodic potentials or more severe solution conditions (strong acids), it is likely that sites of attack at 'complex' inclusions or at the border of the inclusions and the steel matrix will be found, especially in the highly alloyed steels with a low sulphur

content (which are usually applied in aggressive environments). The small spikes measured on micropeened ss 254 SMO already indicated that local activation is possible under certain conditions (chapter 5).

Some phenomena reported in this thesis still ask for an appropriate explanation. For example the current plateaus seen in the current-potential curves of stressed ss 316 surfaces (chapter 5), the current increase seen in the current-time profiles of polished samples (chapter 5) and the mechanism by which acetate and thiosulphate influence localized attack (chapter 3).

Only commercial steels have been investigated. The mechanisms of pit propagation, especially the critical situations which cause progressive localized attack, should be studied at model alloys.

It has been shown that current spikes measurements can provide useful additional information on the pitting susceptibility of an alloy, information that could not be deduced from current-potential curves. The method seems also useful to rank highly alloyed stainless steels, in spite of the scatter in the number and size of the spikes, which is caused by variations in the (cross-sections of) inclusions. The method of measuring current spikes is suitable for more extensive application, if commercial equipment would be developed.

### 6.3 Literature

- 1 P.C. Pistorius and G.T. Burstein, *Phil. Trans. R. Soc. Lond. A* **341** (1992) 531-559.
- 2 N. Sato, *J. Electrochem. Soc.* **129** (1982) 260-264.
- 3 J. Stewart and D.E. Williams, *Corros. Sci.* **33** (1992) 457-474.
- 4 R. Ke, R. Alkire, *J. Electrochem. Soc.* **139** (1992) 1573-1580.
- 5 H.S. Isaacs and G. Kissel, *J. Electrochem. Soc.* **119** (1972) 1628-1632.
- 6 H.S. Isaacs, *Corros. Sci.* **29** (1989) 313-323.
- 7 G.S. Frankel, L. Stockert, F. Hunkeler, H. Böhni, *Corrosion* **43** (1987) 429-436.





## INFORMATION ON THE STAINLESS STEELS

In table A.1, the stainless steels discussed in this thesis are listed with several designations: the American Iron and Steel Institute (AISI) numbering system, the Unified Numbering System (UNS) and the Deutsche Industrie Norm (DIN, Werkstoff-Nr.). In table A.2 the alloy compositions are given.

alloy	AISI	UNS	DIN
304	304	S30400	1.4301
316	316	S31600	1.4436
316L	316L	S31603	1.4404
317L	317L	S31703	1.4438
34LN			1.4439
SAN28		N08028	1.4563
254SMO		S31254	

*Table A.1. The stainless steels with the designation according to some national product standards. SAN28 is an abbreviation for sanicro28.*

Stainless steel type 304 is the most common alloy. By adding molybdenum, the corrosion resistance is improved. Austenitic grades with up to 6% molybdenum (ss 254SMO) can be produced when nitrogen is used to stabilize the austenite phase. Well-known are the differences between ss 304 and 316. The better resistance of ss 316 to pitting corrosion is usually

attributed to the molybdenum content. Stainless steels 317L and 34LN are considered as improved 316 alloys with respect to the corrosion resistance.

Some applications for the steels are listed in table A.3. The ss 316 and 316L used in the studies for this thesis were of "Prodec" quality. This is a designation for alloys with good machining properties due to a high sulphur content.

alloy	Cr	Ni	Mo	C	Mn	P	S	Si	others
304	18-20	8-11		0.08	2.0	0.045	0.03	1.0	
316	16-18	10-14	2.0-3.0	0.08	2.0	0.045	0.03	1.0	
316L	16-18	10-14	2.0-3.0	0.03	2.0	0.045	0.03	1.0	
317L	18-20	11-15	3.0-4.0	0.03	2.0	0.045	0.03	1.0	
34LN	16.5-18.5	12.5-14.5	4.0-5.0	0.03	2.0	0.045	0.03	1.0	
SAN28	26-28	30.0-34.0	3.0-4.0	0.03	2.0	0.03	0.03	1.0	Cu 0.6-1.4
254SMO	19.5-20.5	17.5-18.5	6.0-6.5	0.02	1.0	0.03	0.01	0.8	Cu 0.5-1.0 N 0.18-0.22

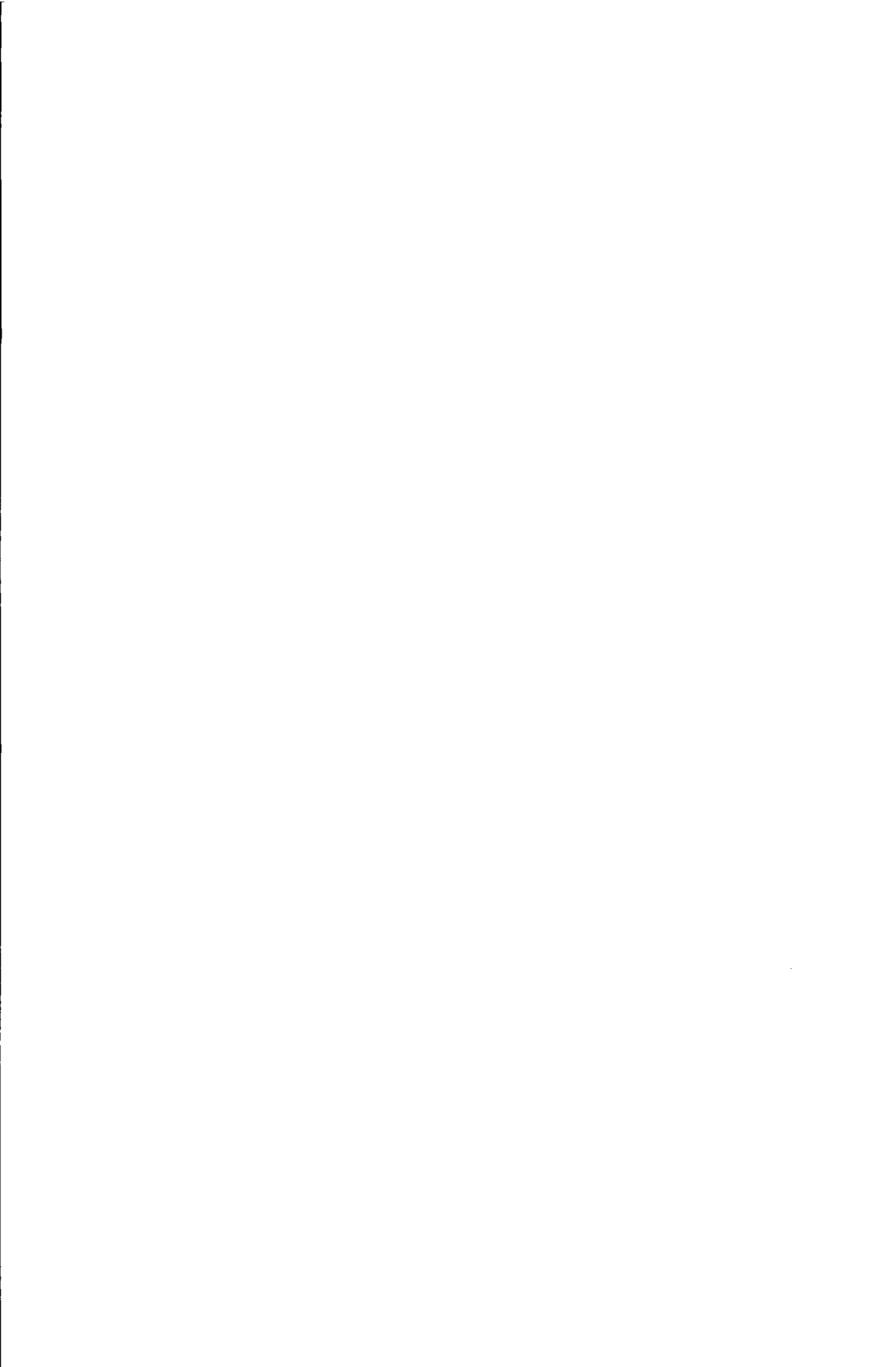
Table A.2. Compositions of the alloys, (maximum) weight per cent, balance of iron<sup>1,2</sup>.

alloy	some applications
304	equipment for use in food industry, chemical industry and breweries
316	equipment for use in the textile industry, chemical industry and swimming pools
317	equipment for use in the cellulose industry and chemical industry, transport containers for chemicals, in dyeing and ink manufacturing equipment
34LN	equipment for use in chloride environments, use in chemical industry and photo industry
SAN28	pipes, fittings, flanges in phosphoric acid environments and chloride environments, piping for oil and gas transportation, heat exchangers in nuclear plants
254SMO	equipment for use in contact with sea water, at pulp bleaching plants, gas cleaning systems, tanks and pipelines and for the distillation of tall oil

Table A.3. Some applications of the stainless steels; information from the steel producers and reference 2.

## References

- 1 R.M. Davison, T. DeBold and M.J. Johnson, in *Metals Handbook Ninth Edition, Vol 13, Corrosion*, American Society for Metals, Metals Park, Ohio, USA (1987).
- 2 *Stahlschlüssel*, Verlag Stahlschlüssel Wegst GmbH, Marbach, Germany (1989).

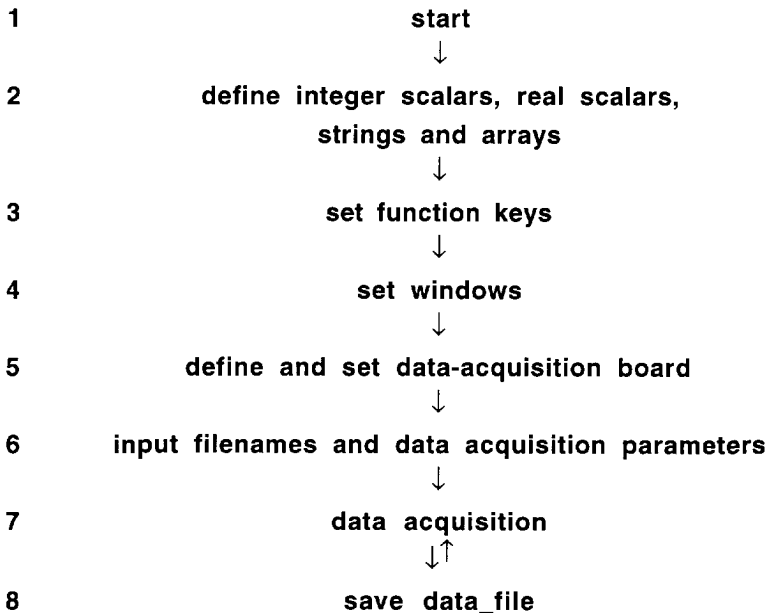


# STRUCTURE OF THE COMPUTER PROGRAMS

## B.1 Data acquisition

The structure of the data acquisition program is as follows (print procedures excluded).

( $\downarrow\uparrow$  = loop)



↓

9                    **transform data from DAS16 format**

↓

10                   **make and save view**

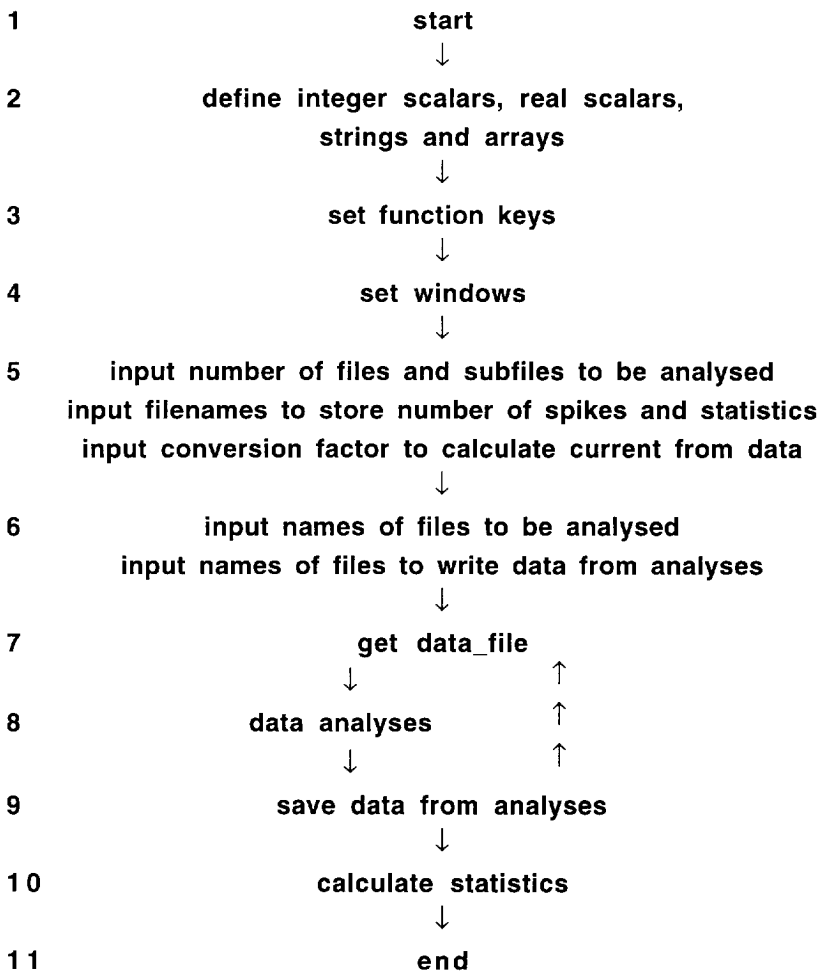
↓

11                    **end**

- ad. 5. A DAS16 board is used for the data acquisition. Defined are: the channel, mode (analog to digital conversion), the buffer length (1024 integers) and data acquisition control by an external clock.
- ad. 6. The number of files and subfiles are defined, at the most 20 files with each 30 subfiles. Each subfile consists of an array of 1024 integers. The gain for the board is set.
- ad.7. Uninterrupted data acquisition by direct memory access. The output from potentiostat ranges between -10 and 10 V, which equals 10 times the selected range of the current. The isolation amplifier multiplies the signal with a factor 0.5. The board is set at 0 to 5 V (the current from the potentiostat is always anodic, thus positive). The overall resolution is 10 times the selected current range divided by 4096 ( $2^{12}$ ). The external clock triggers with the exact frequency of the main electricity supply, about 50 Hz. With 20 subfiles consisting of 30 subfiles, uninterrupted data acquisition lasts 205 minutes. The time is not stored.
- ad.10. View is a file which contains information on the general development of the current during the whole experiment (205 minutes). It is constructed by two points calculated from each array (containing 1024 numbers): the mean of the first 10 numbers and the mean of 10 numbers from 510 to 520.

## B.2 Data analysis

The structure of the data analysis program is as follows (printing routines excluded).



ad.8. Determined are: the start of a spike, the maximum current and the end of the spike. The width, rise (time from the start until the maximum current is reached), fall (time from the moment of



maximal current until the end of the spike, width = rise + fall) and charge are calculated. The procedures to find a spike are as follows. First a copy (work array) is made from the data array (subfile with 1024 integers). Then the 'baseline', the passive current level including the noise, is determined and the work array is made equal to this. Spikes are identified by comparing the two arrays, see figure B.1. Thus no further (high frequency) information on the spikes is lost (as would be the case when filtering procedures are applied). The procedures are described below.

**get data\_array [1024] from data\_file**

find passive current value (incl. noise) and make this the work\_array (incl. noise):

**sort copy\_data\_array values low - high**

**average values 100 to 115 =: basevalue** (=: means 'is assigned to')

**(basevalue)<sup>0.25</sup> \* 1.5 + basevalue =: linefactor1**

**(basevalue)<sup>0.25</sup> \* 1.5 \* 2.5 + basevalue =: linefactor2**

**linefactor2 - basevalue =: differ**

make work\_array:

**I = 1 to 1024**

**if linefactor1 > data\_array[I]**

**and linefactor1 > data\_array[I-1]**

**then data\_file[I] =: work\_array[I]**

**else basevalue =: work\_array[I]**

to recognize a fast rising spike:

**if data\_array [I] > work\_array[I]**

**and data\_array[I+1] > linefactor2**

**then spike is recognized**

to recognize a slow rising spike:

**if data\_array[I+1] > work\_array[I+1]**

**and data\_array[I] < data\_array[I+1]**

**and data\_array[I] < data\_array[I+2]**

**then spike is recognized**

if spike is recognized then find current maximum:

**keep largest value as current.m**

```

current.m - basevalue =: current.max
and find end of a spike:
work.array[l] = data_array[l]
or (end of a 'hidden' spike):
data_array[l] < data_array[l+1]
and data_array[l] < data_array[l+2]
and data_array[l-1] - data_array[l] > differ
a spike is stored if current.m > line.factor2

```

If a current spike is not ended at the end of a data array, the procedure is continued on the next data array. In this case the basevalue is not calculated again.

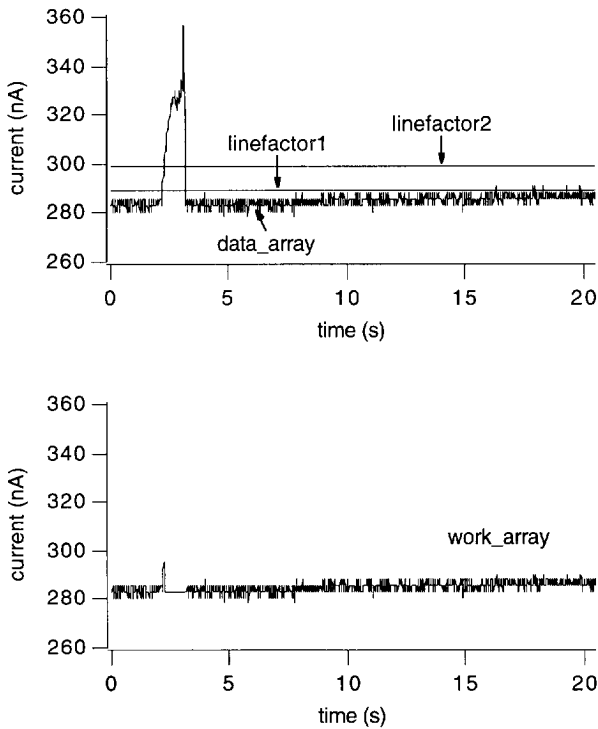


*Figure B.1. Illustration of the search procedure for current spikes. The 1024 values of a data array are plotted as a function of a time array, which can be made independently.*

ad.10. After analysing all the defined files and subfiles, the following data are calculated: total number of spikes, the average width of the spikes, the average rise of the spike (from start of the spike until the current is maximum), the average fall (from the current maximum to the end of the spikes), the average maximum current, the number of spikes excluding hidden spikes, their average width and current maximum. With all the averages, the standard deviations are calculated. All these data are also calculated for all the files minus the first one (614 s).

## SUMMARY

In this thesis some qualitative aspects of pitting corrosion of highly alloyed stainless steels are discussed. Special attention is given to the method and value of current spikes measurements, the role of inclusions in pit initiation and the effect of surface deformation by micropeening.

Current spikes have been measured during polarization in the passive region of stainless steel specimens, usually in 0.1 M NaCl at ambient temperature. Current spikes are shown to reflect local activation of the sample. The activation is only temporary and there is still no irreversible pit growth. The number and size of the spikes indicate the extent of local attack and are considered to be a measure for the susceptibility to pitting corrosion of the steel. The local activation starts with the dissolution of an inclusion leading to occluded cell formation, but has to be followed by attack of the surrounding metal in order to generate a measurable spike. It is shown that prolonged local attack is influenced by the polarization potential, the pH and composition of the electrolyte solution, the size and composition of the inclusions in the steel, stress, the surface roughness, and the steel composition. An increasing number of sites is activated as the polarization potential is increased to more anodic values. Increasing the pH or addition of acetate results in a decreasing number of measurable attacked sites. Thiosulphate in low concentrations as well as an increased chloride concentration promotes localized attack. But high concentrations of thiosulphate have an effect similar to acetate.

Separate manganese sulphide particles have been found, using surface analytical techniques, in large amounts in ss 304, 316, 316L and 317L, but not in ss 34LN, SAN28 and 254 SMO. The latter alloys, with a low sulphur content, are known for their markedly better resistance to localized corrosion.

A considerable difference is demonstrated between the size of the manganese sulphide inclusions in the two 316 steels. Current-potential curves and current spikes measurements showed that the steel with the

largest sulphide inclusions (316L) is more susceptible to pitting corrosion. As the composition of both 316 alloys is similar, the difference in pitting susceptibility is attributed to the difference in size of inclusions.

The alloys 304 and 316 are often compared. The higher pitting resistance of ss 316 is generally attributed to the molybdenum content. Surface analyses of the tested ss 304 and ss 316 demonstrated that the manganese sulphide inclusions in ss 316 are smaller than the inclusions in ss 304. This is likely to contribute to the improved pitting resistance of ss 316. Not only the molybdenum content in ss 316 should be held responsible for the increased resistance to pitting. Moreover, it is shown that the lifetime of current spikes is increased in higher alloyed steels. It is suggested that not only a beneficial effect, an improved repassivation ability, can be expected from alloying, but also a detrimental effect. Better oxide layers, which remain intact longer in acid environments for example, can keep occluded cell conditions for longer times, whereupon localized attack aggravates.

Stress in a steel induces higher current densities. From comparison of ground and polished surfaces it seems that the stress resulting from grinding is beneficial. The stress promotes breakdown of the cover (a thin surface layer) of occluded cells in which the metal is attacked, and thus reduces the time of local activation. Micropeening causes stress and changes the morphology of the surface. Compared with polished surfaces the number of activated sites in a test increases because of micropeening. Compared with ground surfaces the number of activated sites stays the same but the extent of local attack increases, as evidenced by the increased size of current spikes. The effects are probably caused by small crevices which resulted from the surface treatment. The crevices provide solid occluded cells in which attack can proceed relatively long.

## SAMENVATTING

In dit proefschrift komen enkele kwalitatieve aspecten van putvormige corrosie van hoog gelegeerde roestvaste staalsoorten aan bod. Het volgende wordt met name besproken: de methode en de waarde van het meten van stroompieken, de rol van insluitels in de initiatiefase en het effect van oppervlakteformatie door *micropeenen*.

Stroompieken zijn gemeten bij constante potentiaal in het passieve gebied, meestal in 0.1 M NaCl bij kamertemperatuur. De stroompieken geven lokale activering van het roestvast stalen proefstuk weer. De activering is slechts van korte duur en er is nog geen sprake van onomkeerbare putgroei. Het aantal en de grootte van de pieken weerspiegelen het aantal plaatsen respectievelijk de mate van aantasting en worden beschouwd als een maat voor de gevoeligheid van het staal voor putvormige corrosie.

Lokale activering begint met het oplossen van een insluitel waardoor een holte wordt gevormd, maar moet worden gevolgd door aantasting van de omgeving voordat het verschijnsel geregistreerd wordt als een stroompiek. Voortgaande lokale aantasting blijkt te worden beïnvloed door de polarisatiepotentiaal, de zuurtegraad en de samenstelling van de elektrolytoplossing, de grootte en de samenstelling van de insluitels in het staal, spanningen in het metaal, de oppervlakteruwheid en de samenstelling van het staal. Een toenemend aantal plaatsen wordt geactiveerd als de potentiaal wordt verhoogd naar meer anodische waarden. Als de pH wordt verhoogd of acetaat wordt toegevoegd aan de elektrolytoplossing wordt echter een afnemend aantal plaatsen meetbaar geactiveerd. Thiosulfaat in lage concentraties bevordert lokale aantasting, evenals verhoging van de chlorideconcentratie. Maar thiosulfaat in hoge concentraties heeft hetzelfde effect als acetaat.

Afzonderlijke mangaansulfide insluitels zijn in grote hoeveelheden gevonden in de staalsoorten 304, 316, 316L en 317L, maar niet in 34LN, SAN28 en 254 SMO. De laatst genoemde legeringen, met een laag

zwavelgehalte, staan bekend om hun goede weerstand tegen lokale aantasting.

Er is een duidelijk verschil gevonden tussen de grootte van de mangaansulfide insluitsels in de twee onderzochte 316 legeringen. Uit de stroom-tijd curven en de stroompiek-metingen blijkt dat de staalsoort met de grootste insluitsels (316L) het meest gevoelig is voor putvormige corrosie. Omdat de samenstelling van de beide 316 legeringen vrijwel gelijk is, kan het verschil in gevoeligheid toegeschreven worden aan het verschil in grootte van de insluitsels.

De legeringen 304 en 316 worden vaak vergeleken. De hogere weerstand van 316 tegen putvormige corrosie wordt in het algemeen toegeschreven aan de aanwezigheid van molybdeen. Uit oppervlakte-analysen van de geteste 304 en 316 legeringen bleek echter dat de mangaansulfide insluitsels in de 316 legering kleiner zijn dan de insluitsels in het 304 staal. Dit zal bijdragen aan de hogere weerstand tegen putvormige corrosie van het 316 staal. Niet alleen het molybdeengehalte van het 316 staal mag daarvoor verantwoordelijk worden gehouden. Bovendien is gebleken dat de levensduur van de stroompieken toeneemt bij hoger gelegeerde staalsoorten. Naast het gunstige effect van legeren, namelijk verbetering van de repassiverings-eigenschappen, mag ook een nadelig effect verwacht worden. Betere passieve films, die langer intact blijven in agressief milieu bijvoorbeeld, kunnen een holte langer afschermen waardoor de aantasting ter plaatse verergert.

Spanningen in het staal leiden tot hogere stroomdichtheden. Uit vergelijkingen van geschuurde met gepolijste oppervlakken blijkt dat de spanningen ten gevolge van schuren gunstig uitwerken. De spanningen bevorderen breuk van de afdekkende (dunne oppervlakte-)laag over holtes waarin het metaal aangetast wordt, en bekorten daarmee de tijdsduur van lokale aktivering. *Micropeenen* veroorzaakt spanningen en verandert de morfologie van het oppervlak. Vergeleken met gepolijste oppervlakken neemt het aantal geactiveerde plaatsen in een test toe door *micropeenen*. Vergeleken met geschuurde oppervlakken blijft het aantal geactiveerde plaatsen gelijk maar neemt de lokale aantasting toe, getuige de grotere stroompieken. De effecten worden naar alle waarschijnlijkheid veroorzaakt door kleine spleetjes die het gevolg waren van de oppervlaktebehandeling.

De spleetjes voorzien in stevige, afgeschermdde holtes waarin aantasting relatief lang kan voortgaan.





## DANKWOORD

## ACKNOWLEDGEMENT

Met vele medewerkers van Het Laboratorium was het de afgelopen jaren prettig samenwerken en/of gezellig koffie drinken. Ik wil graag een aantal mensen en groepen, ook van buiten het lab, met name noemen, zonder anderen te willen beledigen. Voor alle kleine en grote klussen zoals het vervaardigen van meetcellen, het maken van foto's en dia's, het walsen van proefstukken, het zagen, boren en draaien van van alles en nog wat, talloze tussendoor-klusjes en voor de sfeerverhogende inbreng bedank ik graag: Louis Bakker, Pieter Colijn, Thelma Harmens, Jaap Meijer en alle betrokken medewerkers van de werkplaats, de Centrale Electronische Dienst en het Audio-Visueel Centrum. De ex-collega's uit de gieterij voorzagen mij bovendien van een zitplaats en koffie tot lang nadat ik van vakgroep veranderd was, en van kantoormeubilair (het enige wat ik ooit leende en niet terugbezorgde).

De medewerkers van de oppervlakteanalyse-groep wil ik bedanken voor het uitvoerige werk dat ze voor mij gedaan hebben. In het bijzonder heb ik de samenwerking met Wim Sloof zeer gewaardeerd.

Zonder de (ex-)collega's die altijd bereid waren hun kennis en kunde (of toch kunst?) te delen was het allemaal niets geworden. Twee mensen wil ik met name noemen: Peter Overkamp en Bart Norbart. Peter was ondermeer behulpzaam bij het opstarten van de experimenten. Bart was nooit te beroerd voor welk klusje dan ook. Ook de drie afstudeerders, Johan Elkenbracht, Suling Xu en Richard Ottens, die zich inzetten voor het onderzoek ben ik erkentelijk voor hun bijdrage. De atoomspectrometristen uit onze sectie wil ik niet vergeten; zij voerden snel vele analyses voor mij uit.

Mijn excuses aan Jan-Willem Lenderink, die als kamergenoot moest delen in alle ellende van een gejaagd promovendus. Maar ook bedankt, Jan Willem, voor je steun en behulpzaamheid bij vele klusjes.

*I would like to thank Poul-Erik Arnvig from the Avesta/Sheffield Company. I am grateful for the test material. My stay in Avesta was very instructive and, thanks to you, Poul-Erik, very pleasant. I gained weight.*

*I wish to thank the researchgroup of professor H. Böhni at the ETH in Zürich for the offered hospitality. Rudi Morach, thanks to you I was able to make a quick start with my current spikes measurements.*

Sytze Huizinga, Shell Research, wil ik niet vergeten. Voor de zinvolle gesprekken, het mooie rijtje proefstukken, en vooral voor je belangstelling voor mijn werk ben ik je dankbaar. Hans Verhoef, DSM, ben ik eveneens erkentelijk voor de leerzame gesprekken.

Hoewel de foto in dit proefschrift van een behandeld oppervlak door zijn sterke uitvergroting misschien anders doet vermoeden, zijn alle proefstukken vakkundig en welwillend gemicropeend door het CTB. De bijdrage aan de cultuur in Nederland wordt eveneens zeer gewaardeerd.

Beste professor Hans, jouw onuitputtelijke energie, enthousiasme en vertrouwen zijn onontbeerlijk geweest.

En *last but not least*: Abé, bedankt voor alle steun in hectische tijden!

## CURRICULUM VITAE

Loes Jansen werd op 7 januari 1960 geboren te Altforst (Gld.). Na 5 jaar basisschool in Altforst volgde een jaar MAVO in Beneden-Leeuwen, 2 jaar Atheneum in Druten en vervolgens 4 jaar in Venray alwaar de middelbare school-periode in 1978 met het diploma Atheneum-B werd afgesloten. In 1982 werd de vierjarige HNWO-opleiding (voor researchanalist) afgerond. Een negen maanden full-time stage bij de vakgroep Biochemie van de Katholieke Universiteit Nijmegen (KUN) maakte deel uit van de opleiding. Aansluitend, van mei 1982 tot augustus 1983, werkte ze als analist bij het Antropogenetisch Instituut van de KUN. Vervolgens vervulde ze de functie van technisch medewerker bij de Universitaire Stralingsbeschermingsdienst van dezelfde universiteit. Op 1 januari 1987 werd de overstap naar de Technische Universiteit Delft gemaakt. Ze kwam in dienst als practicumvernieuwer voor de toenmalige Tussenafdeling der Metaalkunde. Met de (avond)studie Scheikunde aan de Rijksuniversiteit Utrecht was reeds een aanvang gemaakt in 1985. Deze studie, met als onderzoeksspecialisatie Chemiedidaktiek en de keuzevakken Informatica en Materiaalkunde, werd afgesloten met het doctoraalexamen in februari 1989. Op 1 september 1989 werd de vakgroep Productietechnologie vervuild voor de vakgroep Toepassingen van Materialen in Constructies, sectie Corrosietechnologie en Electrochemie. Daar was ze vier jaar in dienst als toegevoegd onderzoeker in het kader van een onderzoek gefinancierd door het IOP-metalen. Per 1 oktober 1993 zal ze in dienst treden van het Nationaal Lucht- en Ruimtevaartlaboratorium te Amsterdam (standplaats Marknesse, Noordoostpolder).